Pitt, John Michael

# DEFORMATION RESTRAINT AND THE MECHANICS OF SOIL BEHAVIOR

*Iowa State University* PH.D. 1981

# Deformation restraint and the mechanics of soil behavior

by

John Michael Pitt

A Dissertation Submitted to the
Graduate Faculty in Partial Fulfillment of the
Requirements for the Degree of
DOCTOR OF PHILOSOPHY

Department: Civil Engineering
Major: Geotechnical Engineering

Approved:

Signature was redacted for privacy.

In Charge of Major Work

Signature was redacted for privacy.

For the Major Department

Signature was redacted for privacy.

For the Graduate College

Iowa State University
Ames, Iowa
1981

TABLE OF CONTENTS

# INTRODUCTION AND SCOPE

The geotechnical engineer encounters the problem of having to work with highly variable and complex materials, the properties of which are difficult to measure and often impossible to logically apply to scientifically based theories. In the past, much effort has been devoted to evaluation of the mechanistic behavior of soils, and the result has been the development of a wide variety of test methods and theoretical or empirical techniques dedicated to predicting ultimate strength and deformation. Approaches to evaluating engineering properties of soil might be grouped into two categories. The more conventional tactic is to test representative specimens in the laboratory, under well-defined boundary conditions. However, since it has been observed that the act of taking representative soil specimens can often influence their properties, in situ testing has recently been emphasized. Although the latter approach may circumvent difficulties associated with sample disturbance, one set of problems may have been traded for another. In situ tests involve indeterminate boundary conditions which necessitate a theoretical presumption to evaluate the desired parameters. Theories for soil often involve simplifications not necessarily representative of actual behavior; thus results of many in situ test methods must be empirically correlated to performance.

Regardless of the approach, complexity has been the hallmark of many of the recent soil testing advances, often rendering them useful to understanding soil behavior, but ineffectual when subjected to the

realisms of natural soil deposits. The self-boring pressuremeter represents the results of an extreme effort to reduce the influence of sample disturbance through hole relaxation. Getting the device to self-bore in many soils has been a problem. Laboratory apparatus capable of applying plane strain and truly triaxial boundary conditions have been developed, but their cost and complexity has relegated them to the position of being research tools, not suitable for prosaic engineering practice.

Apparatuses which can provide realistic boundary conditions are certainly valuable and might evolve into practical tools. However, the underlying motivation for this research is to provide theoretical and experimental background for test apparatus and methodologies which are more suited to dealing with the problem of soil variability. The variability factor in geotechnical design could in many situations overshadow the influence of sample disturbance or accurately defined boundary conditions. Soil variability has not gone unrecognized as an obstacle to making valid engineering predictions; however, it has been relegated the status of an unquantifiable nuisance, manifested in the design process through the "factor of safety." Dealing with soil variability means gathering repetitive data, a requirement for which existing tests and prediction methodologies has thus far proven inadequate.

The primary objective of this research is to investigate the suitability of a test in which stress and displacement measurements are made on cylindrical soil specimens, subjected to elastic radial restraint.

The Iowa K-Test (25, 26, 44) is one version of such a test, recently introduced as a quick method for determining the parameters required for many geotechnical predictions. However, the significance of results is not well-understood. The intent of this research is to expand upon previous work by assessing soil behavior tested under such conditions and evaluating and interpreting results within the context of existing theories, tests, and prediction methods. Since results of this research are intended to support a solution to the soil variability problem, an analysis of the significance of this factor in geotechnical design shall be made integral to the evaluation.

# REVIEW AND ANALYSIS OF LITERATURE

## Soil Variability

Quantitative assessment of soil variability is a relatively new addendum to geotechnical engineering. Lumb's (43) 1966 publication seems to represent the first systematic to attack on the variability problem. A total of sixty-six consolidation tests performed on specimens taken from a sandy clay deposit, judgmentally considered a uniform soil, showed that coefficient of variation, CV, for compression index was about 25 percent. Coefficient of variation, a dimensionless quantity, is defined as the sample standard deviation divided by the mean and is useful for comparing variability of different phenomena. As a point of reference, the coefficients of variation for concrete strength is on the order of 10 percent (64). Others, following Lumb's rather tedious methodology, accumulated similar results for many common soil strength and deformation parameters. Harr (28) summarized these data. To provide a feeling for the significance of soil variability, parts of this summary are included as Tables 1 and 2.

Variability in strength parameters for sands and gravels are on the same order as for concrete, whereas cohesive soils display significantly more variation, with an upper limit of 85 percent. Coefficients of variation for compression index for cohesive soils were found to range from 25 to 52 percent.

Table 1. Variability of strength parameters, after Harr (28)

| Material | Frictional Angle, Degrees | Tangent of Frictional Angle | Unconfined Compression Strength, psi | Number of Samples | Mean | Standard Deviation | Coefficient of Variation, % |
|---|---|---|---|---|---|---|---|
| Gravel | X | | | 38 | 36.22 | 2.16 | 6.0 |
| Sand | X | | | 73 | 38.80 | 2.80 | 7.0 |
| Sand | X | | | 136 | 36.40 | 4.05 | 11.0 |
| Sand | X | | | 30 | 40.52 | 4.56 | 11.0 |
| Gravelly Sand | X | | | 81 | 37.33 | 1.97 | 5.3 |
| Sand | | X | | 81 | 0.762 | 0.056 | 7.3 |
| Sand | | X | | 50 | 0.717 | 0.093 | 13.0 |
| Sand: loose | X | | | | | | 14.0 |
| dense | X | | | | | | 12.0 |
| Silty sand | | X | | 82 | 0.692 | 0.096 | 13.8 |
| Clay: depth, ft. | | | | | | | |
| 5 | | | X | 279 | 28.9 | 14.2 | 49.1 |
| 10 | | | X | 295 | 23.3 | 9.6 | 40.9 |
| 15 | | | X | 187 | 20.7 | 8.2 | 39.6 |
| 20 | | | X | 53 | 18.1 | 8.6 | 47.7 |
| Clay | | | X | 231 | 13.5 | 3.6 | 29.0 |
| Clay | | | X | 97 | - | - | 30.0-40.0 |
| Clay shale[a] | | | X | - | - | - | 37.0-51.0 |
| till[a] | | | X | - | - | - | 60.0-85.0 |
| till | | | X | - | 45.0 | 16.3 | 36.1 |

[a]Author notes these two materials are extremely variable and believes that these results are probably close to the upper possible limits of variability for any natural soils.

Table 2. Variability of compression index, after Harr (28)

| Material | Mean Compression Index, $C_c$ [a] | Number of Samples | Standard Deviation | Coefficient of Variation, % CV |
|---|---|---|---|---|
| Sandy clay | .139 | 66 | .0354 | 25.5 |
| Clay: Depth, ft. | | | | |
| 5 | .184 | 108 | .047 | 25.7 |
| 10 | .167 | 95 | .048 | 28.8 |
| 15 | .159 | 40 | 0.048 | 30.1 |
| 20 | .110 | 20 | 0.052 | 47.1 |
| Clay | .33 | 241 | 0.170 | 52.0 |
| Clay | .16 | 314 | 0.060 | 39.0 |
| Clay | 0.09 | 165 | 0.040 | 47.0 |

[a] $C_c = (e_o - e)/\log (\frac{p}{p_o})$, where $e_o$ and e are initial and final void ratios and $p_o$ and p are initial and final effective stresses.

The significance of this variation to geotechnical prediction can be illustrated by considering settlements for a hypothetical situation using data from Table 2. If the most variable clay, CV = 52%, comprised a ten foot thick deposit subjected to a stress increase from 2 to 4 TSF, settlement computed using conventional soil engineering procedures (58) would be 6.6 inches for the mean compression index. Settlements representing one standard deviation of the mean would be 3.4 inches. An initial void ratio of 0.8 was assumed for these computations.

Following Lumb's contention that the compression index is a normal variate (43), the probability of selecting a specimen which would predict a settlement lying within a specified tolerance range can be computed from elementary statistics (8). Results of such an analysis are in Table 3. Assuming that consolidation theory is mechanistically correct, that the net settlement of a structure is the result of an averaging process, and that a chance selection of a single specimen is used for prediction, the probability of predicting settlements even with very large tolerances is quite low. If a prediction goal of 6.6 $\pm$ 1.32 inches were established, a single specimen test program would result in a prediction accurate to $\pm$ 20 percent of the true settlement only about 30 percent of the time. For this highly variable material, the only thing that can be stated with a high degree of confidence (e.g. 95 percent) is that the true settlement can be predicted within $\pm$ 100 percent. A similar analysis was made for the least variable of the soil deposits represented in Table 2. However, to facilitate comparison, the deposit thickness was taken at 27.7 feet such that mean settlements for both cases would be identical. Even for the least variable of deposits for which statistical data are available, the chances of predicting within a reasonable tolerance is not very high. Predictions within $\pm$ 20 percent would occur about half the time.

If the statistical information contained in Tables 2 and 3 truly represents the nature of soil, it is not surprising that the literature abounds with contradictory reports on the adequacy of prediction

Table 3. Single specimen prediction probabilities

| Tolerance Percentage of Mean Settlement | Tolerance Range, $\bar{\delta} \pm t$ [a] (inches) | Chance of Specimen Predicting Settlement, Percent | |
|---|---|---|---|
| | | CV = 52.0 | CV = 25.5 |
| 20 | 1.3 | 30 | 57 |
| 40 | 2.6 | 56 | 88 |
| 60 | 4.0 | 76 | 98 |
| 80 | 5.3 | 88 | 99 |
| 100 | 6.6 | 95 | 99.9 |

[a] $\bar{\delta}$ = mean settlement = 6.6 inches.

methods. From the information available, it is apparent that predictions would be poorest for cohesive soils where a high variability is probably due to complex particulate interaction of the clay fraction. This is unfortunate because cohesive soils are extremely common.

## Mechanical Theory

### Convention

A key element to the application of test results to the available theoretical prediction methods is the mathematical formalization of stress states producing failure or the relation occurring between stress and strain. However, prior to reviewing theory from the literature, the sign convention and nomenclature to be used in subsequent theoretical

developments will be defined.

Compressive stress shall be taken as positive and identified in reference to an orthogonal coordinate system shown in Figure 1a. The stress components on the back side of the cube have been omitted for clarity. Positive shear stresses, designated as $\tau$, are also shown in Figure 1a, with the subscripts identifying the plane and direction upon which the stress is acting. Figure 1b defines the stresses acting on an axisymmetric, cylindrical element. When shear stresses are zero, normal stress in Figures 1a and b shall be taken as: $\sigma_{11} = \sigma_1$, $\sigma_{22} = \sigma_2$, $\sigma_{33} = \sigma_3$, $\sigma_z = \sigma_1$ and $\sigma_r = \sigma_\theta = \sigma_3$. An analogous system shall be used for strain where normal, $\varepsilon$, and shear, $\gamma$, strains replace $\sigma$ and $\tau$ respectively. Compressive strains are considered positive.

Some of the theories used in this research are conveniently expressed in terms of indicial notation which identifies stress or strain components in terms of lettered subscripts taken as 1 through 3. For example, $\sigma_{ij}$ represents all of the stress components shown in Figure 1a when the following substitutions are made: $\sigma_{11} = \sigma_{11}$, $\sigma_{12} = \tau_{12}$, $\sigma_{13} = \tau_{13}$ etc. The summation convention also inferred by indicial notation is described in reference (53).

Failure criteria

The failure criterion most commonly applied to soils is one that states that limiting strength is defined by a unique relation of two extreme values of principal stresses or that shear stress, $\tau$, at yield is a function of the normal stress, $\sigma_n$, acting on the considered plane.

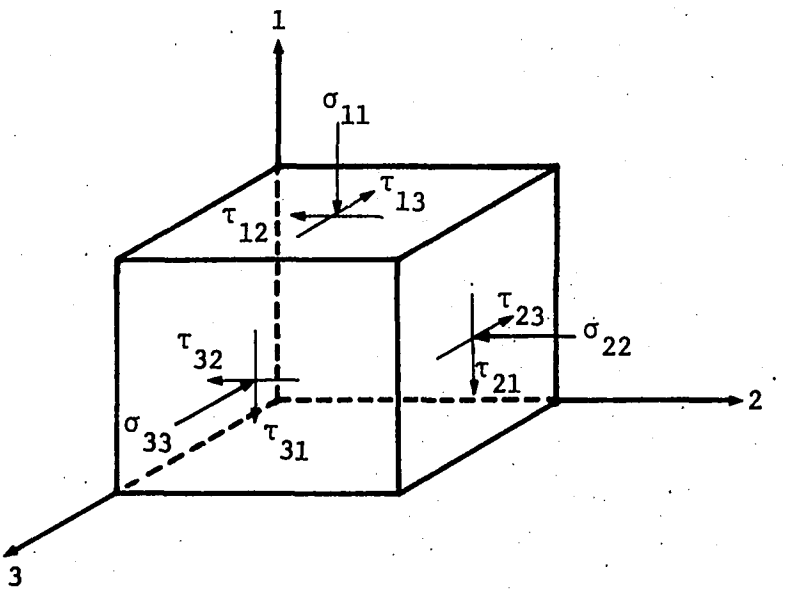


a. Orthogonal coordinates

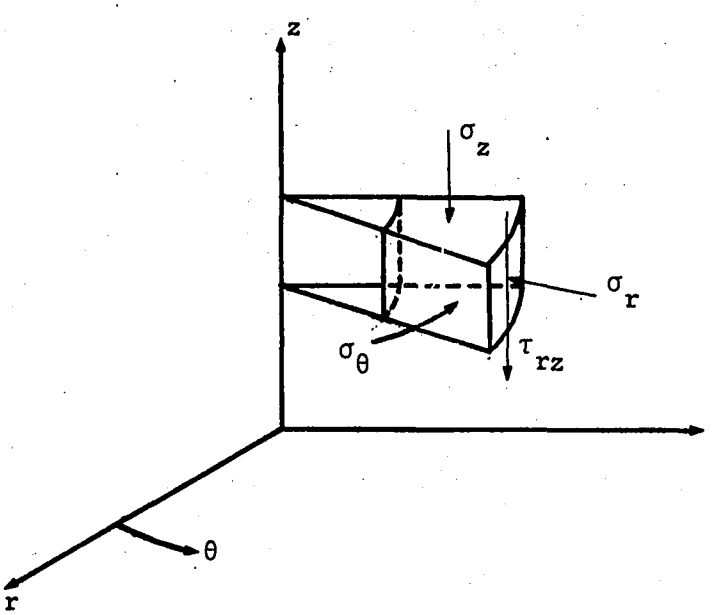


b. Axisymmetric cylinderical coordinates

Figure 1. Convention

Functionally, this statement can take the forms

$$\sigma_{max} - \sigma_{min} = f\ (\sigma_{max} + \sigma_{min})\ \text{cf. Harr (27)} \tag{1}$$

or

$$\tau = f\ (\sigma_n) \quad \text{cf. Harr (27)} \tag{2}$$

known as Mohr's failure criterion. If it is assumed that the relation between $\tau$ and $\sigma_n$ is linear, then from geometry of Mohr's circle describing maximum and minimum principal stresses at failure, the following relation can be written

$$\sigma_1 - \sigma_3 = 2c \cos \phi + (\sigma_1 + \sigma_3) \sin \phi \quad \text{cf. Harr (27)} \tag{3}$$

where c and $\phi$ are parameters referred to as "cohesion" and "angle of internal friction." An alternative representation for equation (3) is

$$\tau = c + \sigma_n \tan \phi \quad \text{cf. Harr (27)} \tag{4}$$

which is known as the empirically derived Coulomb failure criterion. The Coulomb criterion represents a special case of Mohr's general hypothesis.

As a matter of convenience, Lambe (39) introduced an alternate representation of the Mohr-Coulomb failure criterion through the simple transformation $p = (\sigma_1 + \sigma_3)/2$ and $q = (\sigma_1 - \sigma_3)/2$ which identifies

stresses defined by a Mohr's circle with a single point. This convention is particularly useful in that it facilitates definition of stress states or stress paths occurring on an element as loading progresses. Also data reduction can be made easier in that failure stresses expressed in terms of p and q can be statistically regressed to define the slope, tan $\alpha$, and intercept, b, of a line representing the ultimate strength. $\alpha$ and b can be transformed to Mohr-Coulomb parameters by the following relations

$$\sin \phi = \tan \alpha \qquad \text{cf. Lambe (39)} \qquad (5a)$$

$$c = b/\cos \phi \qquad \text{cf. Lambe (39)} \qquad (5b)$$

Although the Mohr-Coulomb failure criterion for many practical applications is a convenient way of formulating a relation for limiting strength, it does have some shortcomings. Harr (27) reports that experiments show the intermediate principal stress can influence a friction angle by as much as 6 degrees. Still another problem is in the fact that experimentation reveals that soil strength is a function of the hydrostatic stress component. The Mohr-Coulomb failure criterion can be generalized to include the influence of all six independent stress components, but the resulting expressions are unwieldy (65). An alternative yield criterion proposed by Drucker and Prager (18) is a more manageable formulation which includes the influence of all the stress components. This hypothesis states that yield is a function of the

first invariant of stress and the second invariant of deviator stress and is expressed as

$$\sqrt{J_{2D}} = \rho + \alpha_f J_1 \quad \text{cf. Zienkiewicz and Humpheson (65)} \qquad (6)$$

where $J_1$ is the first invariant of stress defined by

$$J_1 = \sigma_{11} + \sigma_{22} + \sigma_{33} \quad \text{cf. Zienkiewicz and Humpheson (65)} \qquad (7)$$

and the second invariant of deviator stress, $J_{2D}$, is

$$J_{2D} = \frac{1}{6}\{(\sigma_{11} - \sigma_{22})^2 + (\sigma_{22} - \sigma_{33})^2 + (\sigma_{11} - \sigma_{33})^2\} + \tau_{12}^2 + \tau_{13}^2 + \tau_{23}^2 \quad \text{cf. Zienkiewicz and Humpheson (65)} \qquad (8)$$

$\rho$ and $\alpha_f$ are material constants. Equation 6 is represented in three dimensional stress space as a right circular cone, having a diameter specified by $\alpha_f$ and $J_1/3$ position along the hydrostatic axis. For the special case when $\alpha_f = 0$, the Drucker-Prager criterion reduces to the well-known Von Mises failure law. Thus equation 6 is frequently referred to as the extended Von Mises criterion. In order that the Drucker-Prager and Mohr-Coulomb criterion give identical limit strengths, $\alpha_f$ and $\rho$ must be defined as follows

$$\alpha_f = \frac{\sin\phi}{\sqrt{3}\,(3 + \sin^2\phi)^{1/2}} \qquad (9)$$

cf. Zienkiewicz and Humpheson (65)

$$\rho = \frac{\sqrt{3}\ c \cos \phi}{(3 + \sin^2 \phi)^{1/2}} \quad \text{cf. Zienkiewicz and Humpheson (65)} \qquad (10)$$

A feature common to all failure criteria presented is that nothing is presumed about stress combinations occurring at levels below those producing yield. Thus according to the failure criterion, it should be possible to reach the yield surface via an infinite number of permissible stress paths. Also for a material behaving according to the failure criteria, it is theoretically possible to define stress states at an infinite number of positions on the yield surface.

Except for the experimentally based Coulomb law, the failure criteria represent hypotheses which yet require experimental validation. For the case where the Coulomb and Mohr criteria correspond, tests are relatively easy to perform, and verification is not difficult and has been accomplished many times. The Drucker-Prager criterion has in concept existed for nearly thirty years, but a review of the literature reveals only two physical laboratory validations (53) and no practical application. The value of the Drucker-Prager criterion to this research lies in its capacity to model stresses which contribute to volume change when used in conjunction with a flow rule.

Elastic constitutive law

To determine deformations, a relation between stress and strain must be established. Although soil is known not to behave elastically, it is common practice to use the two-parameter constitutive law of elasticity which can be written in indicial notation as

$$\varepsilon_{ij} = \frac{1+\nu}{E}\ \sigma_{ij} - \frac{\nu}{E} J_1\ \delta_{ij} \quad \text{cf. Rohani (53)} \tag{11}$$

where E is Young's modulus defined as

$$E = \sigma_1/\varepsilon_1 \tag{12a}$$

and $\nu$ is Poisson's ratio

$$\nu = -\varepsilon_3/\varepsilon_1 \tag{12b}$$

Both E and $\nu$ are experimentally defined in a simple uniaxial test. $\delta_{ij}$ is the Kronecker delta which is unity when $i = j$ and zero for $i \neq j$.

Assumptions leading to equation 11 dictate that the material be homogeneous and isotropic, and that the parameters are constants. The elastic connection between stress and strain infers a conservative system in that energy input during loading is recovered upon unloading. The elastic constitutive law also implies that the principle of superposition or law of independence of effects is valid. This feature is the key to the derivation of practical elastic solutions frequently used in geotechnical engineering. For example, one way to develop stress distributions for useful geometric configurations is to integrate results from simpler distributions, such as the Bouissinesq solutions for point loads, over the desired area.

It has been shown that soil behavior bears little resemblance to

many of the requirements of elastic theory (15). A truly elastic material would respond to stress by loading and unloading along the linear path illustrated by curve A in Figure 2, until the yield stress is reached.

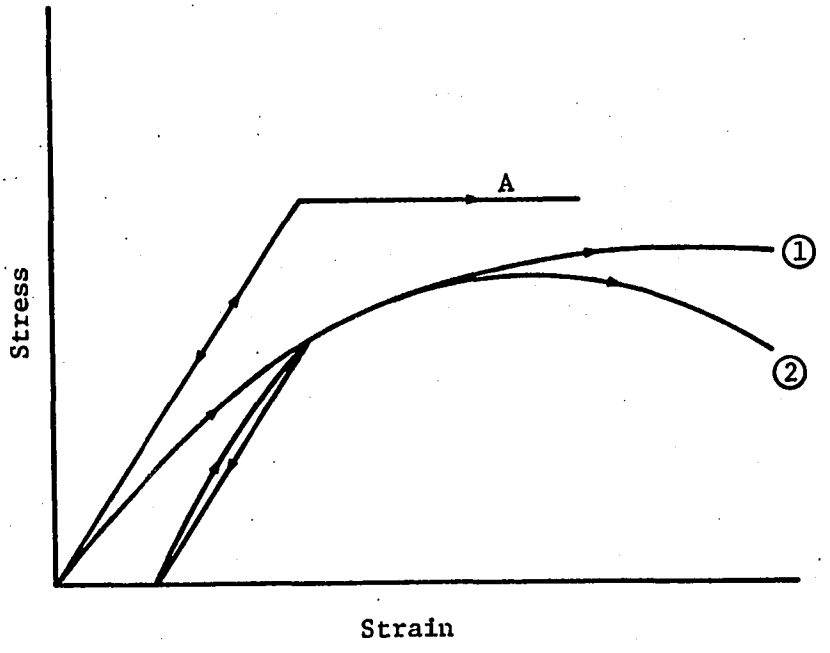


Figure 2. Typical stress-strain behavior (after Desai and Christian (15))

The shape of a stress-strain curve for soil is often nonlinear, and unloadings occurring at stresses below the ultimate strength produce a different relation between stress and strain. Depending upon the nature of the soil, stresses occurring after ultimate strength can either remain constant or decrease as shown by branches 1 and 2.

Even with such differences between the reality of soil behavior and the elastic constitutive law, the idealization or adaptations of this idealization is the basis of many geotechnical predictions. One technique for applying the finite element method is to perform incremental loadings where E and $\nu$ are taken as variables, dependent on stress level and knowledge of whether the material is undergoing a load or unload sequence. Comparisons of numerical and experimental results have been excellent (9) which suggest that many of the inconsistencies occurring between elastic theory and soil behavior may not be significant when appropriate adaptations are made.

Plastic potential

Plastic theory, developed primarily for metals, makes use of plastic flow rules which are based on the concept that increments of plastic strain occurring after yield coincide with the directions of the corresponding stresses according to an instantaneous constant of proportionality. Drucker (17) extended the classic flow rules of plasticity theory to account for volume changes observed for soil. By introducing the concept of a stable material and utilizing energy principles, Drucker demonstrated that there is a relation between the yield criterion and

plastic deformation. The result of this analysis is called the flow rule or plastic potential, and can be expressed as

$$d\varepsilon_{ij}^{p} = \Lambda \frac{\partial f}{\partial \sigma_{ij}} \qquad \text{cf. Rohani (53)} \tag{13}$$

$d\varepsilon_{ij}^{p}$ signifies increments of plastic strain, f is a functional expression of the yield criterion, and $\Lambda$ is a non-negative constant taking on values greater than zero for plastic loading and zero if yield has not occurred. The stipulation that the material is stable means that the stress does not decrease after ultimate strength is achieved, or the material follows branch 1 rather than branch 2 in Figure 2. This restriction could make the flow rule invalid for many soils. A derivation for the plastic potential is provided in Appendix A.

The significance of the plastic potential might best be illustrated by applying a specific form of the yield function. The extended Von Mises criterion can be rewritten as

$$f = \sqrt{J_{2D}} - \alpha_f J_1 - \rho \tag{14}$$

The derivative of f requires the chain rule of partial derivatives which is

$$\frac{\partial f}{\partial \sigma_{ij}} = \frac{\partial f}{\partial J_1} \frac{\partial J_1}{\partial \sigma_{ij}} + \frac{\partial f}{\partial \sqrt{J_{2D}}} \frac{\partial \sqrt{J_{2D}}}{\partial \sigma_{ij}} \tag{15}$$

where the derivatives of the components are

$$\frac{\partial J_1}{\partial \sigma_{ij}} = \delta_{ij} \tag{16a}$$

$$\frac{\partial \sqrt{J_{2D}}}{\partial \sigma_{ij}} = \frac{1}{2\sqrt{J_{2D}}} (\sigma_{ij} - 1/3\ \sigma_{mm}\ \delta_{ij}) = \frac{S_{ij}}{2\sqrt{J_{2D}}} \tag{16b}$$

$$\frac{\partial f}{\partial J_1} = -\alpha_f \tag{16c}$$

$$\frac{\partial f}{\partial \sqrt{J_{2D}}} = 1 \tag{16d}$$

By substituting equations 16 in 15, a statement for a specific form of the plastic flow rule becomes

$$d\varepsilon_{ij}^{\ p} = \Lambda\ (-\alpha_f\ \delta_{ij} + \frac{S_{ij}}{2\sqrt{J_{2D}}}) \tag{17}$$

The increments of plastic strain tensor given in equation 17 can next be separated into volumetric and deviatoric plastic strain components which are

$$d\varepsilon_{vol}^{\ p} = dI_1^{\ p} = -3\ \Lambda\ \ \alpha_f \tag{18}$$

and

$$d\sqrt{I_{2D}}^{p} = \Lambda/2 \tag{19}$$

where the plastic volumetric or first invariant of strain is

$$\varepsilon_{vol} = I_1 = \varepsilon_{11} + \varepsilon_{22} + \varepsilon_{33} \tag{20}$$

and the second invariant of deviatoric strain is

$$I_{2D} = \frac{1}{6}\{(\varepsilon_{11} - \varepsilon_{22})^2 + (\varepsilon_{22} - \varepsilon_{33})^2 + (\varepsilon_{11} - \varepsilon_{33})^2\} + \gamma_{12}^2 + \gamma_{13}^2 + \gamma_{23}^2 \tag{21}$$

Inherent in the flow rule, through the derivative, is a normality condition which indicates that the plastic strain increment, when viewed as a vector, is normal to the yield surface. In terms of the specific yield function being used, the correspondence between volumetric and deviatoric stresses and strains allows the graphical representation shown in Figure 3.

By sign convention, the negative sign in equation 18 means that according to this model, dilation accompanies yield, with the magnitude of volumetric expansion being related to $\alpha_f$. As $\alpha_f$ approaches zero, the yield function approaches the Von Mises criterion, and dilation or

volume change at failure also approaches zero. Since $\alpha_f$ is related to $\phi$, dilatancy would be expected for high friction angle materials.

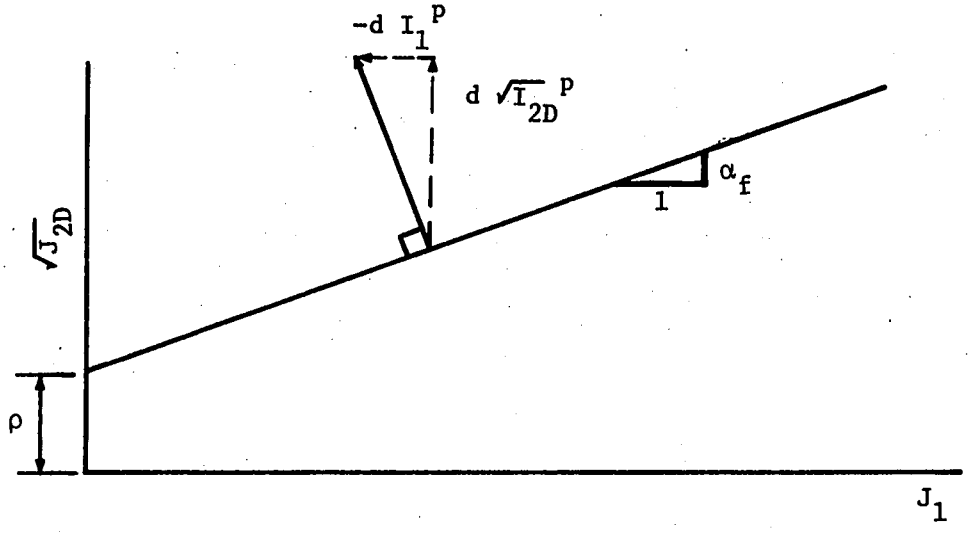


Figure 3. Stress invariant representation of plastic flow rule

Defining the parameter $\Lambda$ in equations 18 and 19 could be a difficult task. However, it is possible to arrive at a relation independent of $\Lambda$ which will be particularly useful to this research. If interest is

directed only to a relation between the ratio of volumetric and deviatoric plastic strain, dividing equation 19 into 18 results in

$$\frac{I_1^p}{\sqrt{I_{2D}}^p} = -6\alpha_f \qquad (22)$$

which is independent of $\Lambda$. The increment of plastic strain can be neglected since the ratio is equal to a constant.

## Conventional Laboratory Tests

A seemingly endless array of test methods has been developed to measure soil properties. Many were devised to answer specific scientific questions about the behavior of soil but their operational complexity makes them unsuitable for engineering. Since this is utilitarian research, the following is a brief review only of apparatus common to engineering practice. These apparatuses will also be used in the experimental aspects of this research. Equipment used to evaluate the parameters necessary to define failure criteria or constitutive laws are the direct shear, triaxial and oedometer tests.

Direct shear dominated the early work in soil mechanics, probably because primary concern was given to the Coulomb failure criterion, equation 4, and this test provides direct measures of shear strength for a given normal stress. Common versions of a direct shear apparatus involve a pair of identical rings into which a short cylindrical specimen

is placed and a normal stress is applied through end caps. Shear stresses are induced by pulling one of the rings while the other remains fixed, until the ultimate strength of the soil is realized. Tests are performed on two or more specimens at different normal stresses, providing data to determine the constants in equation 4. A common objection to this test is that the failure plane is restricted to a limited zone and is thought to bias results by eliminating freedom of a specimen to fail along natural planes of weakness (27). Other objections to the direct shear test include unreconcilable progressive failure thought to occur along the failure plane, inability to use test results for deformation predictions because principal stresses and strains occurring on the specimen are not defined until shear failure occurs, and inability to control drainage and measure pore pressure (27).

The triaxial test represents a versatile and widely-used research tool and probably the limit of sophistication for design practice. Actually the common name for the test is a misnomer because it involves subjecting a membrane-encapsulated, cylindrical specimen to an all-around fluid cell pressure, while additional stresses can be applied to the ends of the specimens by a ram acting on an end cap. Thus, with the condition of symmetry about the axis, the true state of stress acting on a specimen in a triaxial apparatus is $\sigma_1 > \sigma_2 = \sigma_3$. The ability to measure volume change and pore pressure, control drainage, and apply what is thought to be realistic boundary stresses, coupled with the fact that the applied stresses are nearly principal, are undoubtedly

good reasons for its acceptance as a research and design tool. Even with these factors in its favor, there remains a certain degree of uncertainty regarding viability of the test, particularly where radial deformations are involved. Ehrgot (20) has shown that shear modulus, a function of deviator stress and strain derived from the same data, can vary as much as 10%, depending on the treatment of the measurements. This is because specimens do not remain cylindrical during a test, but bulge in the center because of friction between the ends of the specimen and the rigid loading caps. Any other parameter involving radial strain depends upon arbitrary assumptions about radial deformations. Most experimenters use a fictitious average strain computed from axial deformation, volumetric measurements, and a presumed cylindrical geometry, while others use special apparatus to measure radial deformation at the specimen mid-height or at the location of the maximum bulge.

End restraint introduces other complexities in the interpretation of triaxial data in that rather complex stress and strain distributions are thought to occur within the specimen. Observations of compression tests in many materials suggest that conical dead zones in a compressive state of stress occur at both ends of cylindrical specimens. The remaining portion of the specimen undergoes strains commensurate with shear stresses (36). This phenomenon has been the topic of considerable research, and infrequently applied solutions such as lubricating end platens or using special fixtures shaped such that principal stresses actually occur on the contact plane, have been

suggested (3). In practice, end friction is usually neglected, and it has been found to have little influence on ultimate strength provided the length to diameter ratio of the specimen is about 2. Influence of end restraint on volumetric behavior may be another matter. Common practice is to assume that gross volumetric measurements made with conventional apparatus provide an adequate measurement of soil behavior.

The oedometer or consolidation test apparatus involves compressing a short, cylindrical soil specimen along its axis while lateral deformation is held at zero by a stiff confining ring. Porous stones allowing drainage are placed on the top and bottom of the specimen, and timed deformation measurements are taken during application of constant load levels. The objective of the test is to simulate the time dependent deformations resulting from pore water being forced from the soil, and the results are consistent with the well-established consolidation theory proposed by Terzaghi (59). This is probably the most widely used test for predicting settlements, but it has been criticized on the basis that it does not accurately reflect boundary stress conditions thought to prevail under realistic geometries and loads (40). The condition of no lateral deformation within soil deposits is considered to exist when uniform stress is applied over a very extensive area. The lateral deformation due to the applied stress on an element in a deposit is counteracted in equal amounts by the same vertical stress acting on its neighbor. When load acts over a finite area, as would be the case with a foundation, lateral displacements occur within the deposit, giving

rise to vertical deformations which are not measurable with the oedometer.

In addition to the above criticisms of conventional testing, another important objection is the expense of performing these tests, a factor particularly important to defining soil variability. As an example, the conventional technique for defining c and $\phi$ in the Mohr-Coulomb failure criterion is to fail a number of individual specimens subjected to different constant confining or normal stresses, depending upon whether a triaxial or direct shear apparatus is used. A typical triaxial test program expressed in terms of Lambe's stress path is illustrated in Figure 4. Data used for this example are for a natural glacial till and should provide an indication of the problems introduced by soil variability. Since the cost of retrieving and testing laboratory specimens is high, a test program aimed at defining strength parameters is frequently limited to testing 3 or 4 specimens. Depending on drainage conditions, such a program could occupy a technician from one to several days. Thus, the five points used in this example represent a fairly extravagant program for a single soil. By normal regression techniques, the parameters b and $\alpha$ or their transformations c and $\phi$ define expected values for shear strength at different stress, and the squared correlation coefficient, $R^2$, indicates that the linear model selected explains only 61.1 percent of the observed variation. Soil variability accounts for the remaining 38.9 percent. The statistical value of the resultant regression can be expressed in terms of the 90

percent chance of falling between the established limits (8). Prediction intervals differ from the more commonly used or misused confidence bands which merely address the chance that the true mean is contained in some interval. Obviously, the width of the prediction band suggests that in a statistical sense, very little is known about the failure criterion for this soil.

An alternative for defining failure criterion which could improve statistical knowledge of the material takes advantage of experimental observations suggesting that failure conditions are relatively independent of the stress path. Ladd (37) has shown that the failure condition or $K_f$ line can be defined by stress paths such as the one shown by the dashed line in Figure 4. This experimental observation is consistent with failure criteria because, as previously mentioned, they place no stipulation on stresses occurring prior to the limit condition. If this is true, it seems possible that ultimate strength criterion could also be established by defining several points occurring on the failure line from a single specimen. The obvious advantage of such testing is that more data could be realized for about the same cost as a single point derived by the conventional method. Statistical implications are that failure parameters could be defined without the influence of sample variability, and variation occurring in a test would be due to measurement which with adequate apparatus should be small. Statistics of regression involve an entity called degrees of freedom which means each parameter of a model describing a phenomenon reduces the information

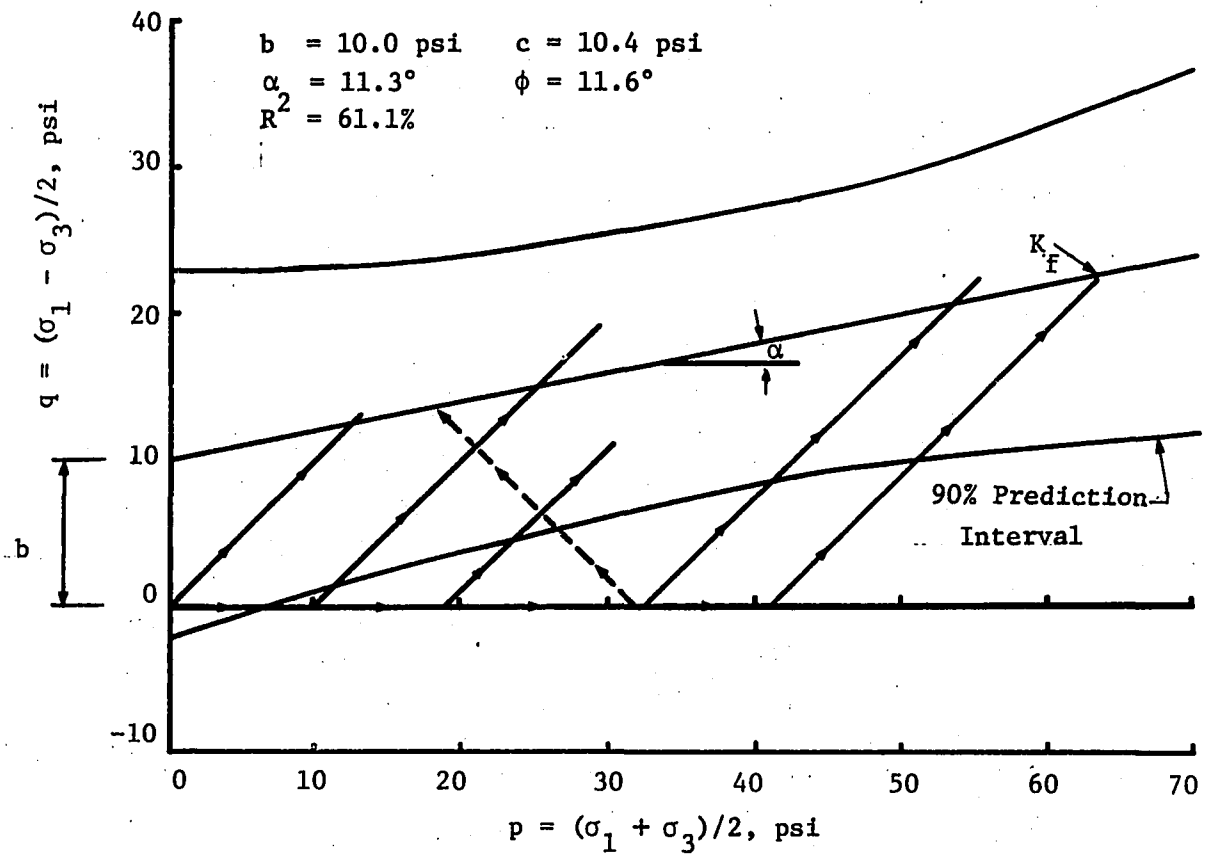


Figure 4. Conventional triaxial results for natural glacial till

available to cope with uncertainty. Thus, for a two-parameter regression on five data points only three points or degrees of freedom remain to define variability, and the prediction interval is wide. If b and α could be defined with numerous measurements from each specimen, the statistics would involve individual variation for five b's and five α's, each having four degrees of freedom. For small numbers of

specimens, a single degree of freedom is very significant. Testing along the $K_f$ line also implies that each specimen has the potential of developing characteristic limit strengths defined by its own failure parameters rather than conditions such as normal or confining stress, arbitrarily set in the laboratory.

Although $K_f$ tests seem a logical way to improve upon the knowledge of ultimate strength parameters, a single experimental study verifying this approach seems to represent the extent of research effort in this area. Flemming (21), using conventional triaxial apparatus, made a comparative study on laboratory specimens. A staged test was performed by loading a specimen at constant confining stress until the axial stress reached a maximum. The process was repeated on the same specimen for several levels of confining stress, and it was found that cohesion compared to within 0.25 psi and friction angle to within 0.2 degrees. Both the differences are well within the range of normal test precision.

## Prediction Methods

Geotechnical engineering covers a wide variety of problems, usually involving ultimate load and deformation predictions. Since the intent of this research is to evaluate and develop a test method that defines design parameters while allowing for assessment of soil variability, a review of the prediction methodologies to which such test results are applied seems appropriate. To keep the review manageable,

it will be limited to a single but very practical case of design for shallow building foundations.

In nearly all instances, prediction theories used in geotechnical engineering are highly idealized. Many phenomena known to exist both in the laboratory and the field are neglected because of complexities introduced to theoretical derivation. Fortunately absence of rigorous solutions has not precluded adequate designs, and success of many imperfect theoretical solutions is due either to insignificance of unreconcilable factors or empirical adjustments based on prototype observations. A good example of this combined theoretical-empirical process is the bearing capacity equation which has its roots in classical plasticity theory.

Bearing capacity

Working from a solution developed by Prandtl and Reissner for the ultimate resistance of a two dimensional punch acting on a Mohr-Coulomb material, Terzaghi (59) formulated a model for ultimate foundation bearing capacity by including the weight of soil. The basic solution involves the assumption that soil is a rigid elastic-plastic material, and that the ultimate bearing capacity is dictated by a geometric failure pattern consisting of three zones shown in Figure 5. Zone I is taken as an active Rankine zone which pushes the Prandtl zone II sideways, and the passive Rankine zone III in an upward direction. Implicit in this model is the fact that all of the soil contained within the rupture zone is in a state of plastic flow when the ultimate bearing

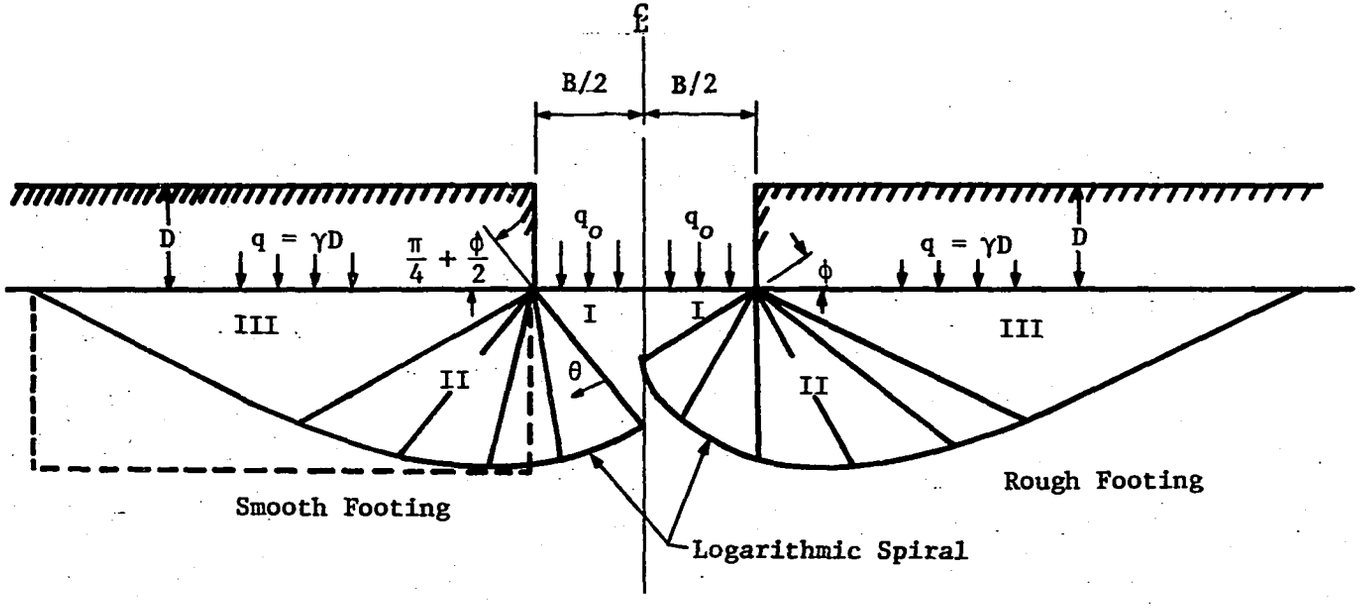


Figure 5. Bearing capacity geometry (after Harr (27))

resistance, $q_o$, is reached. The geometry and extent of the rupture surface is defined by the friction angle of the soil interface, friction occurring at the footing base, and the footing width.

According to Vesic (63), Buisman and Terzaghi are responsible for placing the bearing capacity solution in a workable form by reasoning that the ultimate capacity could be expressed as the sum of resistance components involving cohesion on the rupture surface, surcharge stress caused by the soil lying above the base, and weight of the soil within the rupture zone. Thus the ultimate bearing stress can be expressed as

$$q_o = cN_c\zeta_c + qN_q\zeta_q + \frac{1}{2}\gamma B_\gamma N_\gamma \qquad \text{cf. Vesic (63)} \qquad (23)$$

where $\zeta_c$, $\zeta_q$ and $\zeta_\gamma$ are shape factors which will be discussed later, c = cohesion, q = surcharge stress, $\gamma$ = unit weight of soil, and B = foundation width. The dimensionless parameters $N_q$ and $N_c$ are bearing capacity factors which were determined analytically by Prandtl as being

$$N_q = e^{2(3/4\pi - \phi/2)\tan\phi/2}\cos^2\left(\frac{\pi}{4} + \frac{\phi}{2}\right) \qquad \text{cf. Vesic (63)} \qquad (24)$$

$$N_c = (N_q - 1)\cot\phi \qquad \text{cf. Vesic (63)} \qquad (25)$$

$N_\gamma$ is also a dimensionless bearing capacity factor which can only be

evaluated numerically and according to Vesic (63) is very sensitive to the angle defining the zone I wedge. Extreme boundary conditions occurring at the foundation base are shown in Figure 5. For a perfectly rough surface, Terzaghi indicated that the wedge angle is set by the frictional resistance of the soil. Smooth footing geometry assumes principal stresses at the footing base, and the zone I wedge angle defines the surface upon which the failure stress will occur according to the Mohr-Coulomb criterion. In reality, boundary conditions at the footing base are neither smooth nor rough, and experimental studies done by De Beer (13) indicate that regardless of base friction, the actual angle and bearing capacity are close to that predicted by the frictionless case. This might be because relative displacements at this boundary are small enough such that appreciable friction is not mobilized. Thus, for design purposes $N_\gamma$ is usually based on the frictionless boundary condition and can be approximated by the following relation

$$N_\gamma \cong 2(N_q + 1) \tan \phi \qquad \text{cf. Vesic (63)} \tag{26}$$

The mathematical difficulties associated with solutions for foundation shapes other than that of an infinitely long strip are appreciable. Only a few geometries have been analyzed, and the proposed solutions are at variance with experimental results. Thus, a workable approach to accounting for bearing capacity of rectangular,

circular, and square footings has been modification of the basic bearing capacity equation by geometric shape factors. Based on extensive experiments, Vesic (62) and De Beer (13) recommend the following relations

$$\zeta_q = 1 + \left(\frac{B}{L}\right) \frac{N_q}{N_c} \qquad \text{cf. Vesic (63)} \qquad (27)$$

$$\zeta_c = 1 + \left(\frac{B}{L}\right) \tan \phi \qquad \text{cf. Vesic (63)} \qquad (28)$$

$$\zeta_\gamma = 1 - 0.4 \left(\frac{B}{L}\right) \qquad \text{cf. Vesic (63)} \qquad (29)$$

where B = footing width and L = footing length. For circular footings B and L are identical and are taken as the diameter.

Fortunately for practicing engineers, bearing capacity failures are not very common. On the other hand, this is unfortunate in that information about prototype failures is not available, and most of the information regarding the accuracy of bearing capacity theory comes from relatively small scale model studies. Based on these studies, Vesic (62) found that when soil fails in general shear or through development of limiting shear resistance defined by the geometry in Figure 5, the bearing capacity equation tends to be slightly conservative but accurate to within about 10 percent. When viewed in the context of safety factors of 200 to 400 percent which are applied for

soil variability, the imprecision of bearing capacity theory is not very significant.

A questionable aspect of bearing capacity theory arises when a foundation is supported by a highly compressible soil. Under these circumstances, a phenomenon called local shear occurs and soil comprising zones I and II in Figure 5 undergoes volumetric decrease such that the passive resistance from zone III is not developed. Comparative load-deformation behavior for local and general shear cases are shown in Figure 6. For general shear a definitive ultimate strength is achieved, whereas local shear is characterized by a continuous increase in load capacity, probably representing stiffening and increased strength by virtue of densification. Terzaghi (59) recognized this phenomenon and to satisfy the immediate needs of engineering practice proposed the use of the basic bearing capacity equation, but with reduced strength parameters. Meyerhof (46) established a set of empirical local shear bearing capacity factors to be used when the soil meets certain requirements for relative density or sensitivity. Vesic (63) reports that such empiricism does not hold for all soils and load geometries, and that a rational approach to this aspect of bearing capacity does not exist. However, for building design, it might be possible that bearing capacity analysis for local shear is not necessary. Failures associated with local shear may not result in catastrophic collapse or instability, in which case the governing design criterion may be settlement. The form of the load-settlement curve in Figure 6

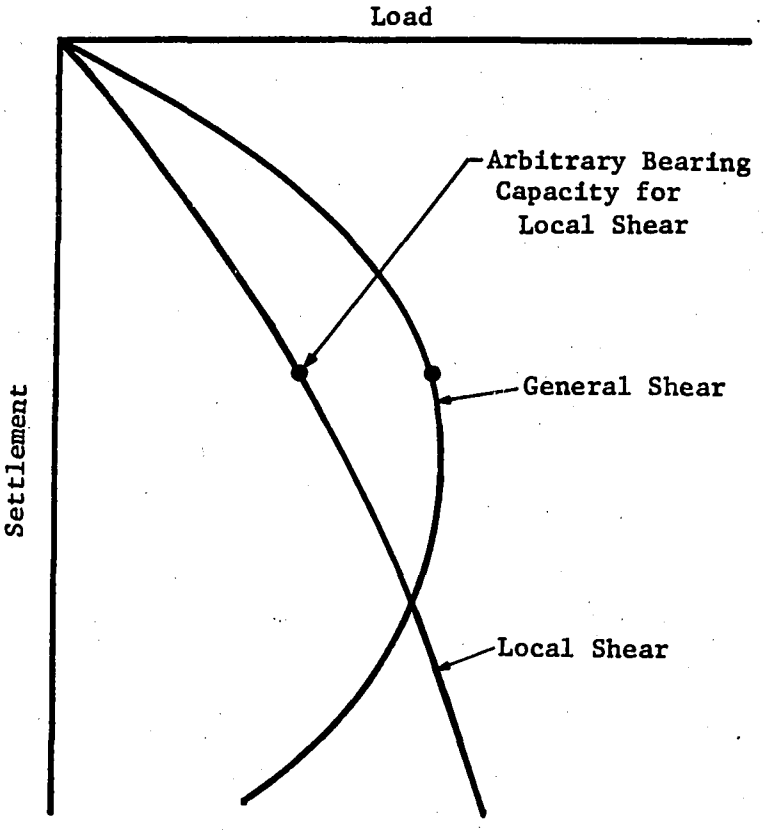


Figure 6. Load-settlement response for local and general shear (after Vesic (63))

suggests that establishment of an ultimate bearing capacity may in reality represent limits on settlement.

Settlement

Settlement prediction methods available to the geotechnical engineer range from the elaborate finite element method which demands comprehensive test data defining complex relationships between material properties, to the more widely used conventional techniques which rely on fragments of theory and less testing. As previously mentioned, the finite element method is very accurate when the material is adequately defined (9). However, this accuracy has been proven only for model studies where soil variability has been well-regulated. As variability has been demonstrated as being a very significant factor, attention will be given to the conventional prediction methods for which testing is simpler and collection of repetitive data seems more plausible. In the conventional context, settlement occurring beneath a shallow foundation is often viewed as being separable into three components (30). Initial settlement is considered independent of time and is attributed to compression of air in voids and distortion of the soil mass. Consolidation settlement is due to the time-dependent flow of pore water and the resultant decrease in volume. The third settlement component is called secondary compression and is thought to involve the time-dependent adjustment of soil structure under constant effective stress. Secondary compression settlement is often a small fraction of the total settlement component and is frequently neglected in engineering estimates.

Although there is no reason to suspect that settlement resulting from the components occurs independently, design convenience is realized by adapting theories and physical tests to the parts.

Prerequisite to estimating any of the settlement components by conventional methodology is knowledge about stress levels occurring within the soil mass. Even though soil is known not to be an elastic material, the availability of elastic solutions for problems having boundary conditions which correspond approximately to those for soil engineering problems, and the lack of anything better, have promoted the use of elastic theory. A landmark study aimed at evaluating the validity of elastic theory was performed at the U.S. Army Waterways Experiment Station (22, 61). It was found that for fine-grained, cohesive soils, elastic stress distributions beneath a uniformly loaded circular area corresponded to within 10 percent of measured values. However, the same theory applied to predicting deformations from constant-confining-stress triaxial test results on carefully prepared laboratory specimens predicted far greater settlements than were observed. The apparent validity of one aspect of elastic theory and not the other might be explained by considering results for the appropriate elastic solutions. The vertical and radial stress occurring beneath the center of a uniformly loaded circular area, acting on a homogeneous half space is given by the equations

$$\sigma_z = \sigma_1 = q_s \left\{1 - \frac{1}{((a/z)^2 + 1)^{3/2}}\right\} \quad \text{cf. Harr (27)} \qquad (30)$$

$$\sigma_r = \sigma_3 = \frac{q_s}{2}\left\{(1 + 2\nu) - \frac{2(1 + \nu)}{(a^2 + z^2)^{1/2}} + \frac{z^3}{(a^2 + z^2)^{3/2}}\right\} \quad (31)$$

cf. Harr (27)

where $q_s$ = surface stress, z = depth below the loaded area, and a = radius of the loaded area. From equation 30, it can be seen that vertical stress distribution is only a function of geometry and is not influenced by material properties. Radial stress distribution invokes Poisson's ratio but agreement with experimental results reported in references 22 and 61 was realized only after adjusting $\nu$. Vertical displacement, $\delta_\nu$, for the same geometry is given by the equation

$$\delta_\nu = \frac{2a\, q_s\, (1 - \nu^2)}{E} \qquad \text{cf. Harr (27)} \quad (31a)$$

which depends on both E and $\nu$. Elastic theory appears to work well for predictions which do not involve material properties but is of questionable value unless an appropriate assessment of E and $\nu$ is possible. The Waterways Experiment Station work was done prior to the realization the E and $\nu$ for a soil are not constant but depend on stress. Thus, attempts to use the elastic parameters from constant confining stress triaxial tests without appropriately dealing with the problem of stress dependency resulted in sizable errors. For some predictions all that is required from elastic theory is the vertical stress distribution. In these situations, the 10 percent accuracy is

probably adequate.

Because of the inaccuracy of predicting initial or distortional settlements with laboratory tests and elastic theory, attention has been focused on empirical modifications of basic elastic theory. A common approach is to assume a value for $\nu$ and back-compute values for E using equation 31a and data from field load tests or observed foundation settlements. Back-computed values for E are then correlated to an easily measured property for future predictions. Unconfined compression strength, $q_u$, seems to be the most widely used correlative parameter. Perloff (50) reports the following relation as being appropriate

$$E \approx (250 \text{ to } 500) q_u \qquad \text{cf. Perloff (50)} \qquad (32)$$

while British investigators (7) recommend a multiplier ranging between 140 to 150 for soils occurring near London. Unless the multipliers can be calibrated for a specific deposit, this technique can obviously result in a wide range of settlement predictions. A more complex methodology for estimating initial settlements has been proposed by D'Appolonia, Poulos, and Ladd (12). This method includes the influence of local yield by using conventional elastic theory together with a series of elastic-plastic finite element solutions for idealized soil profiles and geometries. However, an essential element of this analysis is still an empirical correlation between back-computed values of E and undrained shear strength. For the three clays used in the correlation, this prediction method worked quite well. The original paper appears

to represent the only application.

In many saturated soils, consolidation represents the most significant component of total settlement. An analysis proposed by Terzaghi (59) is the mainstay of engineering practice and often represents the full extent of settlement evaluations. Although somewhat time-consuming, conduct of the test is simple. A specimen placed in an oedometer is subjected to different levels of constant stress. During the application of each stress level, vertical deformations are measured with respect to time until pore pressures are dissipated. Since the oedometer is not suited for pore pressure measurements, effective stress is defined by graphical manipulation of time-deformation plots. Results of this test are traditionally presented as a plot of void ratio versus the logarithm of effective vertical stress $\sigma_z'$. A more recent trend has been to replace void ratio with axial strain. Typical results are shown in Figure 7. Consolidation settlement, $\delta_c$, can be graphically estimated by reading the change in void ratio associated with a stress increase computed from elastic theory, and the relation

$$\delta_c = H \left(\frac{e_1 - e_2}{1 + e_1}\right) \quad \text{cf. Spangler and Handy (58)} \qquad (33)$$

where H is the thickness of the compressible layer and $e_1$ and $e_2$ represent the initial and final void ratios. Alternatively, the slope of the straight line part of the e - log $\sigma_z'$ plot can be reported and used to determine the void ratio difference in equation 33. This slope is called

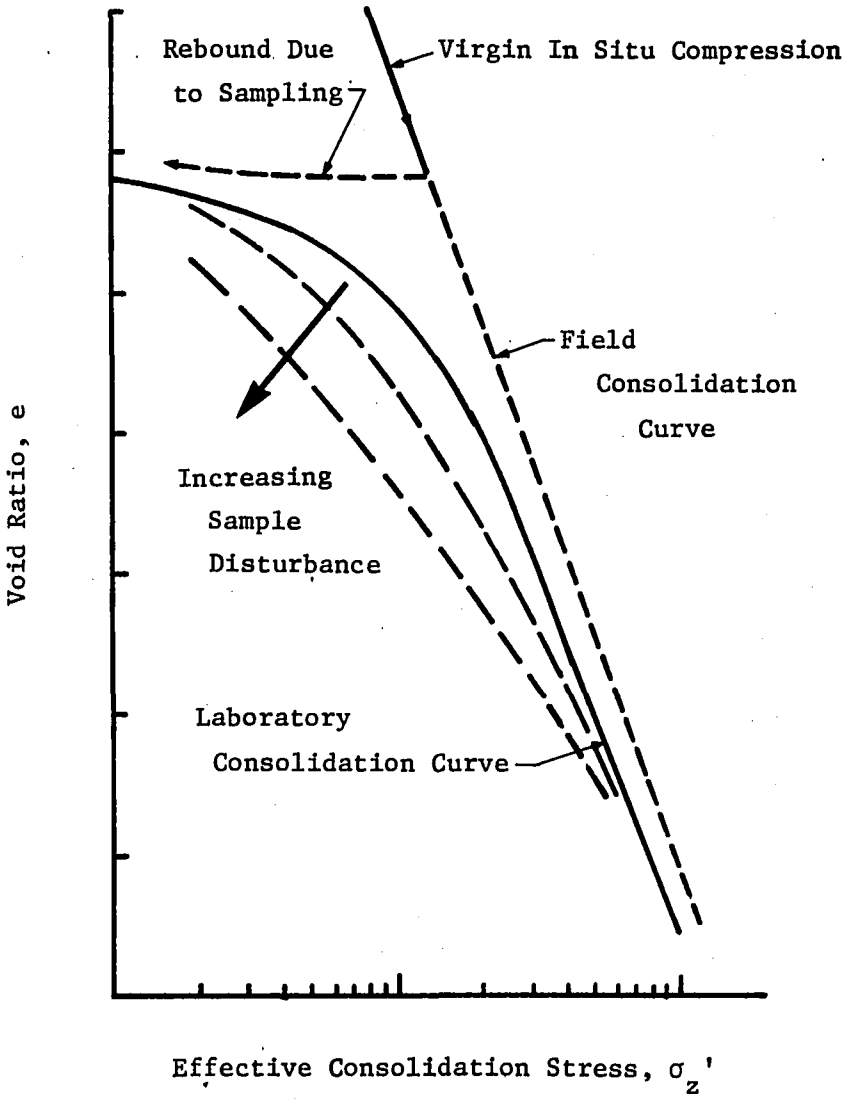


Figure 7. Typical void ratio-log pressure (after Holtz and Kovacs (30))

the compression index.

The semi-logarithmic plot of void ratio versus effective vertical stress has been the subject of much evaluation and speculation. The deformation behavior of a soil relative to the maximum past effective stress has been found to correspond to the shape of different parts of the curve (30). The straight line part of the laboratory consolidation curve represents stress levels in excess of those to which the soil specimen has been previously subjected, while curvature is thought to represent reloading of a specimen having been subjected to the unloading process associated with sampling. Several empirically substantiated graphical techniques have been proposed for determining the maximum past vertical stress, which occurs in the vicinity of the knee of the laboratory curve. Where the maximum past stress exceeds the existing overburden pressure, the material is said to be overconsolidated. Overconsolidation is frequently observed and is attributed to such factors as glaciation, removal of overburden, or development of internal stresses by desiccation. In terms of design, this merely means that the nonlinear part of the curve is used to estimate the change in void ratio for a given stress increment.

A factor considered more important to settlement predictions is the influence of sample disturbance. Field sampling, extrusion, trimming, and inserting the specimen in apparatus does to some unknown degree alter the fabric and the stress-strain behavior of a soil (30). Figure 7 shows changes inferred for consolidation curves as disturbance

increases: the compression index tends to decrease with disturbance, hence underestimating settlements, and the point of maximum curvature becomes obscured. Schmertmann (56) studied the influence of sample disturbance and proposed a graphical procedure for reconstruction of the field consolidation curve, the validity of which is difficult to evaluate because the position of a true field curve is unknown.

The e - log $\sigma_z'$ curve in Figure 7 represents a stress-deformation relation that supposedly occurs after pore pressures have dissipated to zero. Terzaghi's (59) most significant contribution to consolidation theory is the development of an analytical procedure describing the time it takes for the consolidation procedure to occur. A detailed description of the rate theory will not be presented here, but the essence of the development involves the assumption that fluid in a saturated soil flows in one direction according to Darcy's law when stress is applied. The rate theory is based on a solution to the one-dimensional diffusion equation in which pore pressure and position are the variables. The settlement at any time is estimated from the proportion of pore pressure dissipated.

Janbu (35) proposed an alternative method for estimating settlements. This scheme uses data from the oedometer test but stress-strain properties of the material are expressed in terms of parameters more consistent with classic mechanics. The tangent modulus, $M_t$, representing the slope of an arithmetic axial stress-strain curve, is formulated in terms of the following power function

$$M_t = m \, p_a \left(\frac{\sigma_z'}{p_a}\right)^{1-\omega} \qquad \text{cf. Janbu (35)} \qquad (34)$$

where m = modulus number, $\omega$ = stress exponent, $\sigma_z'$ = axial effective stress and $p_a$ = reference pressure introduced to keep the parameter m dimensionless. One-dimensional stress-strain behavior is quantifiably categorized by $\omega$ which can range from 0 to 1. For $\omega = 1$, the modulus is constant, meaning a linear stress-strain relation and as defined by Janbu, an elastic material. Rock, overconsolidated clays, and highly-cemented soils have been found to fall in this category. The other extreme, $\omega = 0$, characterizes normally consolidated clays and means that an arithmetic plot of stress versus strain is exponential. Intermediate values for $\omega$ are for sands and silts which also display non-linear stress-strain behavior but to a lesser degree than the $\omega = 0$ case. Having a functional expression for the modulus, Janbu suggests that settlements be computed by integrating strain over the vertical extent of the deposit. He went one step further and developed a simple one-dimensional vertical stress distribution based on a polynomial decay of vertical stress with depth.

In an attempt to include both the distortional and consolidation settlement components in a unified procedure, Lambe (38) introduced the concept of performing tests in which field boundary stresses are simulated in the laboratory. This procedure presumes that the in situ stresses, acting on a representative specimen can be reconstituted by following stress paths defined by the zero lateral strain condition.

Once in situ stresses have been reconstituted, vertical strains, resulting from stress paths dictated by the ratio of superimposed radial and axial stresses from elastic theory, are used to evaluate settlement. The triaxial apparatus is used to perform these stress path tests, and the superimposed stress ratio requirements, $K = \sigma_r/\sigma_z$, are taken from positions beneath the structure and on an axis of symmetry such that theoretical boundary stresses correspond to the principal stress conditions of the test. This means settlement predictions are keyed to specimen performance subjected to boundary conditions representing a small fraction of the soil supporting the structure.

Figure 8 is a schematic p-q representation of a stress path settlement analysis where the principal stresses in the test correspond to the vertical and horizontal orientations of the specimen relative to field orientation. $K_o$ represents the ratio of $\sigma_3/\sigma_1$ developed when $\varepsilon_3$ is maintained at zero. The line labeled $K_o$ is the stress path representation of such a test which is very difficult to perform in a triaxial apparatus. Thus, Lambe and Whitman (41) suggest that in situ stress conditions be determined from the following empirical relations for at-rest earth pressure

$$K_o = 1 - \sin \phi \qquad \text{cf. Jaky (34)} \qquad (35)$$

$$K_o = 0.95 - \sin \phi \qquad \text{cf. Brooker and Ireland (6)} \qquad (36)$$

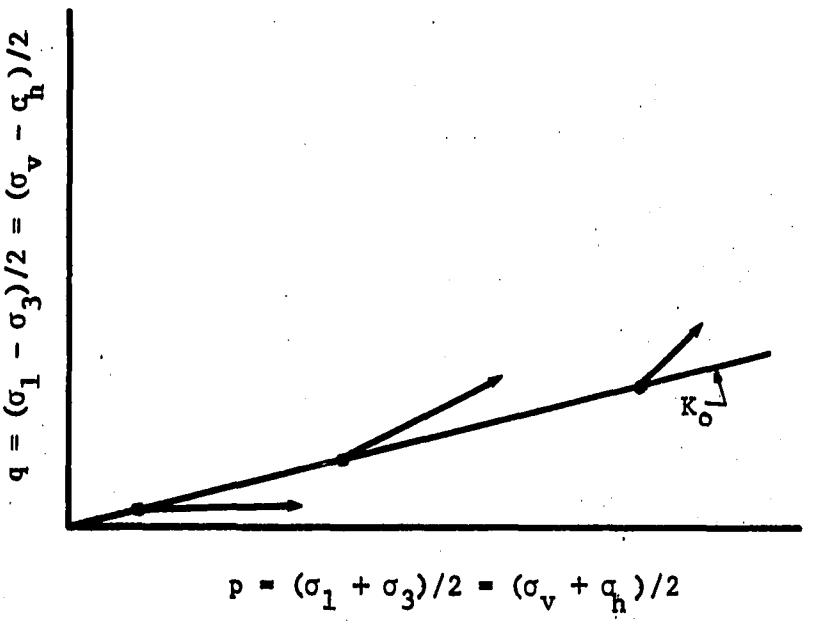


Figure 8. Typical stress path settlement analysis

Equation 35 is for cohesionless soil while equation 36 represents at-rest conditions for cohesive materials.

Equations 30 and 31 are the elastic solutions frequently used to define the stress ratio conditions for the settlement phase of the test. This phase is represented by vectors originating at the $K_o$ stress path in Figure 8. Since the superimposed stress ratio, $K = \sigma_3/\sigma_1$, is a function of position or z, an infinite number of boundary stress conditions is possible, approximated in the stress path method by several tests. Settlements are computed by summing deformations occurring at several points within a deposit. To circumvent the

multiple test requirement, Lambe (39) suggests using an average element selected from a position such that settlement from this single element is equivalent to that produced by the multi-element analysis. Location of the average element was determined experimentally as being located at a depth 1.5 times the radius. Evidently Lambe does not consider this position critical, because in applications presented in references 38, 39, and 41, the average element was selected at a single radius depth.

Lambe and Marr (40) contend that either initial or total settlement can be evaluated with the stress path method by controlling the drainage. For initial settlements, the test would be performed rapidly and without drainage. However, from a practical view, it seems the time required to run tests simulating the pore pressure dissipation of consolidation could be phenomenal. Pore pressure dissipation for the thin oedometer specimens of some soils takes days. According to Terzaghi's theory, pore pressure dissipation varies with the square of the distance to a free drainage surface (58). Achieving zero pore pressure in the longer triaxial specimens should increase the test time by a factor of five or more. Even in its most convenient form where initial settlements are evaluated by rapid, undrained loading, the stress-path test is still rather time-consuming and requires a degree of operational sophistication which is not frequently available in working laboratories. In the author's experience, it takes 3-4 hours to run a single test, during which time, continual computations and cell pressure adjustments

must be made to maintain the appropriate stresses.

Another disadvantage of the procedure is in the fact that $\phi$, $\nu$, and the footing dimensions should be known prior to performing a stress path analysis. Measuring $\phi$ so $K_o$ can be defined is itself an expensive process. $\nu$ is seldom measured and is usually estimated at 0.5, and the footing size often is the objective rather than a starting point of the investigation.

One factor consistent with all of the available prediction methods is that they are to some degree inconsistent with theory and at best represent approximations of the actual phenomenon. A straightforward methodology for assessing the value of these approximations is to compare predictions with prototype performance, and to this end the literature abounds with seemingly contradictory results from case studies involving the more common prediction techniques. In view of the potential for soil variability, it is not unreasonable to expect that isolated evaluations will produce contradictory results, which say little or nothing about the mechanistic validity of the method. However, when viewed as a whole, a pattern might emerge.

One way of assessing the validity of settlement predictions and the associated variability is to consider several prediction attempts and treat the error or difference between observed and predicted settlements as a statistic. If the phenomena underlying settlement parameter variability are described in sum by a normal distribution, the process of predicting settlements should also be described by the

same function. Also, if the prediction technique or theory is valid, the mean of the normal frequency distribution of errors should be zero. One statistical technique for detecting normalcy is through use of "rankit" plots (55). The basic idea comes from the notion that when taking a sample from a normal distribution and ranking the observations from smallest to largest, there will be certain values which, on the average, one would expect each of the ranked observations to attain. Thus, "rankits" are defined as the expected values of $n$ ordered observations for a random sample of size $n$ from a standardized normal population. If the sample in fact comes from a normal population, a plot of the variable versus "rankits" is a straight line. The mean is defined by the value of the variable at the intersection of the straight line, and the zero rankit and standard deviation is defined by the slope of the line. In essence, rankit plots accomplished the same thing as a probability plot but are more suited to computer analysis.

Figure 9 is a rankit plot for error observed in 46 attempts at predicting settlement using Terzaghi's consolidation theory for soil deposits occurring in Europe and the United States. Prediction error, defined as the difference between observed and estimated settlements, divided by the observed settlement, was computed such that negative values indicate that the test under-predicts true settlement. The data were taken from five sources and represent predictions in both normally and overly consolidated saturated clays. The linearity is evidence that settlement prediction error is a random process described

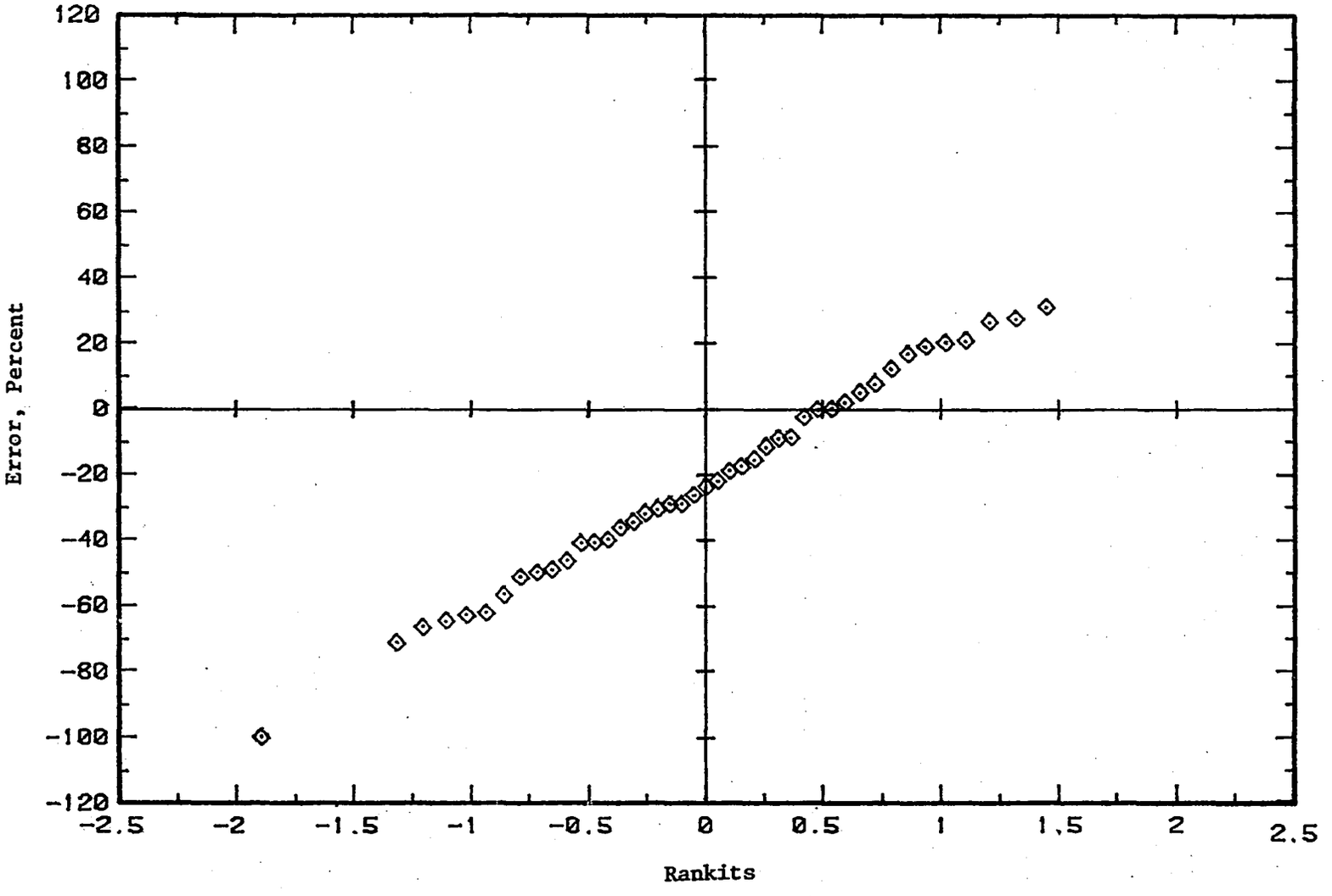


Figure 9. Analysis of settlement predictions by consolidation theory

by the Gaussian probability distribution function.

Table 4 is a summary of similar analyses performed where adequate data was available on other prediction techniques. An indication of normality is expressed in the correlation coefficient, R, from the regression of error on "rankits". On the average, the conventional consolidation theory underpredicts settlement by about 22 percent. This is consistent with the logic that the settlements resulting from distortion are not included in the oedometer analysis, and that sample disturbance does to some unknown degree tend to reduce the compression index. Although Janbu's method also involves the oedometer, a series of 17 predictions indicate a 8.9 percent overprediction on cohesionless soils. This positive error might be the result of Janbu's modified stress distribution or systematic error introduced in reconstituting the cohesionless specimens to field conditions. This can be done on the basis of void ratio or relative density but the field values are seldom known. Janbu (35) was not clear about how this was accomplished.

The value of empirical methods for estimating initial settlement with modified parameters and elastic theory is demonstrated in case III in Table 4 by a series of case studies on materials occurring near London. Here the factor in equation 32 was taken as 140 and the resulting mean prediction error was very close to zero. On the other hand, case IV illustrates the danger of empiricism. The case III calibration was used, but for heavily overconsolidated soils, located in Canada. The result was to increase the prediction error to nearly 27 percent.

Table 4. Analysis of settlement predictions

| Case | Analysis | n [a] | Mean Prediction Error, % | Standard Deviation % | Error Range % | R [b] | Soil Type | References |
|---|---|---|---|---|---|---|---|---|
| I | Terzaghi One-dimensional consolidation | 46 | -22.4 | 54.8 | -100 to 57 | 0.99 | Normally and overly consolidated cohesive | 2, 11, 14, 49, 54 |
| II | Janbu Tangent Modulus | 17 | 8.9 | 16.0 | -11 to 44 | 0.97 | Cohesionless | 35 |
| III | Empirical Elastic Theory for Initial Settlement | 27 | 5.0 | 17.9 | -40 to 40 | 0.98 | Cohesive over-consolidated | 7 |
| IV | Empirical Elastic Theory for Initial Settlements | 6 | 26.6 | 26.4 | -7 to 72 | 0.94 | Cohesive/ Highly Over-consolidated Glacial Deposits | 7 |

[a] n = number of prediction attempts.

[b] R = correlation coefficient.

An attempt was made to include Lambe's stress path technique in this analysis; however, data were available for only one field evaluation. Moore and Spencer (47) report that the stress path method underpredicted settlement by 54 percent. However, in view of the influence of soil variability, this error does not mean very much nor does it represent a fair evaluation. This single example could easily be from the fringe of the distribution. The fact that very few field evaluations have been reported using a prediction technique which has been available for over 17 years, may speak to the practicality of the approach. Incidentally, Lambe's work involved no field evaluations.

This analysis serves to illustrate some of the difficulties encountered in assessing the accuracy of prediction methods. In contrast to bearing capacity theory, where some degree of validation has been realized through carefully controlled model studies, the assessment of settlement prediction techniques has been left to happenstance and subject to the whims of material variability. Since much settlement prediction involves cohesive soils, the indication that consolidation theory underpredicts settlements by an appreciable amount is adequate justification for improving the test. However, if the improvement results in procedures so demanding that they cannot be applied, little is gained.

## Reliability Analysis

From the information thus far presented, it may be assessed that soil variability is a dominant factor in settlement predictions and

should be equally important to ultimate strength evaluation. If the problem of material variability is to be solved by providing better knowledge through improved tests and prediction methods, a systematic means of incorporating such information in design would be useful. In other engineering fields, variability has been included in the design process through a methodology called reliability analysis.

Reliability analysis had its beginnings in the aircraft industry during the early 1940s, and a few years later was introduced into structural engineering by Freudenthal (23). In concept, reliability analysis is quite simple. It involves measuring uncertainties associated with strengths and loads on structural components by statistical methods, and the evaluation of performance in terms of failure probability. Deterministic design lumps inevitable uncertainties into the rather nebulous domain called engineering experience, common sense, or the safety factor. Reliability analysis offers a more precise scale, amenable to communication and systematic refinement. It also acknowledges the reality that a finite risk is associated with any design.

One impediment to the application of reliability analysis is deciding on acceptable failure probabilities. Even if accurate uncertainty measurements and the consequent reliability assessment are available, a specific failure probability is of little value unless it is associated with a viable target. Where the cost of failure can be stated, schemes such as one proposed by Turkstra (60), where total cost of a structure and failure are optimized, can be used to arrive at an

acceptable probabilistic target. More frequently the consequence of structural failure involves loss of life. Assignment of monetary value to life is exceedingly complex and not considered morally justifiable. Thus the approach used to establish realistic, acceptable failure probabilities in structural engineering has been to use fatality rates, associated with other socially accepted activities, as reference points. Mac Gregor (45) summarizes the decision process which has led to the criterion that structures should be designed so the probability of failure is $10^{-5}$. In fact, this criterion is the design goal in the current American Concrete Institute (ACI) reinforced concrete building code (1, 64). For ease of design, the rather complex reliability analysis has been simplified through the use of partial load and strength factors which when used in conjunction with expected or mean values, produces a probability of material understrength on the order of $10^{-2}$, and a $10^{-3}$ chance of overload.

Although a few excursions into reliability analysis of geotechnical problems are reported in the literature, most end up generating failure probabilities with little being said about their significance. Hoeg and Murarka (29) evaluated a gravity retaining wall, Harr (28) a footing, and both find a safety factor of 3 corresponds to a 1/100 chance of failure. Other than questioning the relatively high risk associated with what is commonly considered to be an adequate safety factor, nothing firm was concluded about these results. Thus, the state-of-the-art in geotechnical design centers about the safety factor for bearing capacity

design and a guess for settlement.

Vesic (63) offers rather detailed guidance for the application of safety factors to ultimate bearing capacity. These suggestions, reproduced in Table 5, indicate that the safety factor depends on the type of structure, the consequence of failure and the thoroughness of soil exploration. Most of the criteria seem reasonable except for dependence of safety factors on soil exploration. Table 5 suggests that the nature of investigation rather than the variability that might be discovered, dictates the safety factor. Also the integer safety factor values surely cannot represent the intergrades of soil variability possible in nature.

Table 5. Minimum safety factors for design of shallow foundations after Vesic (63)

| Category | Typical Structures | Characteristics of the Category | Soil Exploration | |
|---|---|---|---|---|
| | | | Thorough, Complete | Limited |
| A | Railway bridges<br>Warehouses<br>Blast furnaces<br>Hydraulic retaining walls<br>Silos | Maximum design load likely to occur often; consequences of failure disastrous | 3.0 | 4.0 |
| B | Highway bridges<br>Light industrial and public buildings | Maximum design load may occur occasionally, consequences of failure serious | 2.5 | 3.5 |
| C | Apartment and office buildings | Maximum design load unlikely to occur | 2.0 | 3.0 |

Although the safety factor scheme deserves criticism, reliability analysis in its present state of development does not offer a solution. The elements necessary for a reliability analysis include probability frequency distributions for loads and material strength and a target failure probability. Hoeg and Murarka (29) have established distributions for soil loaded by its own weight, but this does not apply to all geotechnical applications. Also, existing soil testing techniques are incapable of defining strength distributions, and probabilistic targets have not been established. It may be possible, however, to improve upon geotechnical reliability analysis simply by using information developed by structural engineers. This idea is particularly valid when viewed from the standpoint that an important aspect of geotechnical engineering is in direct support and should be consistent with requirements for structural design.

Bearing capacity

If the probability frequency distribution for loads, L, and strength, Q, can be established, the chance of failure can be computed by simply determining the area common to both distributions relative to the area of a single distribution. This process is shown graphically in Figure 10. A specific example should illustrate the potential and the problems of using the reliability approach to geotechnical design. Assume that it is desired to transfer average 100 kip column loads of a reinforced concrete building through individual footings to a soil deposit characterized by $\phi$. Tests on specimens taken from five random locations

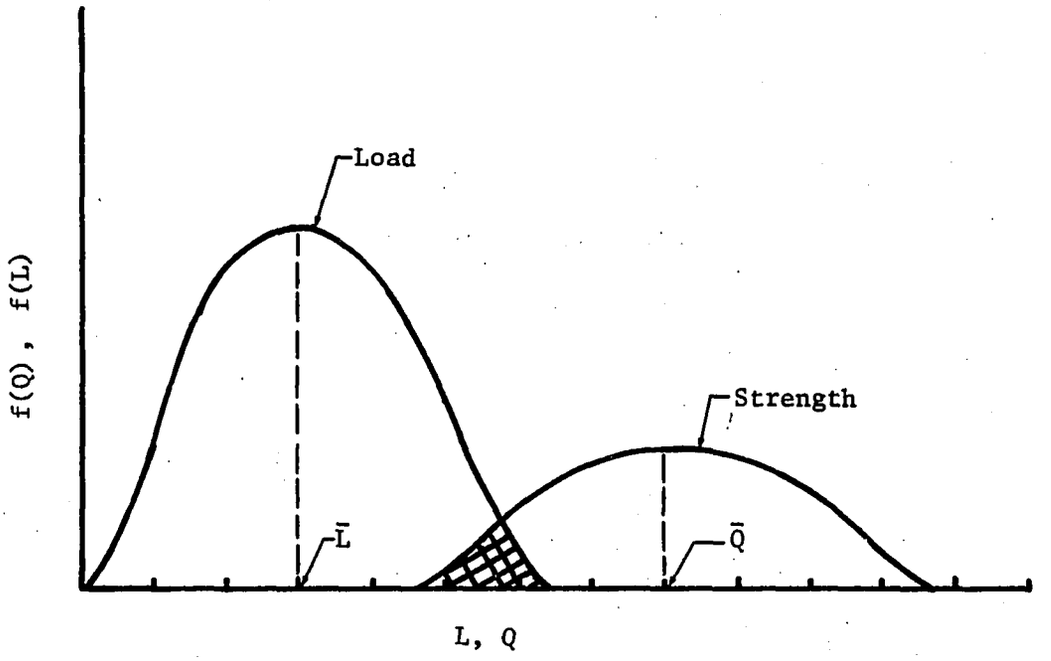


Figure 10. Frequency distributions

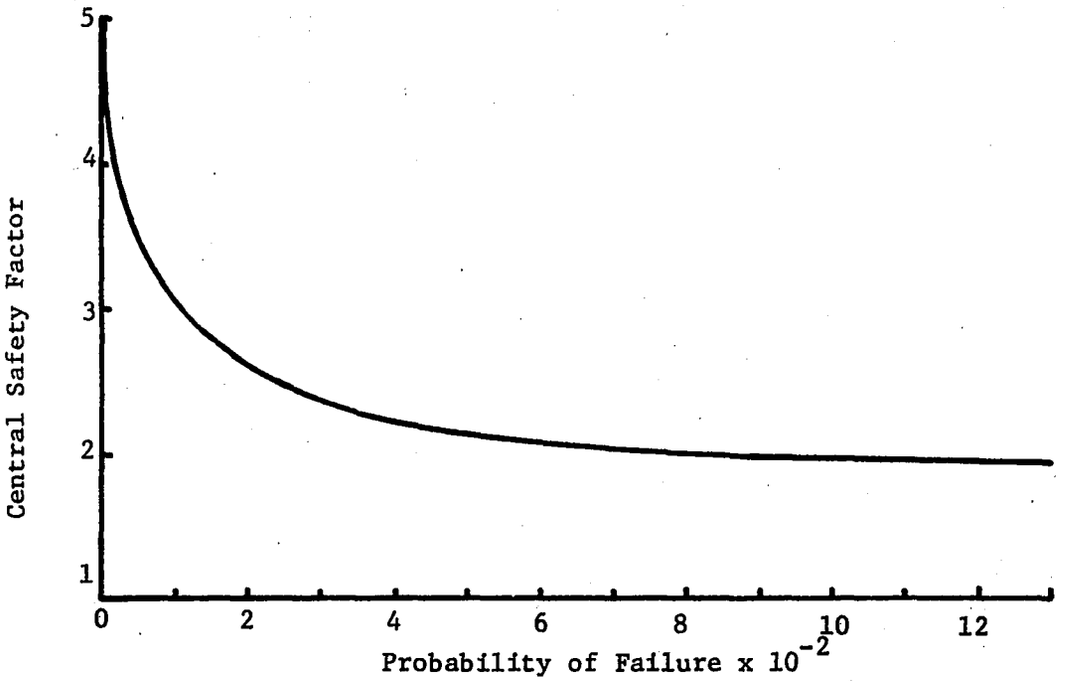


Figure 11. Reliability analysis example

throughout the deposit resulted in friction angles of $\phi_1 = 28°$, $\phi_2 = 30°$, $\phi_3 = 29°$, $\phi_4 = 28°$ and $\phi_5 = 25°$. These are hypothetical data taken from reference 28 and represents a deposit characterized by a mean friction angle of 28° and a coefficient of variation of 7 percent. The bearing capacity relation as given by equations 23 to 29 transform the fundamental soil properties to loads which are consistent with the design requirement. For an 8 foot square footing and 120 pcf soil, the ultimate load for each of the measured friction angles is: $Q_{25} = 201$, $Q_{28} = 313$, $Q_{28} = 313$, $Q_{29} = 360$, and $Q_{30} = 413$ kips. The mean or expected capacity is 322 kips. Next comes the task of selecting and determining parameters for the probability frequency distribution. In past statistical evaluations, the normal or Gaussian distribution has been presumed for soil properties. This is consistent with Lumb's analysis of experimental data (43), but Harr (28) contends that it is physically impossible for material parameters and the consequent strengths to follow the normal distribution. This is because normality requires that observations take on a finite probability of having negative values (i.e. negative strengths and unit weights). While the Gaussian distribution is convenient and may adequately define material variability near the mean, a nonsensical representation could result at the tails of the distribution, and this is the important region for reliability analysis. To overcome objections to the normal distribution, Harr suggests the beta-distribution which imposes bounds on the variate. Substantiation for using the beta-distribution is not overwhelming

because it is based on empirical fits of limited data, and other more convenient distribution forms having as much logical support might be used. Some examples are the log-normal distribution which imposes a lower bound or extreme value distributions, specifically developed to predict the occurrence of large or small quantities (24). An objection to the beta-distribution is that it is a four-parameter model requiring considerable data to define its form.

Since defining the appropriate frequency distribution for soil strength is not the intent of this research, the beta-distribution having the following functional form will be used for this example.

$$f(Q) = \frac{1}{(n-m)B(\lambda + 1, \mu + 1)} \left(\frac{Q - m}{n - m}\right)^{\lambda} \left(\frac{n - Q}{n - m}\right)^{\mu} \qquad (37)$$

cf. Harr (28)

where Q is ultimate load. $\lambda$ and $\mu$ are parameters defining the shape of the distribution, m is the lower limit for the random variable, and n the upper limit. The function B $(\lambda + 1, \mu + 1)$ depends on the gamma function. Details of defining the four parameters for this example are given in Appendix B where the following probability density function is formulated.

$$f(Q) = 2.385 \times 10^{-17} (Q - 82)^3 (562 - Q)^3 \qquad (38)$$

The frequency distribution for loads can be generated from the fact that research supporting the ACI code indicates that live and dead building loads are normal variates (42), conforming to the following design conditions (1).

$$P\ (L_{DL} \geq 1.4\ \bar{L}_{DL}) \leq 0.001 \tag{39}$$

$$P\ (L_{LL} \geq 1.7\ \bar{L}_{LL}) \leq 0.001 \tag{40}$$

where P indicates the probability of the bracketed statement, L is the load variate, $\bar{L}$ is the expected value and the subscripts LL and DL refer to live and dead loads. The factors 1.4 and 1.7 are the design factors used to impose the 1/1000 chance of loads exceeding the mean or nominal design value. Equations 39 and 40 are adequate to define the standard deviation, $S_q$, for the Gaussian frequency distribution given as

$$P\ (L > 0.001) = \int_{\tilde{L}}^{\infty} \frac{1}{S_q \sqrt{2\pi}}\, e^{-(L - \bar{L})^2/2S_q^2}\, dL \tag{41}$$

where the lower limit on the integration, $\tilde{L}$, defines a value for which the probability condition is met. To allow use of probability tables, equation 41 can be normalized with the transformation

$$Z = \frac{L - \bar{L}}{S_q} \tag{42}$$

which leads to

$$P\ (Z \geq 0.001) = \int_{\tilde{Z}}^{\infty} \frac{1}{\sqrt{2\pi}} e^{-Z^2/2}\, dZ \qquad (43)$$

From normalized Gaussian probability tables (8), $\tilde{Z} = 3.09$ results in the 1/1000 chance that the variate will be exceeded. Thus the standard deviation for frequency distributions consistent with equations 39 and 40 can be determined from equation 42, and the following relations can be established

$$S_{qDL} = \frac{1.4\ \bar{L}_{DL} - \bar{L}_{DL}}{\tilde{Z}} = \frac{0.4\ \bar{L}_{DL}}{3.09} \qquad (44)$$

$$S_{qLL} = \frac{1.7\ \bar{L}_{LL} - \bar{L}_{LL}}{\tilde{Z}} = \frac{0.7\ \bar{L}_{LL}}{3.09} \qquad (45)$$

Because live and dead loads are additive and occur simultaneously, a combined probability frequency distribution is required. Fundamental relations for expected values and variance can be used to establish the parameters for the desired frequency distribution. These relations are

$$E_x\ (L_{DL} + L_{LL}) = E_x\ (L_{DL}) + E_x\ (L_{LL}) \quad \text{cf. Chatfield (8)} \qquad (46)$$

$$V_{ar}\ (L_{DL} + L_{LL}) = V_{ar}\ (L_{DL}) + V_{ar}\ (L_{LL}) \tag{47}$$

cf. Chatfield (8)

where $E_x$ signifies the expected or mean value of the variate and $V_{ar}$, the variance or squared standard deviation.

For this example, the total expected load, $\bar{L}$, is 100 kips and if the dead load is equal to the live load, standard deviations for the individual distributions are

$$S_{qDL} = \frac{(50)(0.4)}{3.09} = 6.47 \tag{48}$$

$$S_{qLL} = \frac{(50)(0.7)}{3.09} = 11.32 \tag{49}$$

and for the combined distribution the definitive parameters are

$$E_x\ (L_{DL} + L_{LL}) = 100 \text{ kips} \tag{50}$$

$$S_q\ (L_{DL} + L_{LL}) = ((6.47)^2 + (11.32)^2)^{1/2} = 13.04 \text{ kips} \tag{51}$$

and the resulting frequency distribution is

$$f(L) = 0.159\ e^{-(L - 100)^2/340} \tag{52}$$

With both load and strength distributions defined, the final step in the reliability analysis is to compute the area common to both frequency distributions. A preferred technique is mathematical integration but numerical integration is easier. In this case, the intersection of the load and strength curves was determined graphically, and the area was computed using the Romberg numerical integration scheme pre-programmed for a Texas Instruments, TI 59 calculator. For the 100 kip nominal load, the probability of failure is $9 \times 10^{-3}$. For comparative purposes, a device known as the central safety factor (CSF), defined as the ratio of the mean load and strength can be used. In this case CSF is 3.22. By assuming different nominal loads and maintaining constant soil variability, a relation between CSF and failure probability was developed. The results are shown in Figure 11 and Table 6.

If the structure is indeterminate and senses a single bearing capacity failure as an overload, the targeted 1/1000 chance of this occurring corresponds to a CSF of 4, a rather inflated value when compared to the standards established by Vesic in Table 5. In fact, the type of construction covered by the ACI code probably corresponds best to Vesic's category B which suggests safety factors ranging from 2.5 to 3.5. However, it should be recognized that the normal design safety factor and the CSF from the statistical analysis are not necessarily the same. Consider a situation where information from a complete, thorough soil investigation or all of the strength data is made available

to a prudent engineer. Under such circumstances, use of the most conservative bearing capacity, along with Vesic's suggestion for a 2.5 safety factor leads to a design load of 80.4 kips. As Figure 11 or Table 6 indicates, this results in a failure probability consistent with the ACI goal of 1/1000 and corresponds to a CSF of 4. Conversely,

Table 6. CSF and failure probability

| CSF | Failure Probability x $10^{-3}$ | $\bar{L}$ (kips) |
|---|---|---|
| 5.0 | 0.083 | 64.4 |
| 4.5 | 0.306 | 71.6 |
| 4.0 | 1.080 | 80.5 |
| 3.5 | 3.490 | 92.0 |
| 3.0 | 10.700 | 107.3 |
| 2.5 | 24.500 | 128.8 |
| 2.0 | 94.600 | 161.0 |
| 1.0 | 668.200 | 322.0 |

consider what is probably the more common event where the engineer has access to a single soil strength parameter. A limited soil exploration would dictate a safety factor of 3.5, and the result could be any one of the outcomes listed in Table 7. Two designs are consistent with the expectations of the structural engineer and one represents excessive overdesign. Greater significance may be in the fact that according to this analysis, risky designs could be the result of forty percent of the time.

This example illustrates a logical format by which design goals can be established. Also, for the data used, the reliability analysis is quite consistent with current practice in the event that a complete suite of data is available. In essence, a poorly defined, undetermined form of statistical analysis is performed by using worst-case conditions. It seems that a better design method would include a more concise measure and treatment of variability. For the bearing capacity problem applied to building foundations, load frequency distributions and a design target have been established. Practical difficulties in applying such a methodology come from definition of soil variability.

Table 7. Failure probabilities using a conventional safety factor of 3.5

| $Q_u$ kips | I (kips) | CSF | Probability of Failure |
|---|---|---|---|
| 201 | 57.4 | 75 | 1/100,000 |
| 313 | 89.4 | 4.0 | 1/1000 |
| 313 | 89.4 | 4.0 | 1/1000 |
| 369 | 105.4 | 3.0 | 1/100 |
| 413 | 118.0 | 2.75 | 1.6/100 |

Settlement

Two independent surveys of rather significant structures conducted by Bjerrum (4) and Skempton and Mac Donald (57) revealed that of 193 buildings evaluated, 100 suffered some degree of damage associated with

differential settlement. This 50 percent chance of damage resulting from settlement suggests that improvement in current design practice is certainly warranted, and the cause could well be the inability to statistically evaluate a given problem.

Unlike the bearing capacity problem, settlement damage does not usually involve loss of life, and the consequences are frequently serviceability factors such as machinery alignment, cracked walls or partitions, and function of doors and windows. Standards for current design practice are based on building surveys such as the ones previously mentioned with a widely used source being taken from the U.S.S.R. Building Code. Portions of this code are presented in Table 8. In geotechnical design, settlements are usually thought of in terms of total and differential settlements where the former represents the least demanding design goal and is governed by such factors as drainage and utility access. In Table 8, it can be seen that structures can tolerate total settlements of up to 12 inches. For differential settlements, which are more difficult to evaluate, the toleration limit can be fractions of an inch. For example, the defection ratio, $\delta/l$, for a reinforced concrete building is 0.002. If column loads for such a building were supported by independent footings spaced at 20 foot intervals, the tolerable differential settlement would be slightly less than one half inch. Meeting such a design goal means not only an accurate prediction method but one which can account for the chance of poor predictions by virtue of material variability.

Table 8. Allowable settlement criteria: 1955 U.S.S.R. Building Code (after Polshin and Tokar (51))

| Type of Structure | Average Settlement, in. | Angular Distortion $\delta/\ell$ [a, b] |
|---|---|---|
| Allowable Total Settlement | | |
| Building with plain brick walls | | |
| $\ell/h$ [c] $\geq 2.5$ | 3 | |
| $\ell/h \leq 1.5$ | 4 | |
| Building with brick walls, reinforced with reinforced concrete or reinforced brick | 6 | |
| Framed building | 4 | |
| Solid reinforced concrete foundations of smokestacks, silos, towers, etc. | 12 | |
| Allowable Differential Settlement | | |
| Civil and industrial building column foundations: | | |
| a. For steel and reinforced concrete structures | | 0.002 |
| b. For end rows of columns with brick cladding | | 0.001 |
| c. For structures where auxillary strain does not arise during nonuniform settlement of foundations | | 0.005 |
| Tilt of smokestacks, towers, silos, etc. | | 0.004 |
| Craneways | | 0.003 |

[a] $\delta$ = differential settlement between two points.

[b] $\ell$ = distance between adjacent columns or two reference points.

[c] $h$ = height of building.

One scheme proposed to assess the uncertainty of total settlement predictions was proposed by Corotis, Krizek, and El-Moussi (10). Results of more than 700 consolidation tests on alluvial, marine, aeolian, and residual soils were used as a data base for correlation of variability in compression indices to dry density. Gaussian distributions of the compression index and loads were assumed, and using the method of derived distributions a log-normal frequency distribution for settlements was developed. Application of this scheme presumes that pertinent statistical characteristics of specific deposits can be determined from average dry density, and the method results in a statement about the chance of realizing settlements in excess of a specific amount. This technique has the advantage of keying easily measured properties to parameters which would be difficult to measure in sufficient quantity to define variability of specific deposits. A criticism is the validity of indexing seemingly unrelated properties, and perhaps of more importance is the value of the result. Being able to state the probability of realizing settlements in excess of a specific value is superfluous, unless a realistic design goal can be defined. Furthermore, this approach does not address differential settlement which may be the more important design factor.

A partial solution to defining a probabilistic design target might be possible by considering observations of structures near failure, because of differential settlement. Bjerrum (4) found that settlement ratios exceeding 0.007 occurred for buildings at impending failure.

If a frequency distribution using deflection ratio as the random variable were available, a design goal consistent with ACI code would be allowable footing stresses producing 1/1000 chance of achieving $\delta/l = 0.007$. This implies that structural integrity is due to overloads induced in an indeterminate structure through the mechanism of differential settlement. Deflection ratio distributions could be generated by dividing differences in settlements predicted at different locations on a building site by separation distance for all permutations of the available data. Obviously, this process will generate a symmetric probability density function because each deflection ratio or slope will take either a positive or negative sense depending upon which test location is taken as reference. This has not been done because the data supporting such an analysis cannot be developed by conventional test and prediction methods.

Sample and test requirements

Including the influence of soil variability in design, either through reliability analysis or the less systematic approach of designing with conservative results from a series of experiments, means repetitious testing. The amount of testing required to define the statistical character of a soil deposit also depends on variability, the importance of which can be demonstrated by a simple statistical relation. The number of samples, n, required to estimate the mean of a population can be computed from the equation,

$$n = \frac{Z^2 S^2}{L^2} \qquad \text{cf. Chatfield (8)} \qquad (53)$$

where S = standard deviation, L = interval defining precision of the estimate, and Z is a statistical parameter stipulating the form the parent probability distribution and the likelihood that the true mean will be contained in the interval L. For a 90 percent chance that the interval L contains the population mean from a Gaussian distribution, Z = 1.65. A priori information is required about population standard deviation before equation 53 can be used. However, if S can be estimated from experience, the relation can be a useful starting point.

To provide a feeling for sampling requirements in soil deposits, Table 9 contains a summary of sample size estimates for extremes in variability represented by the statistical data from Tables 1 and 2. Precision intervals were somewhat arbitrarily selected and are thought to represent laboratory precision or design significance. If the data in Tables 1 and 2 are a true representation of soil variation, Table 9 suggests that the number of samples and tests needed for definition of variation by conventional practice and methodology would in many cases be out of the question. For example, definition of friction angle for the least variable of deposits requires eleven independent measurements which at a minimum should mean 33 specimens tested to failure by conventional techniques. The requirement for 9 unconfined compression tests is reasonable, but the results may in some materials inadequately define parameters demanded by prediction theories. Except for

exceptionally large projects or statistical research, results from 31 to 111 consolidation tests is probably a dream.

Table 9. Sampling requirements

| Parameter | C.V. % | S | L | n | Variability |
|---|---|---|---|---|---|
| Friction angle | 5.3 | 1.97° | 1° | 11 | Low |
| | 11.0 | 4.56° | 1° | 57 | High |
| Unconfined Compression Strength | 29.0 | 3.6 psi | 2 psi | 9 | Low |
| | 49.1 | 14.2 psi | 2 psi | 137 | High |
| Settlements | 25.7 | 1.7 in. | .5 in. | 31 | Low |
| | 48.5 | 3.2 in. | .5 in. | 111 | High |

## Iowa K-Test

As a means of inexpensively obtaining mechanical soil properties, Handy and Hoover (25) proposed an alternative laboratory apparatus. Known as the Iowa K-Test, this device consists of a split steel mold into which a Proctor specimen is inserted and loaded along its axis through a pair of discs. When the specimen has expanded sufficiently to contact the inside walls of the mold, shown in Figure 12, radial stresses are developed by the reaction of the mold. The radial stress magnitude can be evaluated from measurements of mold expansion through a calibration between radial stress and mold deformation. A later development is the commercially produced apparatus shown in Figure 13.

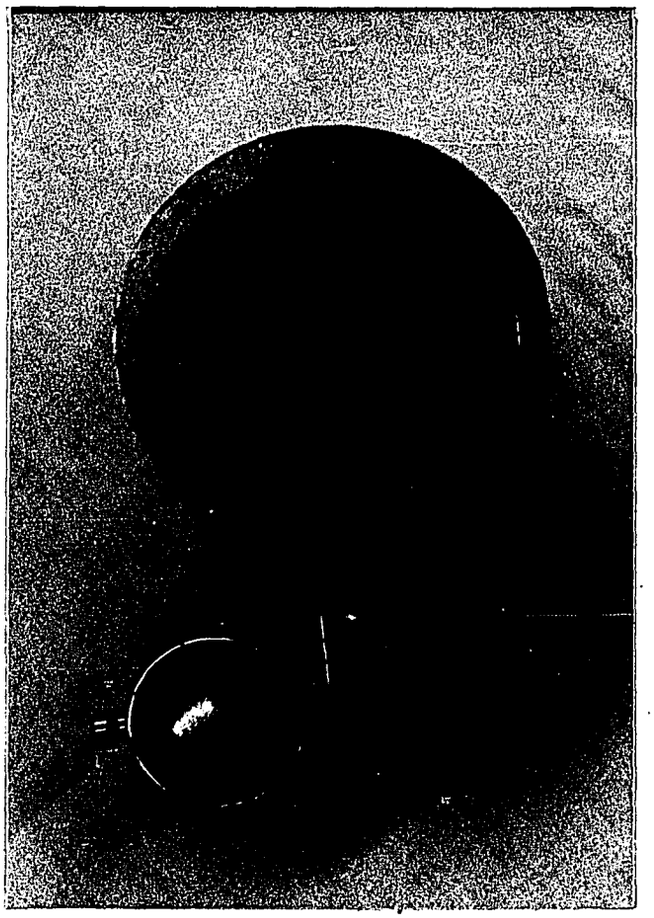

Figure 12. Early version of Iowa K-Test

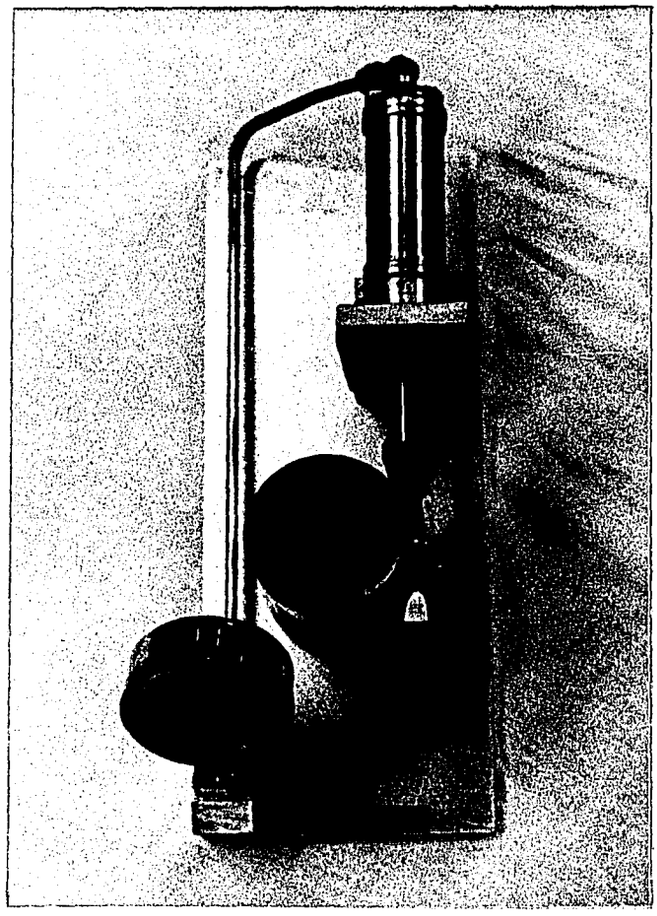

Figure 13. Commercial version of Iowa K-Test

This apparatus is comprised of a split, thin-walled mold, restrained by a closed hydraulic system. Radial stress is measured from a calibration to hydraulic pressure, and the operator also has the option of controlling radial stress with a pump connected to the hydraulic system.

A desirable feature of the K-Test is its automatic, continuous increase in radial stress during axial loading. Set-up and test time are roughly equivalent to that required for unconfined compression testing, the apparatus is relatively inexpensive. Since no stress control is required during a test, technicians can be easily trained.

One interpretation of results from the Iowa K-Test is based on the concept that radial and axial stresses measured during the test approximate principal stress components and define ultimate strength according to the Mohr-Coulomb failure criterion (26). Lutenegger (44) reports c and $\phi$ parameters derived from K-Test results for several soils, many of which seem reasonable. However, an exception is the persistent measurement of significant negative cohesion for sands and natural loess. Lutenegger (44) also reports results of a comparative analysis between K-Test and conventional triaxial results on a natural glacial till where the K-Test produced excessive measures of both c and $\phi$. This comparison is of questionable significance because few tests were performed on specimens taken from different locations. Although the nature of the parameters defined by the K-Test is not clearly defined, Hoover and Handy (31) have demonstrated that the test does

have capacity of providing logical differentiations in strength parameters with respect to variation in moisture content and unit weight of laboratory compacted specimens.

Boundary friction, present on all surfaces rather than just the ends as with the triaxial apparatus, is an objection of the K-Test. Handy, Lutenegger, and Hoover (26) proposed a correction technique based on measurements from a hydraulic load cell used in place of the bottom loading disc. With vertical support at the bottom of the mold, and both the load cell piston and top loading disc free, a soil-to-steel mold friction component occurring on the sides of the specimen was measured during the test. Knowing the normal stress and assuming an average shear occurring throughout the specimen, the failure envelope was graphically adjusted using Mohr-circles. Such adjustments tend to reduce $\phi$ and increase c but validity of this correction was not verified.

One question arising from the K-Test results is the influence of the amount of restraint on the results. The models thus far developed represent extremes in mold stiffness, and Lutenegger (44) reports the softer, thin-walled mold tends to produce higher friction angles and lower cohesion than the stiff mold. In fact, the negative cohesions reported by Lutenegger occurred most frequently with tests performed using the thin-walled, hydraulic apparatus.

Another factor considered in reference 26 is the significance of vertical deformation moduli measured during the conduct of the test. For the soils tested, axial stress-strain plots were very linear and

did not reach limiting strength. Both observations are inconsistent with data usually obtained from conventional triaxial tests.

The idea of testing geotechnical materials under conditions where radial deformation dictates the magnitude of stresses in that particular direction did not originate with the Iowa K-Test. Hveem and Davis (32) report that as early as 1932, the California Department of Transportation tested flexible pavement materials, including soils, using apparatus made from thin steel tubing split lengthwise along one side. The split was reinforced with springs and measurements identical to those for the K-Test were made. This apparatus has since evolved into the now standard Hveem Stabilometer, a device in which reactions to radial deformation are produced by closed hydraulics acting on the specimen through a rubber membrane. Early attempts to analyze Stabilometer data involved definition of the strength parameters c and $\phi$, but this was criticized on theoretical grounds and present application is through empirical correlation (32).

# DEFORMATION RESTRAINT THEORY

Because of its potential for providing a rapid measure of soil properties, the deformation restraint (DR) test seems a likely candidate for solving at least some of the problems associated with soil variability and prediction accuracy. Potential applicability of the test might be viewed from two perspectives. By analogy to staged triaxial testing, the DR test could represent a convenient method for determining ultimate shear strength parameters. Alternatively, it could also represent an improvement to settlement prediction accuracy in that radial deformation occurring in a DR test may represent distortion shown to be a partial cause of underpredictions with the oedometer. Based on the review and analysis of the literature, there is a definite need for both applications of the DR test.

The work done thus far with DR testing has been exploratory in nature, and little attention has been given to what may be a very important aspect of the test; specifically, the influence of the degree of restraint on the resulting parameters. Lutenegger's work suggests it does make a difference on ultimate strength parameters. In terms of settlement predictions, a hint might be taken from Lambe's stress path method, where radial stress is increased as a function of axial stress. If radial strain were measured, a radial stress-strain relation would exist as with the DR test. However, an important, but unknown factor, is whether arbitrarily dictating this restraint by the

properties of an apparatus is adequate. Evaluation of this factor shall be attempted through theory and experimentation.

## Restraint Function

Presently, the only thing known about deformation restraint tests is that the radial stress is some function of radial strain. For this analysis it will be presumed that the following linear relation, expressed in terms of axisymmetric principal stress and strain, is appropriate

$$\sigma_3 = -k\,\varepsilon_3 \tag{54}$$

where k is a constant defining stiffness of the apparatus. The negative sign is used to make $\sigma_3$ positive for negative radial expansive strain that occurs during the test. Equation 54 infers that for an unconfined test $k = 0$ since $\sigma_3 = 0$ and $\varepsilon_3 \neq 0$. The other extreme for k represents the constrained or oedometer test because in the limit k approaches infinity as $\varepsilon_3$ approaches zero. Even from this very basic analysis, it might be speculated that deformation response is highly dependent on k. It is known that unconfined and constrained test results are certainly different.

## Restraint and the Elastic Constitutive Law

Since some elements of elastic theory provide relatively good estimates in geotechnical materials, the DR test might offer a means of evaluating parameters consistent with elastic theory. If equation 11 is expanded with stress and strain expressed for the axisymmetric case, expressions for axial and radial strain can be written as

$$\varepsilon_1 = \frac{1}{E} (\sigma_1 - 2\nu\, \sigma_3) \tag{55}$$

$$\varepsilon_3 = \frac{1}{E} ((1 - \nu)\sigma_3 - \nu\sigma_1) \tag{56}$$

Equation 54 solved for $\varepsilon_3$ and substituted in equation 56 results in

$$\sigma_3 = \left(\frac{\nu\, k}{k(1 - \nu) + E}\right) \sigma_1 \tag{57}$$

An expression for axial stress in terms of axial strain can next be obtained by substituting $\sigma_3$ from equation 57, in equation 55, resulting in an axial stress-strain relation for a restrained test

$$\sigma_1 = \left\{\frac{k\ (1 - \nu)\ E + E^2}{k\ (1 - 2\nu)(1 + \nu) + E}\right\} \varepsilon_1 \tag{58}$$

The bracketed term in equation 58 represents an apparent modulus or restrained modulus, $M_r$, dependent on the restraint parameter, k, and elastic constants. This equation can be checked by looking at the limits on k. For k = 0 in equation 58, $M_r = E$ which is consistent with basic definition for E. The other limit, $K = \infty$, results in the indeterminate form, $M_r = \infty/\infty$ and by applying L'Hospital's rule

$$\lim_{k\to\infty} M_r = \lim_{k\to\infty} \left(\frac{k(1 - \nu)E + E^2}{k(1 - 2\nu)(1 + \nu) + E}\right) = \left(\frac{(1 - \nu)}{(1 - 2\nu)(1 + \nu)}\right)E$$

This means for infinite restraint $M_r$ becomes the constrained modulus, $M_c$, defined as

$$M_c = \left(\frac{(1 - \nu)}{(1 - 2\nu)(1 + \nu)}\right) E \qquad (59)$$

The constrained modulus represents the elastic counterpart to the oedometer test.

## Plastic Flow

Mohr-Coulomb theory is not readily adaptable to modeling deformation relations for a material subjected to yield stress components. However, the link between volumetric strain, deviatoric strain, and the failure parameter $\alpha_f$ provided by the Drucker hypothesis in equation 22 could explain the linear deformation results reported by Handy,

Lutenegger, and Hoover (26). Strain invariants in equation 22, expressed in terms of axisymmetric principal strains are

$$\frac{(\varepsilon_1^p - \varepsilon_3^p)/\sqrt{3}}{\varepsilon_1^p + 2\varepsilon_3^p} = -\frac{1}{6\alpha_f} \tag{60}$$

Solving equation 60 for $\varepsilon_3^p$ results in

$$\varepsilon_3^p = \varepsilon_1^p \left\{\frac{6\alpha_f + \sqrt{3}}{6\alpha_f - 2\sqrt{3}}\right\} \tag{61}$$

Drucker-Prager or the extended von Mises failure criterion for axisymmetric principal stresses is

$$(1/\sqrt{3})(\sigma_1 - \sigma_3) = \rho + (\sigma_1 + 2\sigma_3)\alpha_f \tag{62}$$

Solving equation 62 for $\sigma_1$ results in

$$\sigma_1 = \sigma_3 \left\{\frac{1 + 2\sqrt{3}\,\alpha_f}{1 - \sqrt{3}\,\alpha_f}\right\} + \frac{\sqrt{3}\,\rho}{1 - \sqrt{3}\,\alpha_f} \tag{63}$$

Imposing the deformation restraint condition defined by equation 54 on equation 61 and substituting the result in equation 63, results in the following major principal stress-strain relation

$$\sigma_1 = k \left\{ \frac{1 + 2\sqrt{3}k}{1 - \sqrt{3}\,\alpha_f} \right\} \left\{ \frac{6\alpha_f + \sqrt{3}}{2\sqrt{3} - 6\alpha_f} \right\} \varepsilon_3{}^p + \frac{\sqrt{3}\,\rho}{1 - \sqrt{3}\,\alpha_f} \qquad (64)$$

Equation 64 indicates that for material having a linear failure envelope and a constant restraint function, the major principal stress-strain relation occurring under conditions of restrained plastic flow is also linear. The last term in equation 64 represents the stress level for the onset of plastic failure. Further evaluation of equation 64 reveals that the plastic stress-strain relation depends on the volumetric characteristics of the material through the parameter $\alpha_f$. By this model, $\alpha_f > 0$ means the material dilates while for $\alpha_f = 0$ no dilation occurs and equation 64 reduces to

$$\sigma_1 = \frac{k}{2}\ \varepsilon_1{}^p + \sqrt{3}\ \rho \qquad (65)$$

Additionally, no restriction being placed on k means that an infinite number of restraint functions are capable of producing a failure stress path. Each function will, however, produce a unique stress-strain relation. If this model is valid, it infers that $\alpha_f$ can be determined from a deformation restraint test by arbitrarily setting k, and that other stress-strain relations can be predicted for any desired degree of restraint.

Numerous assumptions, not necessarily consistent with the behavior of all soils, were used to develop the deformation relations for

restrained plastic flow. Thus, the validity of such a model should be experimentally verified. If the model works, it could represent a valuable predictive tool. If not, it may serve the useful purpose of raising a pertinent question. If an infinite number of k-dependent major principal stress-strain relations is possible, which one is appropriate for field deformation predictions?

## Restraint Function for Settlement Predictions

Further consideration of Lambe's stress path method reveals that boundary stresses are dependent not only on material properties but also on geometry, as can be seen from equations 30 and 31. Working from elastic solutions, it may be possible to formulate a methodology which defines a restraint function, dependent on the same factors as the stress path technique. For load acting over a circular area, an expression for radial stress occurring beneath the center of the loaded area is given by

$$\sigma_3 = q_s (2 \nu A + C + (1 - 2\nu)F) \quad \text{cf. Poulos and Davis (52)} \quad (66)$$

where $q_s$ = stress at surface, and A, C, and F are geometric parameters dependent on the radius of the loaded area, a, and depth below the surface, z. Equation 66 is nothing but a more manageable form of equation 31, and the parameters A, C, and F can be found in reference 52. The second element necessary to establish restraint function is an

expression for the radial strain. From the same elastic solution this equation is

$$\varepsilon_3 = q_s \frac{1 + \nu}{E} \quad ((1 - 2\nu)F + C) \text{ cf. Poulos and Davis (52)} \quad (67)$$

Solving equation 67 for $q_s$ and substituting the result in equation 66 results in

$$\sigma_3 = \left\{\frac{E}{1 + \nu}\right\} \left\{\frac{(2\nu A + C + (1 - 2\nu)F)}{(1 - 2\nu)F + C}\right\} \varepsilon_3 \quad (68)$$

where the two terms in brackets represent k in equation 54.

Equation 68 could represent a convenient control for a settlement test. Obviously, a priori knowledge about the two elastic parameters E and $\nu$ is necessary. Since both $\nu$ and E for soil are known to be stress dependent, an adequate approximation might be obtained from the elastic constitutive relations and soil response from early phases of a test. Should part of the test sequence involve loading under constrained conditions, $\nu$, can be computed by setting $\varepsilon_3 = 0$ in equation 56 which results in:

$$\nu|_{\varepsilon_3 = 0} = \frac{\sigma_3}{(\sigma_1 + \sigma_3)} \quad (69)$$

An estimate for E can also be made from the results of a constrained

phase if a value can be assessed for constrained modulus. By substituting $\nu$ from equation 69 in equation 59 and solving for E, the following expression in terms of $M_c$ and principal stresses can be written

$$E = M_c \left\{ \frac{(\sigma_1 + 2\sigma_3)(\sigma_1 - \sigma_3)}{\sigma_1 (\sigma_1 + \sigma_3)} \right\} \tag{70}$$

A possible scheme for a deformation restraint test would involve the following:

1. Reconstitute the in situ vertical stress by following the $K_o$ stress path shown schematically in Figure 14a.
2. Upon reaching what is presumed to be initial in situ stress conditions, compute values for $\nu$ and E using equations 69 and 70 respectively. $\nu$ comes from in situ stress conditions while E depends on stresses and the tangent value of $M_c$ taken at point a, Figure 14b.
3. The vertical stress-strain relation of interest can be determined under the restraint conditions defined by equation 68 where it is understood that $\sigma_3$ represents radial stresses imposed on that produced during the $K_o$ loading. The resulting stress path should then be dictated by an estimate of material properties occurring under in situ conditions. Depending on drainage conditions allowed during the test, it might also be possible to evaluate initial or a combination of initial and consolidation settlements

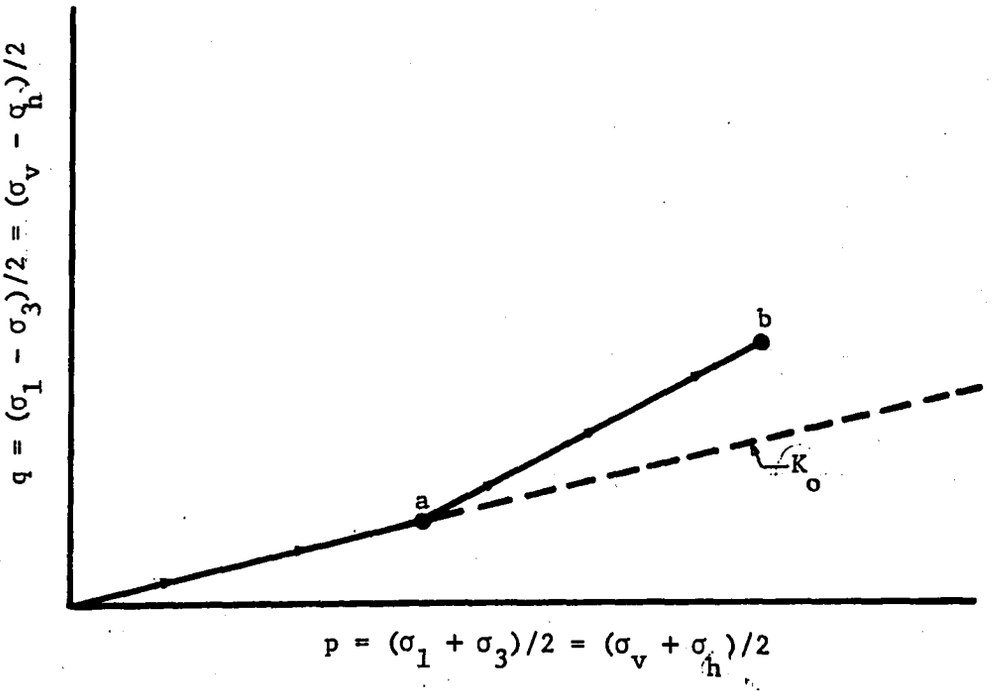


a. Stress path

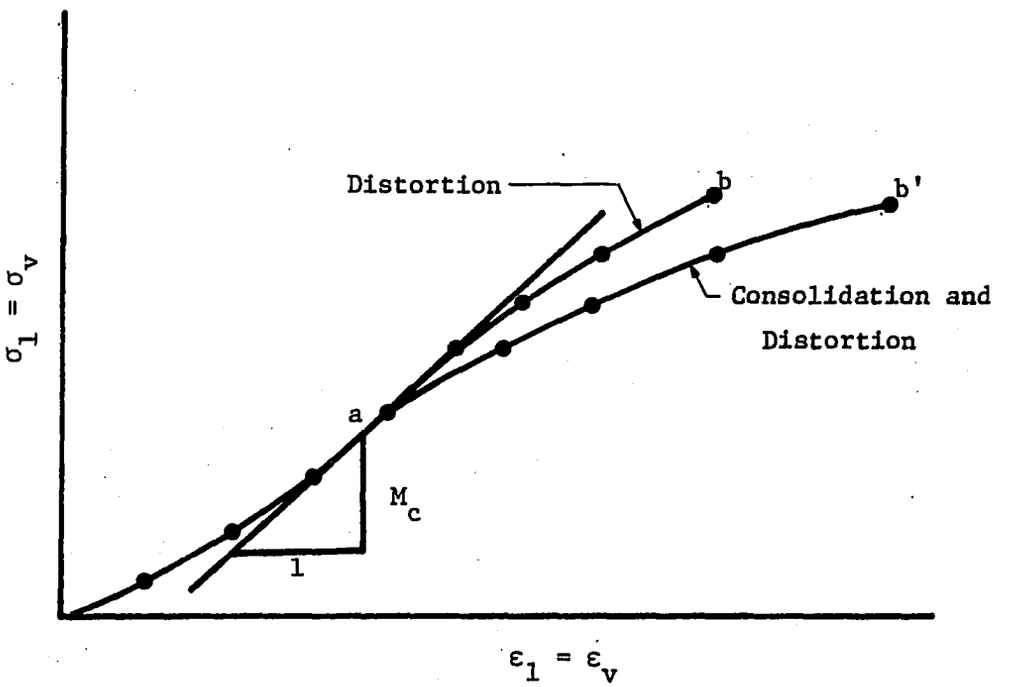


b. Stress-strain

Figure 14. k-path settlement evaluation

as shown by deformation responses ab or ab'.

The same general criticism of using elastic theory to estimate boundary conditions is valid for both the proposed k-path and Lambe's stress path methods. A reason for either technique providing acceptable settlement estimates might lie in the fact that elastic theory is only used to provide an approximation of boundary conditions, while the actual settlement parameters are derived from the inelastic response of the primary element being tested. If the performance of the primary element is somewhat insensitive to its boundary conditions, it may be possible that a precise definition of boundary conditions is not essential. Thus the elastic estimate may be adequate. This rather nebulous concept of boundary condition insensitivity is something that probably cannot be analytically proven but might be experimentally illustrated. Nevertheless, both Lambe's method and the proposed k-path method may in the least offer partial improvement to the underpredictions characteristic of the oedometer or consolidation test.

A closer look at the restraint function given by equation 68 reveals that by elastic theory, the equation 54 definition may not be adequate. Figure 15a shows the distribution of vertical and radial stresses occurring along the axis of symmetry for the circular load area. Since $\sigma_1$ is independent of material properties, a single curve describes the distribution. $\sigma_3$ depends on $\nu$, thus a sizable range of radial stress distributions is possible. In terms of the sign convention, both $\sigma_1$ and $\sigma_3$ are always positive, and at different positions beneath the

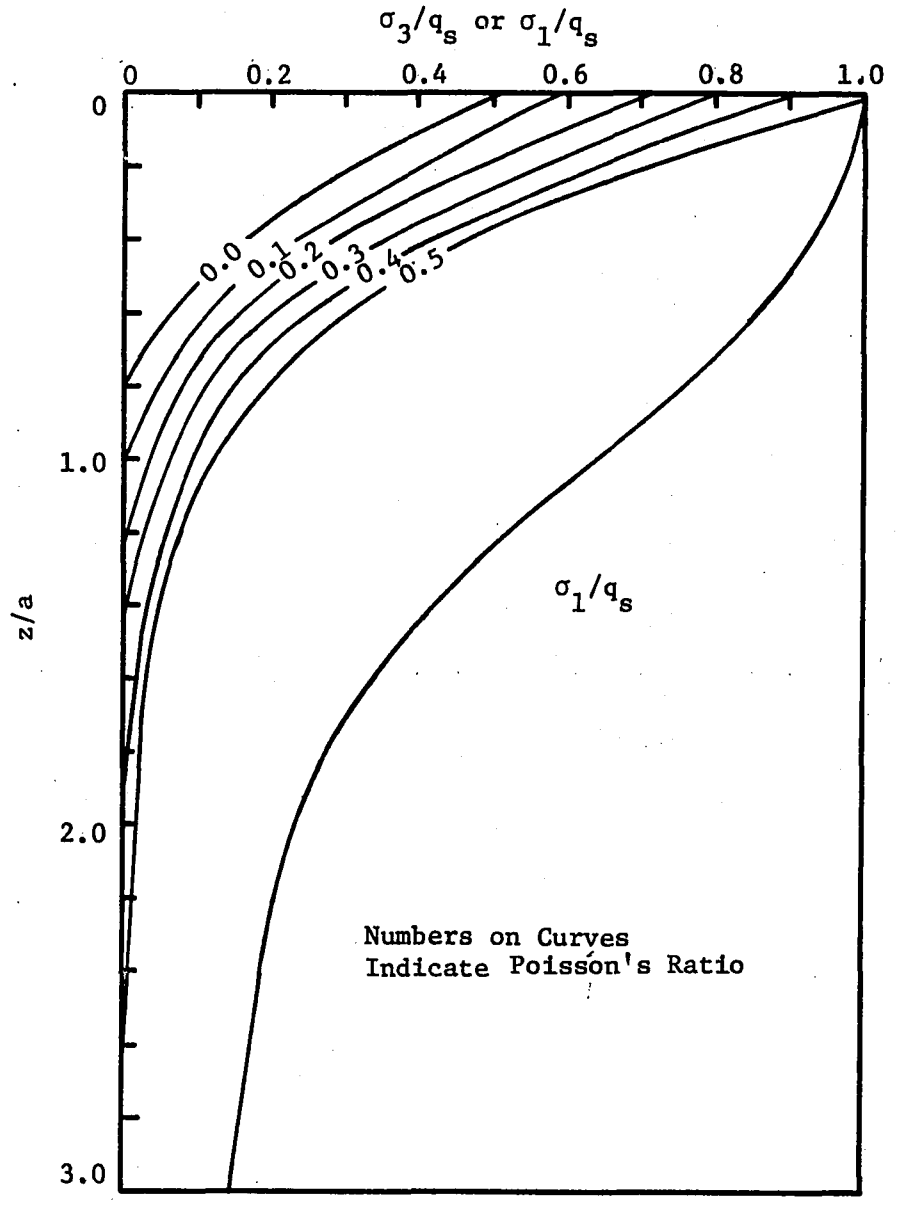


Figure 15a. Elastic stress distribution for a circular footing

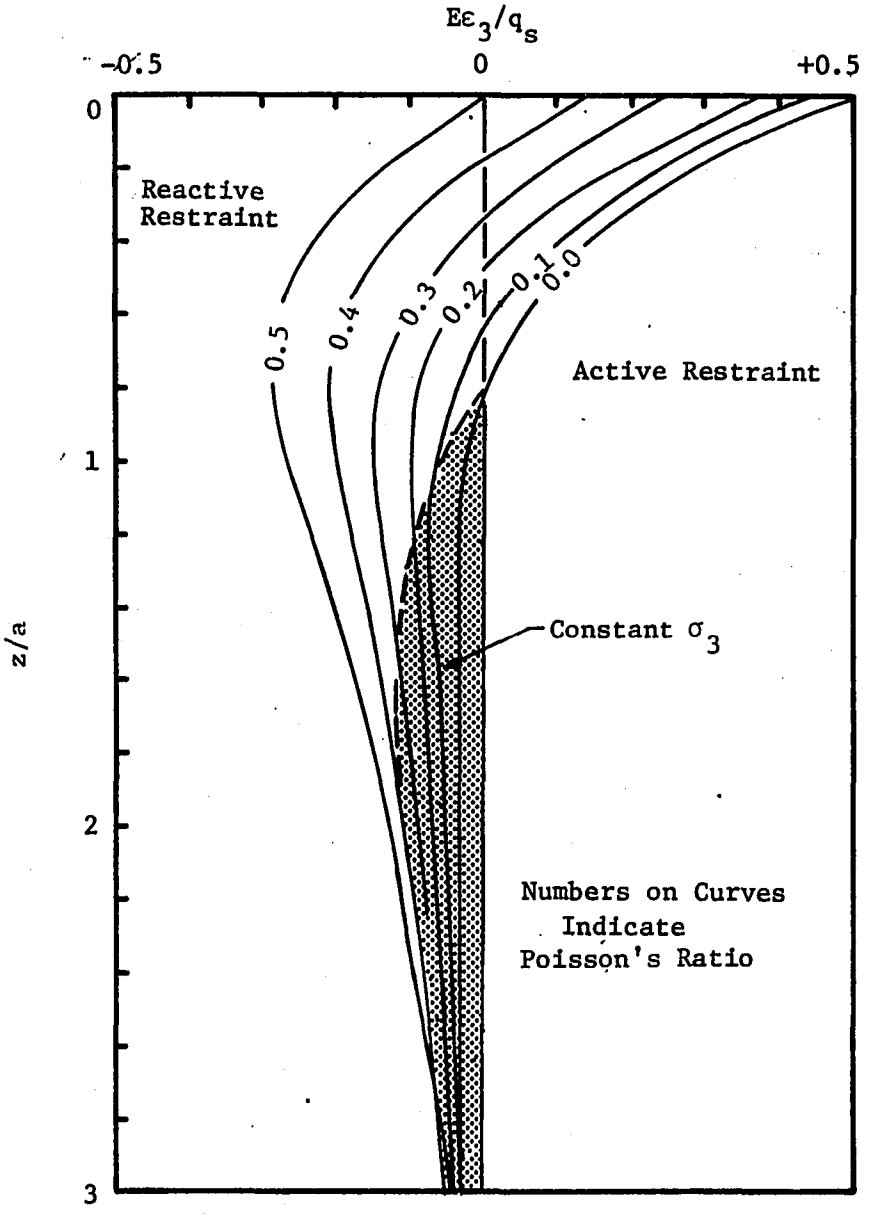


Figure 15b. Elastic strain distribution for a circular footing

footing $\sigma_3 = 0$. This means for stress path control the superimposed radial stress is zero or the test is conducted at constant, in situ radial stress.

The quantity $E\varepsilon_3/q_s$ for different values of Poisson's ratio is shown in Figure 15b. Since E, $q_s$, and $\sigma_3$ are always positive, the occurrence of positive and negative strain means that the restraint relation given by equation 68 can be either of an active or reactive form where elastic theory calls for negative strain and compressive stress, equation 54 and reactive restraint of the Iowa K-Test are consistent. Conversely, where compressive strains are called for, the spring constant defined by equation 68 should produce radial compression or work as an active spring against the specimen. When $\nu = 0.5$, a reactive response is always appropriate until z/a is such that the superimposed $\sigma_3$ should be zero. Other values of $\nu$ dictate combinations of restraint responses including $k = \infty$ when $E\varepsilon_3/q_s = 0$ and $k = 0$ when the superimposed $\sigma_3$ is 0.

The main advantage that could result from formulating the test response in terms of deformation restraint is convenience in testing. Stress control requires a triaxial apparatus and continual computations and adjustments throughout the test. A solution might be an expensive pre-programmed servomechanism. On the other hand, the k-path method would require intervention at point a on the stress path shown in Figure 14a, but the remaining portion of the test could be conducted in a fashion similar to that of the oedometer with a physical analogy to

the restraint function being a spring. The inconvenience of having active and reactive springs might be circumvented by using Lambe's average element concept. Since the average element occurs near z = a, elastic theory stipulates reactive response for $\nu \geq 0.1$ and constant $\sigma_3$ for $\nu < 0.1$. Since few soils are known to have Poisson's ratio less than 0.1, a reactive restraint apparatus should suffice.

Another potential advantage of the k-path test is in the definition of the $K_o$ phase and the elastic parameters. A constrained test performed in a triaxial apparatus is difficult to perform and requires special equipment. Thus, $K_o$ is usually defined from empirical relations. Additionally the measurement of $\nu$ is difficult in a triaxial apparatus, so this parameter is usually estimated at 0.5, a value for which graphical stress distributions are published. A criticism of the proposed k-path method is that the restraint function is defined at the conclusion of the $K_o$ loading phase and held constant thereafter. As the stress state in the primary element changes, the definitive parameters E and $\nu$ could vary, thus changing restraint constant computed in equation 68. Material parameters are also assumed constant in the stress-path test; however, for the k-path test, it is entirely feasible that E and $\nu$ could be updated at points along the stress path ab, Figure 14a, according to the procedure previously discussed but with the elastic solutions for restrained conditions being the source of E and $\nu$. Such a procedure would certainly eliminate the convenience of k-path testing.

# EXPERIMENTAL METHODS

Although the primary goal of this research is to investigate the influence of the restraint function on the deformation and strength characteristics of soil, the proposition of a new test apparatus essential to accomplishing the desired goal introduces some factors not encountered with conventional testing. The significance of specimen dimensions, the influence of imposing rigid boundaries, and the effects of boundary friction are all factors common to a deformation restraint test. The philosophy of this experimentation is to presume that conventional techniques yield valid parameters, or at least they yield parameters consistent with prediction methods currently used. Thus, if results from the proposed test are to be implemented within the framework of current engineering practice, a viable evaluation can be made in the laboratory by simply comparing results of the proposed test to accurately defined properties determined from conventional methods.

## Test Material

The diverse nature of soil makes a monumental task of experimentally evaluating all of the possible ramifications. For this study, a single soil was selected on the basis of uniformity and ease of specimen preparation. A total of 31 specimens was made from Monona series soil from western Iowa. The physical and mineralogical properties of the

soil were determined for previous research, and the results are tabulated in Table 10. To reduce variability associated with moisture content and dry unit weight, the material was compacted at constant moisture content in a 2.8 inch diameter steel mold with a hydraulic ram. The compaction apparatus was arranged such that the desired unit weight was achieved by compacting a given weight of the soil to the appropriate dimensions. Unit weight and moisture content were arbitrarily set at the standard Proctor density and optimum moisture content given in Table 10. Table 11 is a summary of the volumetric and gravimetric properties of all specimens used in the test program. The mean dry unit weight and moisture content were quite close to the targets. More importantly, variation in these properties was low, meaning the chances of evaluating a test mechanism rather than variability between specimens are better. For comparison, Harr (28) reports field variability for the same properties in excess of 30 percent. Also it was anticipated that the low saturation levels would eliminate pore pressure as a variable.

## Apparatus

The two existing versions of the K-Test apparatus were used during a preliminary evaluation for this research. The stiff mold, Figure 12, performed admirably, but it lacked the capacity of changing the restraint function. Stiffness of the thin-walled model, Figure 13, can be changed by retracting the hydraulic cylinder and placing

Table 10. Physical and mineralogical properties of Monona loess (after Hoover and Handy (31))

| Name or Series Location | Monona, Sioux City, Iowa |
|---|---|
| Horizon sampled | B/C |
| Textural Composition, % | |
| Gravel (>4.76 mm.) | 0.0 |
| Sand (4.76 - 0.074 mm.) | 0.6 |
| Silt (0.074 - 0.005 mm.) | 78.4 |
| Clay (<0.005 mm.) | 21.0 |
| Colloids (<0.001 mm.) | 17.0 |
| Physical properties: | |
| Liquid limit, % | 32 |
| Plastic limit, % | 26 |
| Plasticity index, % | 6 |
| Specific gravity | 2.71 |
| Std. dry unit weight, pcf | 103.8 |
| Std. opt. moist. cont., % | 18.5 |
| Classification: | |
| Textural | Silty clay loam |
| Engr. - AASTHO | A-4 (8) |
| Predominant Clay Mineral | Montmorillonite |
| Other Clay Minerals | Illite[a]<br>Kaolinite[a] |
| Geological Description | Loess<br>calcareous |

[a]Indicated clay mineral present in small amounts only.

Table 11. Volumetric and gravimetric properties of test specimens

| | Mean | Standard Deviation | CV, % |
|---|---|---|---|
| Unit weight, PCF | 102.9 | 2.2 | 2.1 |
| Moisture Content, % | 18.3 | 0.3 | 1.6 |
| Void Ratio | 0.63 | 0.01 | 1.6 |
| Saturation, % | 79.5 | 1.42 | 1.7 |

different sized springs between the piston and one of the ears on the mold, and a few tests were performed using this technique. However, tensile cracks in specimens, occurring at and parallel to the slot in the side of the mold raised questions about the validity of assuming axisymmetric stress conditions. Thus, it was decided to design and construct experimental apparatus capable of performing deformation restraint or conventional stress controlled tests under approximate axisymmetric boundary conditions. The resulting deformation restraint (DR) apparatus is shown in Figures 16 and 17.

Radial stress is applied to 2.8 inch diameter cylindrical specimens of varied length by eight radially oriented Bellofram (rolling diaphragm) cylinders acting on individual segments. The segments were cut from thick-walled aluminum tubing, having an inside diameter matching that of the specimen and grooves were milled on the exterior to index the cylinder pistons at the middle of the segments. Opposing

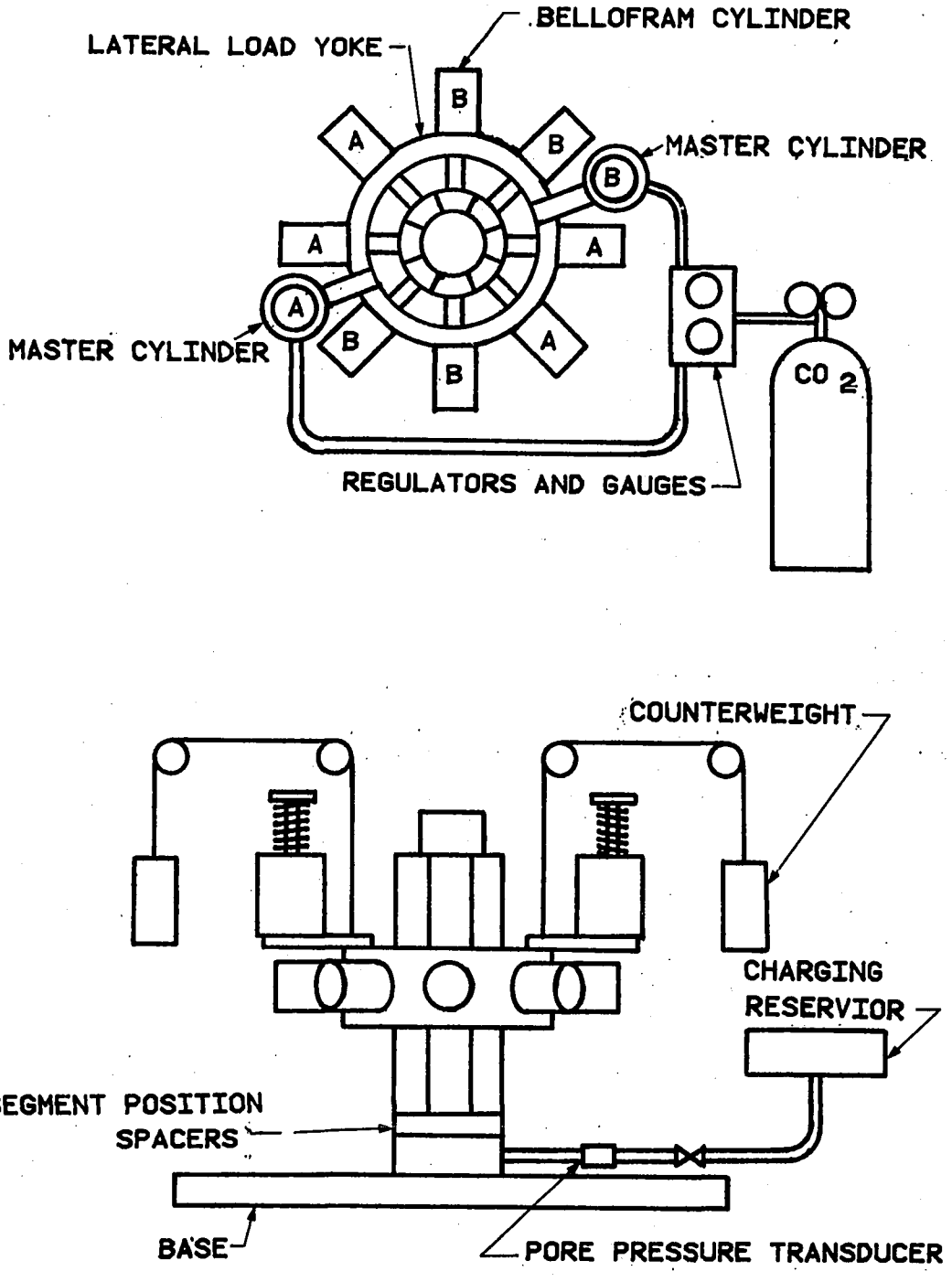


Figure 16. Schematic of deformation restraint apparatus

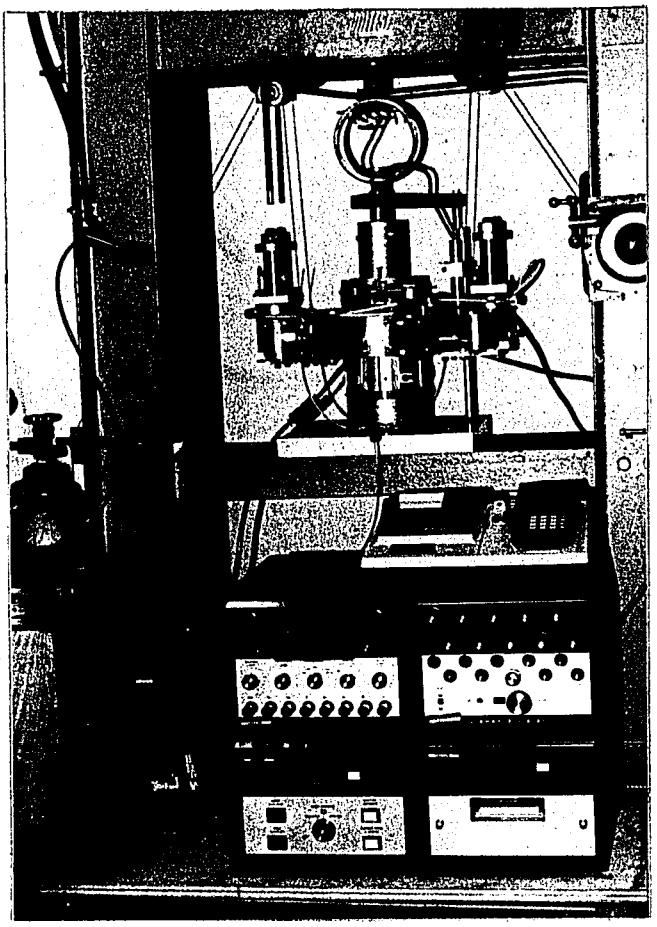

Figure 17. Deformation restraint test system

pairs of radial cylinders were connected in series to a pair of master cylinders which react against springs. The intended design was to allow the option of stress control or automated lateral deformation. With the master and radial cylinders charged with hydraulic fluid and operated as a closed system, deformation restraint is automatic and can be altered by changing the springs. The stress control option involves application of $CO_2$, with manually controlled pressure regulators. The dual master cylinder system is intended to allow application of truly triaxial stresses, either by using reaction springs of different stiffness or by manual pressure control. To avoid downward thrust on the specimen and interference between the bottom of the segments and the base, the weight of the lateral load yoke and the segments was balanced by a counterweight system attached to a commercial load frame.

Radial and axial displacements are measured with LVDTs (linear variable differential transformers), and axial loads with a load cell fabricated from a proving ring and electrical resistance strain gages. A diaphragm-type pressure transducer is used to monitor pore pressure at the base of the specimen as is done with conventional triaxial apparatus. The electrical load and deformation sensors are monitored with an automated, digital strain gage indicator. Calibration revealed that displacements could be measured to a precision of 0.0005 inches, axial stress to 0.2 psi, and pore pressures to 0.04 psi.

A pretest evaluation of the apparatus revealed that the radial Bellofram cylinders were nearly frictionless. They could be activated at pressures slightly less than 0.6 psi, meaning hysteresis expressed in terms of radial stress on the 5.6 inch long specimen would be less than 0.12 psi. This is well within the precision of the 1/4 percent, 250 psi pressure gages used in the control console. The pretest evaluation also revealed that the O-ring seal at the shaft on the spring side of the master cylinders was far from frictionless, and changing to a double-acting Bellofram system was attempted. However, nonavailability of proper sized diaphragms also cause that system to stick. Thus a decision was made to conduct deformation restraint tests under manual control.

The test procedure developed is an incremental feedback system where radial stresses are computed and adjusted based on radial deformations and the desired restraint function through use of a Texas Instruments, TI 59 programmable calculator. The programs developed also have provisions to account for stress adjustments based on changing geometry occurring during a test.

## Boundary Friction

Two options are available for the treatment of shear occurring at the specimen boundaries in deformation restraint tests. As suggested in reference 26, a measure of the net frictional force acting on a specimen can be made. This, however, requires assumption of a stress

distribution about which little is known. In fact a solution to the simpler case of friction on ends of triaxial specimens has eluded researchers for many years, and it seems unlikely that an accurate analysis of boundary friction as an element of routine testing is easily achievable. The second alternative, other than neglecting friction, is to minimize its influence by providing a near frictionless boundary.

A part of this research was devoted to evaluating potential interface materials and their properties. Results of interface friction tests performed in a direct shear apparatus on several materials are presented in Table 12. Tests were conducted over normal stresses ranging from 10 to 50 psi and the subscript, I, on c and $\phi$ are used to designate frictional resistance occurring on an interface. Shear strength of Monona loess is included as a reference. A soil-Teflon interface which is used with the thin-walled Iowa K-Test developed surprisingly high frictional resistance. The other extreme is represented by Teflon interface lubricated with a silicone oil spray, where the direct shear apparatus could not measure an interface shearing resistance. The frictional properties of lubricated rubber triaxial membrane and Teflon are of particular interest because this represents a workable solution for reducing friction in the experimental apparatus. At a normal stress of 50 psi, the ultimate friction that can be developed is about 0.2 psi. Thus, by incapsulating specimens in a triaxial membrane, lining the interior faces of the mold segments with

Table 12. Interface frictional properties

| Interface Description | $C_I$, psi | $\phi_I$, degrees | $R^2$ | CV, % | n |
|---|---|---|---|---|---|
| Soil-Soil | 12.25[a] | 34.6[a] | 0.9829 | 7.9 | 3 |
| Soil-Teflon | 0.96 | 24.4 | 0.9632 | 11.1 | 5 |
| Teflon-Teflon | 0.78 | 4.9 | 0.9963 | 2.9 | 7 |
| Rubber-Teflon (Lubricated) | 0.05 | 0.2 | 0.9982 | 8.3 | 7 |
| Teflon-Teflon (Lubricated) | -[b] | -[b] | - | - | - |

[a]Not an interface property as tests were performed on solid specimens.

[b]Not measurable.

overlapping strips of the Teflon sheet, and using the same interface combination at both ends of a specimen, it can reasonably be assumed that boundary friction is zero. Pore pressures were monitored by cutting a small hole in the center of the Teflon and rubber discs used at the base of the specimen. This technique has a secondary advantage of eliminating the potential for variable boundary friction resulting from the collection of pore fluid at the surface of the mold. Lutenegger (44) reports a variation in net side friction measurements as specimens become saturated.

## Computational Methods

A key aspect of the experimental test program is comparison of volumetric and radial strain from triaxial and deformation restraint apparatus. Volumetric strain is measured directly in a triaxial apparatus and $\varepsilon_3$ is a computed value. For the deformation restraint apparatus, the inverse is true. For small deformations, volumetric or radial strain for axisymmetric situations can be computed from the simple relation

$$\varepsilon_{vol} = \varepsilon_1 + 2\varepsilon_3 \tag{71}$$

However, in soil mechanics strains are not always small, which could have a significant influence on a comparison of computed versus measured values. Consider a cylindrical specimen of initial height, $H_o$, and diameter, $D_o$. A deformed measure for height, $H_i$, and diameter, $D_i$, can be expressed in terms of engineering strain as:

$$H_i = H_o\ (1 - \varepsilon_1) \tag{72}$$

$$D_i = D_o\ (1 - \varepsilon_3) \tag{73}$$

Volumetric strain can be expressed in terms of deformed and undeformed volumes as

$$\varepsilon_{vol} = \frac{\Delta V}{V_o} = 1 - \frac{V_i}{V_o} \tag{74}$$

Substituting volumes in terms of deformed and under-formed heights and diameters in equation 74 and cancelling terms leads to

$$\varepsilon_{vol} = 1 - (1 - \varepsilon_1)(1 - \varepsilon_3)^2 \tag{75}$$

The assumption of small strains means the product of terms in equation 75 is essentially zero; thus it becomes equation 71. However, if the products are not small, the true volumetric strain can be conveniently computed by taking logarithms, such a manipulation results in

$$\varepsilon_{vol} = 1 - \exp \left\{ \ln (1 - \varepsilon_1) + 2 \ln (1 - \varepsilon_3) \right\} \tag{76}$$

Differences in volumetric strain computed from equations 71 and 75 can be as great as 10 percent for deformations encountered in soil testing. To compute $\varepsilon_3$ from measured values of $\varepsilon_{vol}$ and $\varepsilon_1$, equation 76 can be solved for $\varepsilon_3$ which results in

$$\varepsilon_3 = 1 - \left( \frac{1 - \varepsilon_{vol}}{1 - \varepsilon_1} \right)^{1/2} \tag{77}$$

Equation 77 presumes that triaxial specimens remain cylindrical.

A common convention for presenting constant confining stress triaxial test results is to plot deviator stress, $\sigma_1 - \sigma_3$, against axial strain and call the slope of the resulting curve E. If E is to

be consistent with the elastic constitutive law, the fact that such tests are conducted in a combined stress field might be important. Thus, from equation 55, E is theoretically defined as

$$E = \frac{\sigma_1 - 2\nu\sigma_3}{\varepsilon_1} \tag{78}$$

and depends not only on stress but Poisson's ratio. For the special case where $\nu = 0.5$, the conventional soil mechanics approach is valid. Otherwise, a measure of $\nu$ is needed to define E which leads to a second problem. Again by convention, $\nu$ is frequently taken as the ratio $-\varepsilon_3/\varepsilon_1$, from tests conducted under a combined stress field. To arrive at a theoretically consistent measure for $\nu$, a ratio formed from equations 55 and 56 when solved for $\nu$ results in the expression

$$\nu = \left( \frac{\sigma_3 - R\sigma_1}{\sigma_1 + \sigma_3 - 2R\sigma_3} \right) \tag{79}$$

where $R = \varepsilon_3/\varepsilon_1$, a quantity computed directly from test results. Experimental results from this research will be presented in the conventional soil mechanics format. Deviator stress versus axial strain relations will be plotted under the presumption that $\nu = 0.5$, and the slope of such plots will be designated $E_D$. However, the significance of evaluating E and $\nu$ such that they are consistent with the elastic constitutive law will be considered. Also it is important to realize that the parameters E and $\nu$ derived in such a manner for a soil are not in reality elastic parameters.

# PRESENTATION AND DISCUSSION OF RESULTS

## Conventional Tests

The purpose of this part of the study is to define strength and deformation parameters and observe the character of the soil tested by conventional methods. It might be speculated that differences observed between the results obtained from conventional and deformation restraint apparatus might be attributed to conditions imposed by the apparatus itself. For example, the proposed apparatus enforces a nearly cylindrical geometry on a specimen. Knowing whether this geometry influences the strength or deformation properties of a soil is important to the analysis of results from deformation restraint tests.

### Unconfined compression

Six specimens were tested in unconfined compression while pairs of opposing, radial deformation measurements were made at the mid-height. To minimize end restraint bulging, lubricated rubber-teflon interfaces were provided at the ends of the 5.6 inch long specimens. Unconfined ultimate or maximum strength, $q_u$, and deformation modulus, $E_u$, were found to be:

$$q_u = 33.8 \pm 3.74 \text{ psi}$$

$$E_u = 909 \pm 91.5 \text{ psi}$$

The numbers following the $\pm$ sign represent sample standard deviation, and CV for $q_u$ and $E_u$ were 11 and 10 respectively. The fivefold increase in CV over that measured for volumetric properties suggests that such factors as dry unit weight or void ratio may not be indicative of variation in strength or deformation modulus.

Figure 18 is a typical stress-strain plot from which the summarized data were obtained. Hysteresis occurring with unloading cycles indicates the relatively linear nature of the loading curve and does not imply a truly elastic material. Upon reaching ultimate strength, failure was abrupt, implying inconsistency with the Drucker model which requires a stable material.

Results of the radial deformation measurements are plotted in terms of $\nu$ and $\sigma_1$, in Figure 19. The tests show varied linear relations up to $\sigma_1$ = 30 psi, a stress level which also results in $\nu$ exceeding 0.5. This phenomenon is common for many soils displaying a tendency for volumetric dilatancy. Erratic values for $\nu$ occurring near failure stress levels are attributed to the measurement technique. All of the unconfined specimens failed along well defined shear planes, which if by happenstance were oriented perpendicular to the direction of radial deformation measurements would produce exaggerated values of $\nu$. An important result, observable in Figure 19, is that for this soil $\nu$ is not a constant as is often presumed in many geotechnical adaptations of elastic theory. Also the material appears to be totally compressible, $\varepsilon_3 = 0$ up to stress levels ranging from 5 to 15 psi.

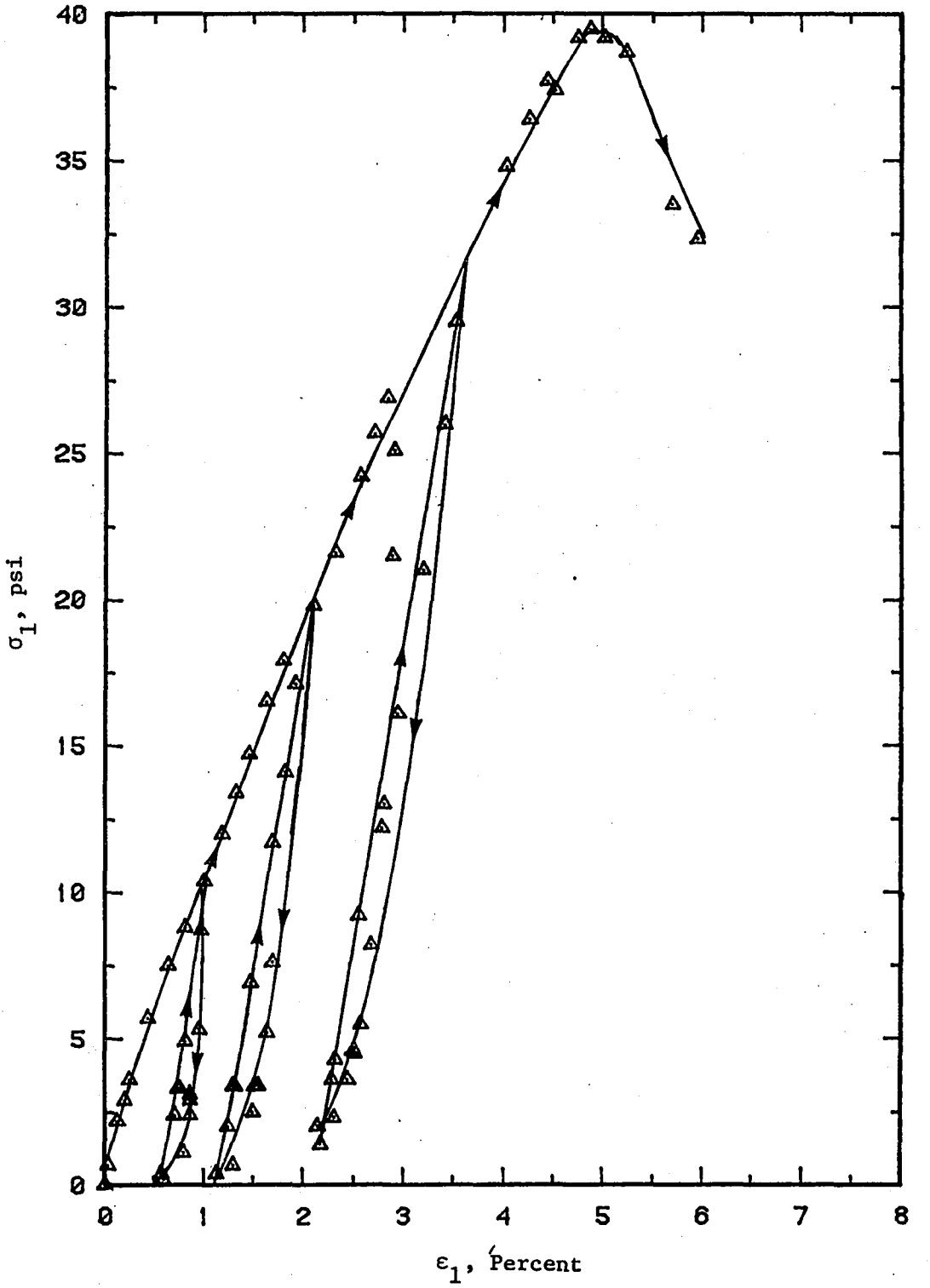


Figure 18. Typical unconfined test

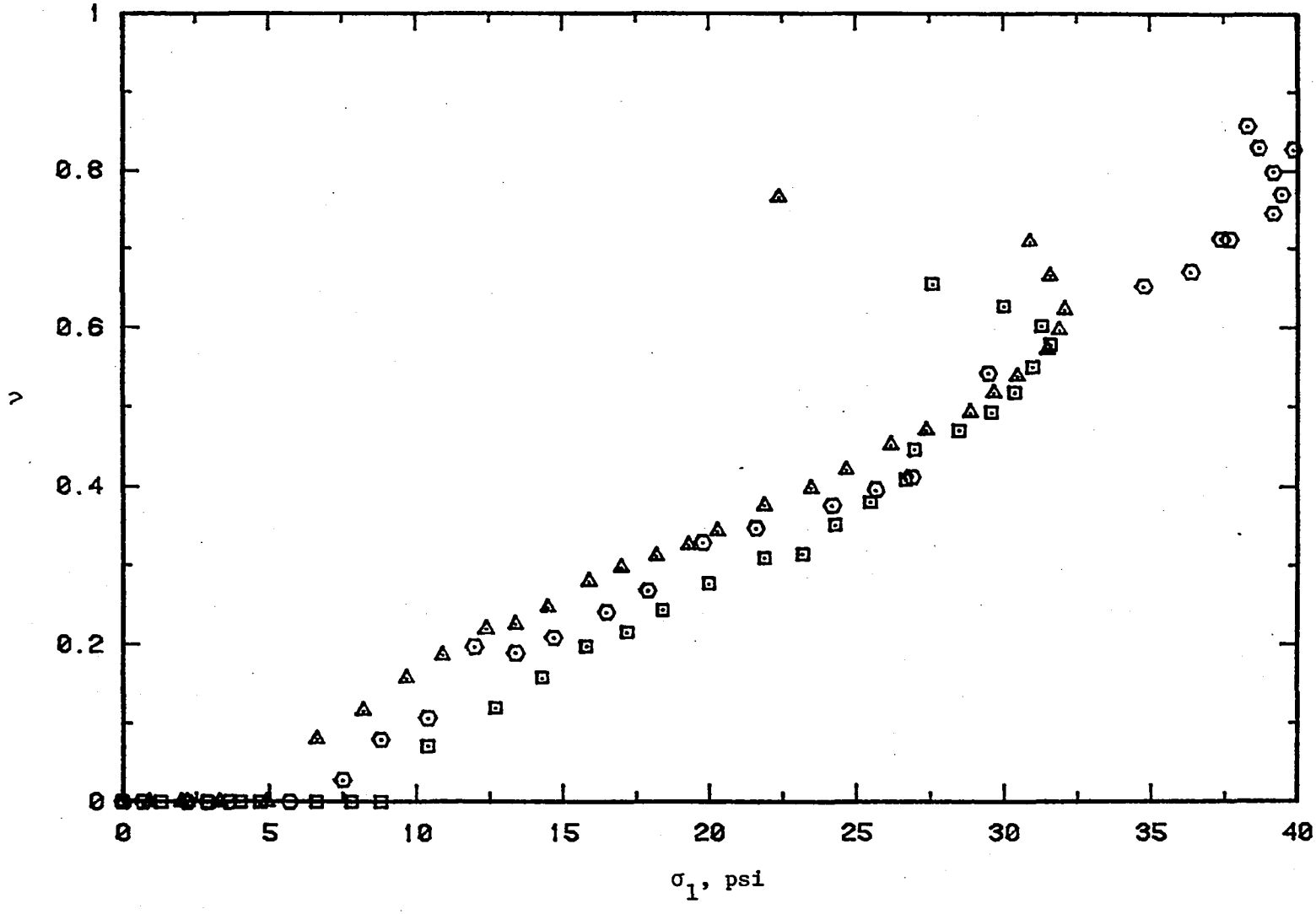


Figure 19. Poisson's ratio versus axial stress

Shear strength

Twenty hydrostatically consolidated 5.6 inch long specimens were sheared at different constant confining stresses in conventional triaxial apparatus and in the experimental deformation restraint device. Drainage was allowed during consolidation, and the shear phase was conducted under undrained conditions with pore pressure measurements. For all specimens, the maximum pore pressure measured was less than the precision of the principal stress measurements; therefore, it is presumed that the consolidation drainage phenomenon is not a factor in this evaluation.

The first three lines in Table 13 are a summary of the shear strength parameters derived from a least squares linear regression on the data shown in Figure 20. A linear relation more than adequately defines the failure envelope, and comparison of c and $\phi$ obtained from the two apparatuses indicates that the rigid boundaries of the DR apparatus have little if any influence on the strength of the material. The 0.6 psi difference in cohesion and the 1.4 degree difference in expected friction angle could easily be due to variations in specimens and measurements. The near identical strength parameters also suggest that boundary friction is minimal, and that ultimate strength resulting from total plastic flow within the bounds of the cylindrical geometry established by the deformation restraint device is the same as a more localized failure occurring in the middle zone of triaxial specimens. Another interesting outcome from these tests is the fact that CV on the

Table 13. Summary of ultimate strength parameters, $\sigma_3$ = constant

| Test Description | n[a] | b[b] psi | tan $\alpha$[c] | c[d] $\pm$ s[e] psi | $\phi$[f] $\pm$ s[e] degrees | $R^2$[g] | CV[h] % |
|---|---|---|---|---|---|---|---|
| Triaxial Test | 18 | 7.60 | 0.5635 | 9.2±0.4 | 34.3±0.3 | 0.9987 | 2.2 |
| Deformation Restraint Apparatus | 18 | 6.97 | 0.5840 | 8.6±0.4 | 35.7±0.4 | 0.9983 | 2.3 |
| Composite Triaxial & Deformation Restraint | 30 | 7.47 | 0.5706 | 9.1±0.4 | 34.8±0.3 | 0.9978 | 2.3 |
| Direct Shear | 3 | - | - | 12.3±3.3 | 34.6±5.2 | 0.9830 | 7.9 |
| Stage Triaxial Test A | 4 | 9.81 | 0.4423 | 10.9±0.4 | 26.3±0.3 | 0.9997 | 0.6 |
| Stage Triaxial Test B | 4 | 11.57 | 0.4849 | 13.2±0.7 | 29.0±0.5 | 0.9993 | 0.9 |
| Composite Secondary Failure | 17 | 4.81 | 0.5415 | 5.7±3.2 | 32.8±2.0 | 0.94109 | 6.8 |

[a] n = number of tests.
[b] b = intercept from q - p regression.
[c] tan$\alpha$ = slope from q - p regression.
[d] c = cohesion.
[e] s = standard deviation.
[f] $\phi$ = friction angle
[g] R = correlation coefficient.
[h] CV = coefficient of variation.

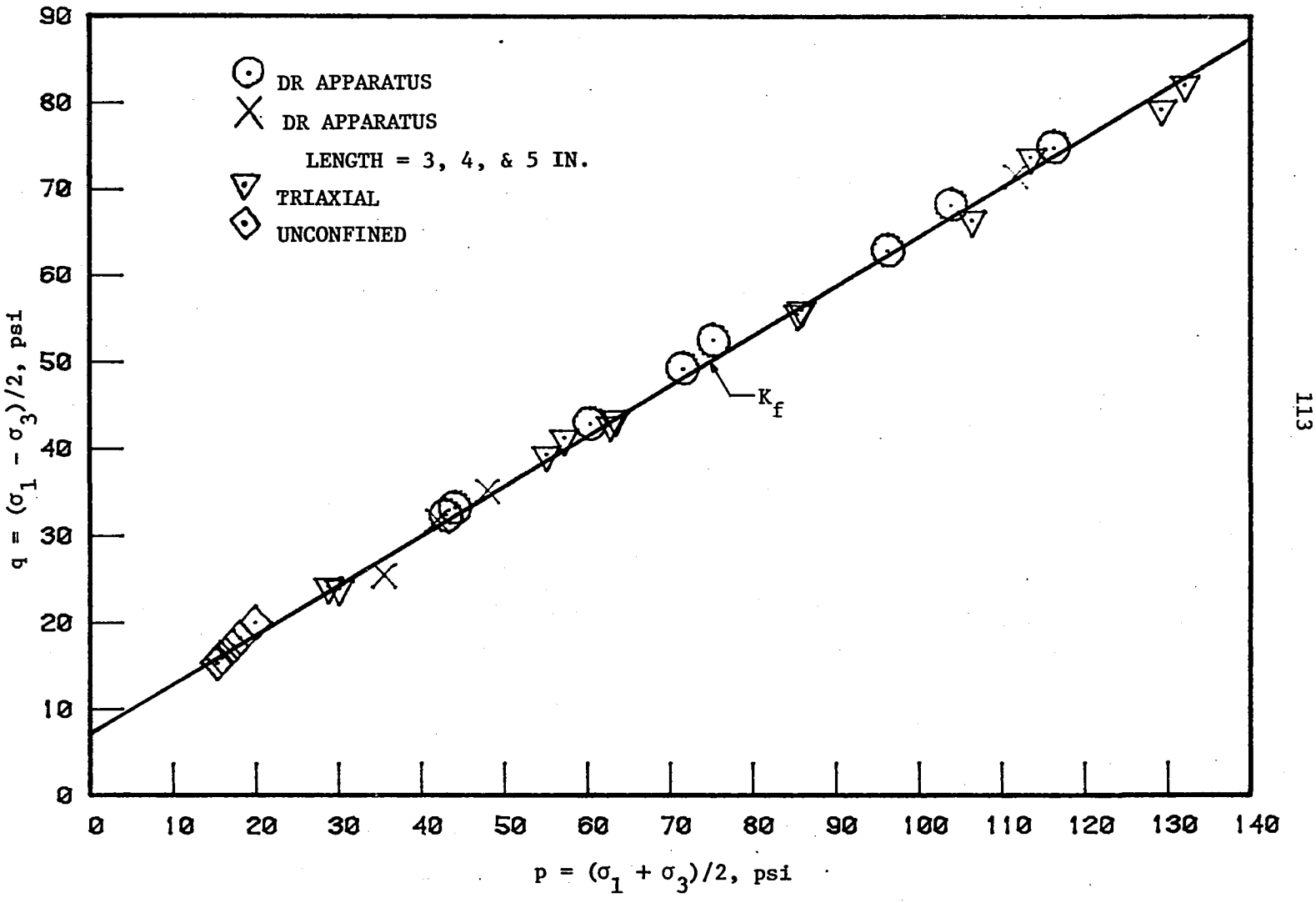


Figure 20. Constant confining stress shear strength

model is of the same magnitude as the physical properties of the original specimens. For a linear regression of q on p, CV is the standard deviation divided by the expected value for q at the mean value for p. Since data from the triaxial and deformation restraint apparatus are quite similar, the regression on the pooled data, (line 3, Table 13), shall be used as a reference for further comparisons.

Four of the tests plotted in Figure 20 were performed on specimens in violation of the length to diameter criterion established for triaxial testing. Specimens of 3, 4, and 5 inch lengths were tested in the deformation restraint apparatus with the resulting strengths showing no apparent difference in shear strength realized from the longer specimens. This observation also supports the contention that boundary friction is not significant because side shear stress should be a function of specimen length. Also, use of shorter specimens to achieve the same result could be important to the practitioner. Field sampling sometimes produces fragmented specimens.

Results of the direct shear tests previously discussed are also presented in Table 13 for comparison with the triaxial data. The relatively small number of direct shear data points produced results quite consistent with those from triaxial and DR apparatus. Apparently, difficulties such as progressive failure and predetermined failure planes were not significant for the compacted loess.

Another aspect of the conventional shear strength analysis is to evaluate the influence of staged triaxial testing on strength parameters. Stage tests A and B in Table 13 are results from two experiments in which

one data point was measured by normal procedures. However, rather than conclude the tests, confining stress was increased at the first sign of limiting deviator stress, and loading was continued. When compared to results from normal tests, the staged technique produced a pronounced decrease in friction angle and increase in cohesion. Strength parameters from a regression on several secondary failures excluding first failure points are also in Table 13. For these data, the friction angle is near that obtained from the conventional first failure tests, but cohesion is nearly halved. These observations tend to support the contention that the strength of the compacted loess is sensitive to the disruption of cohesion. A test sequence producing one point from an intact specimen, which includes the full cohesive component, followed by tests producing additional strength from inter-particulate friction would tend to rotate the failure enveloped clockwise, amplifying c and understating $\phi$. Parameters derived from tests excluding intact cohesion suggest that $\phi$ is relatively independent of progressive failures, and that about one half the cohesion is destroyed by strain producing ultimate strength. For this soil, practical implications of continuous staged testing are that shear strength could be overestimated by as much as 45 percent at low normal stress and underestimated by 25 when normal stress is high.

Deformation properties

This portion of the investigation is an analysis of the deformation response of specimens subjected to direct shear and constant confining stress in the triaxial and deformation restraint apparatus. Stress and volumetric strain versus displacement results for three direct shear

tests are in Figure 21. In this apparatus, the material should be characterized as unstable because of the lower residual shear strength occurring after ultimate strength is achieved. During shear, the material displayed a slight volumetric decrease or positive volumetric strain followed by more pronounced dilation, commencing before very much of the ultimate strength was realized. This suggests that particle overriding is a major contributor to shear strength, and that the void ratio is less than the critical value.

Figure 22 illustrates the influence of the triaxial apparatus on the deformation behavior of the material. The deviator stress versus major principal strain curves suggests a stable material and demonstrates difference in behavior of the same soil subjected to failure on a discrete plane as opposed to that occurring in a zone. Specimens tested under constant confinement in the triaxial apparatus did not display discrete single failure planes as naturally occurred in unconfined tests or was forced in the direct shear tests. At the conclusion of the test, triaxial specimens displayed a pronounced bulge over the middle one third of the specimens, but this highly deformed zone contained no observable slip planes. Availability of more material to resist deformation in the triaxial mode should enhance the potential of strong elements picking up load after weaker neighbors have failed, thus explaining why the deviator stress in Figure 22 did not decrease after reaching a limiting value. A comparison of soil behavior in a triaxial apparatus to that for unconfined tests suggests that stability is also influenced by

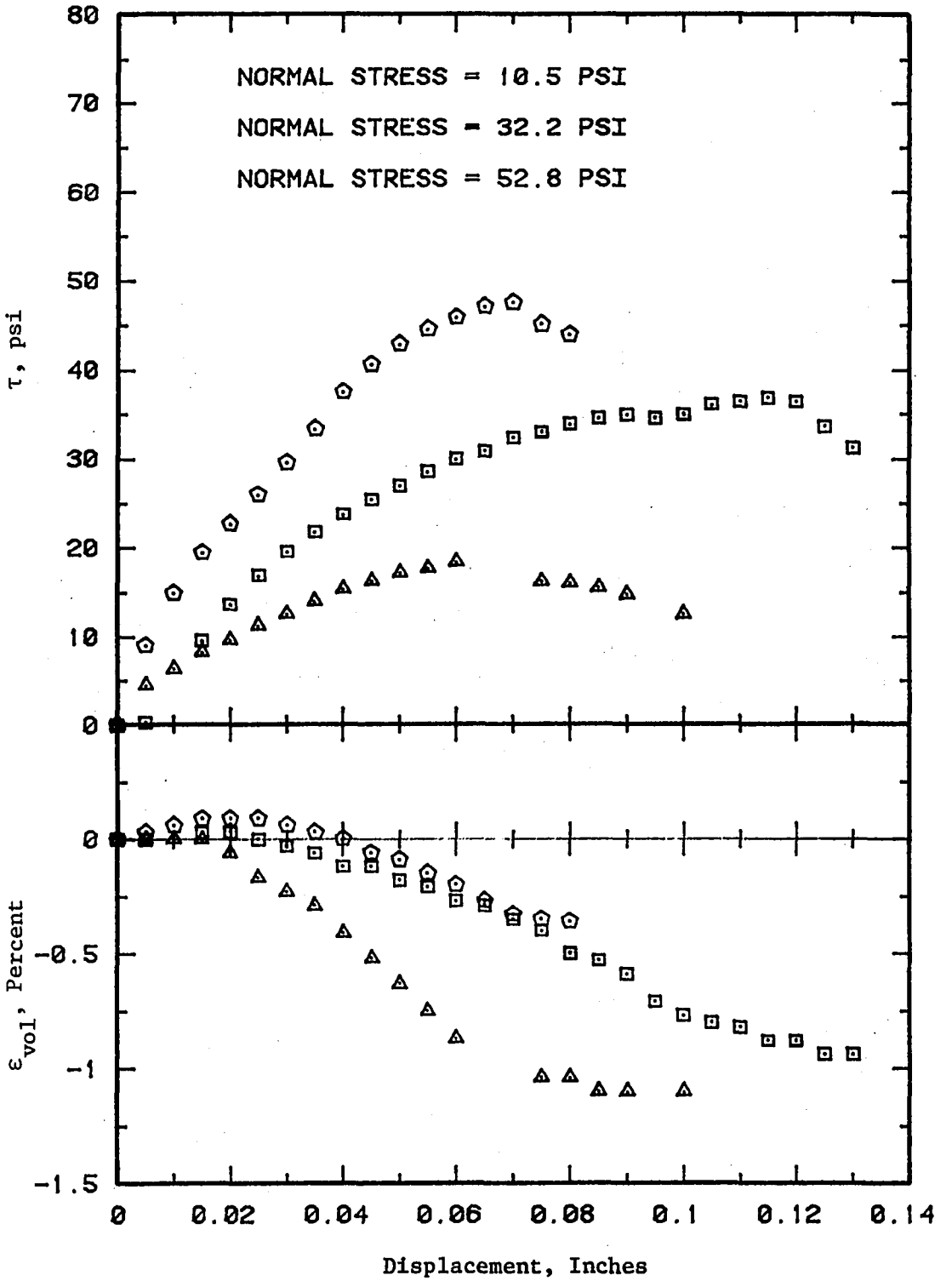


Figure 21. Stress-deformation response from direct shear tests

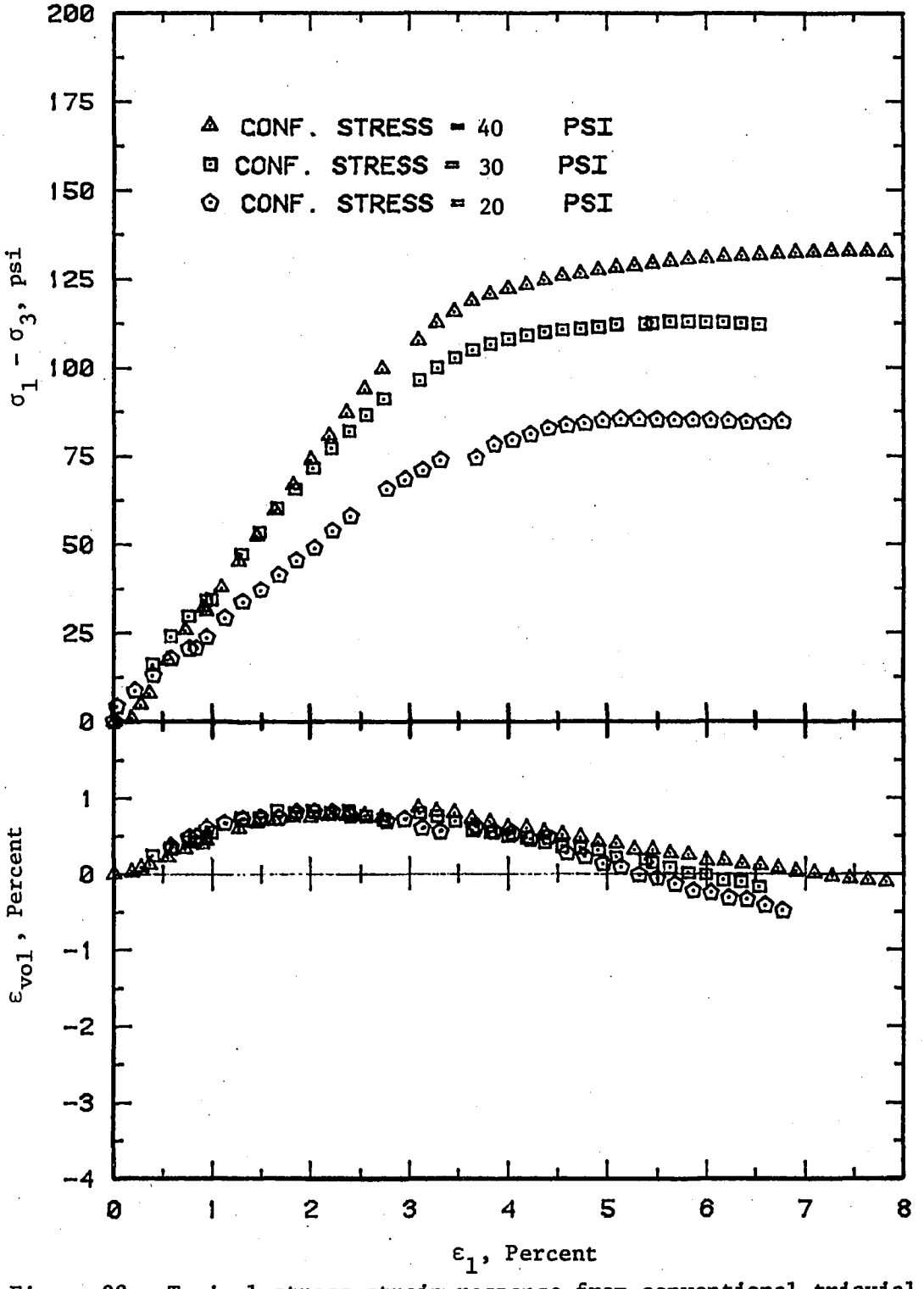


Figure 22. Typical stress-strain response from conventional triaxial apparatus, $\sigma_3$ = constant

degree of confinement. Thus the validity of a yield condition load-deformation model as that proposed by Drucker may not only be a function of the material but also operational stress states.

Stress-strain and volumetric behavior of the remolded loess under constant confinement in the deformation restraint apparatus is shown in Figure 23. In terms of stability, both the triaxial and deformation restraint apparatus produced very similar results. Comparison of volumetric responses in the lower graphs of Figures 22 and 23 shows measurements from the deformation restraint apparatus produced much greater compressive and dilative volumetric strains than the conventional triaxial apparatus. This seems logical in that end friction associated with normal triaxial testing should induce a complex combination of compressive and dilatory zones. Thus, the triaxial volumetric measurements and dependent strain computations represent an average. Since the deformation restraint apparatus insures that all elements of a specimen undergo similar volumetric activities, a more truthful measure should be possible. Unrealistic volumetric measures from triaxial tests may be a partial explanation for Drucker's plastic potential overpredicting dilative behavior. Thus far, verification has been based on triaxial testing, and if the dilation occurring within the active zone could be measured, better correlation between experiment and theory might be possible.

The ratio of principal strain is plotted against the axial strain for triaxial and DR tests in Figures 24 and 25. An obvious difference between the two sets of results is absence of initial radial strain and

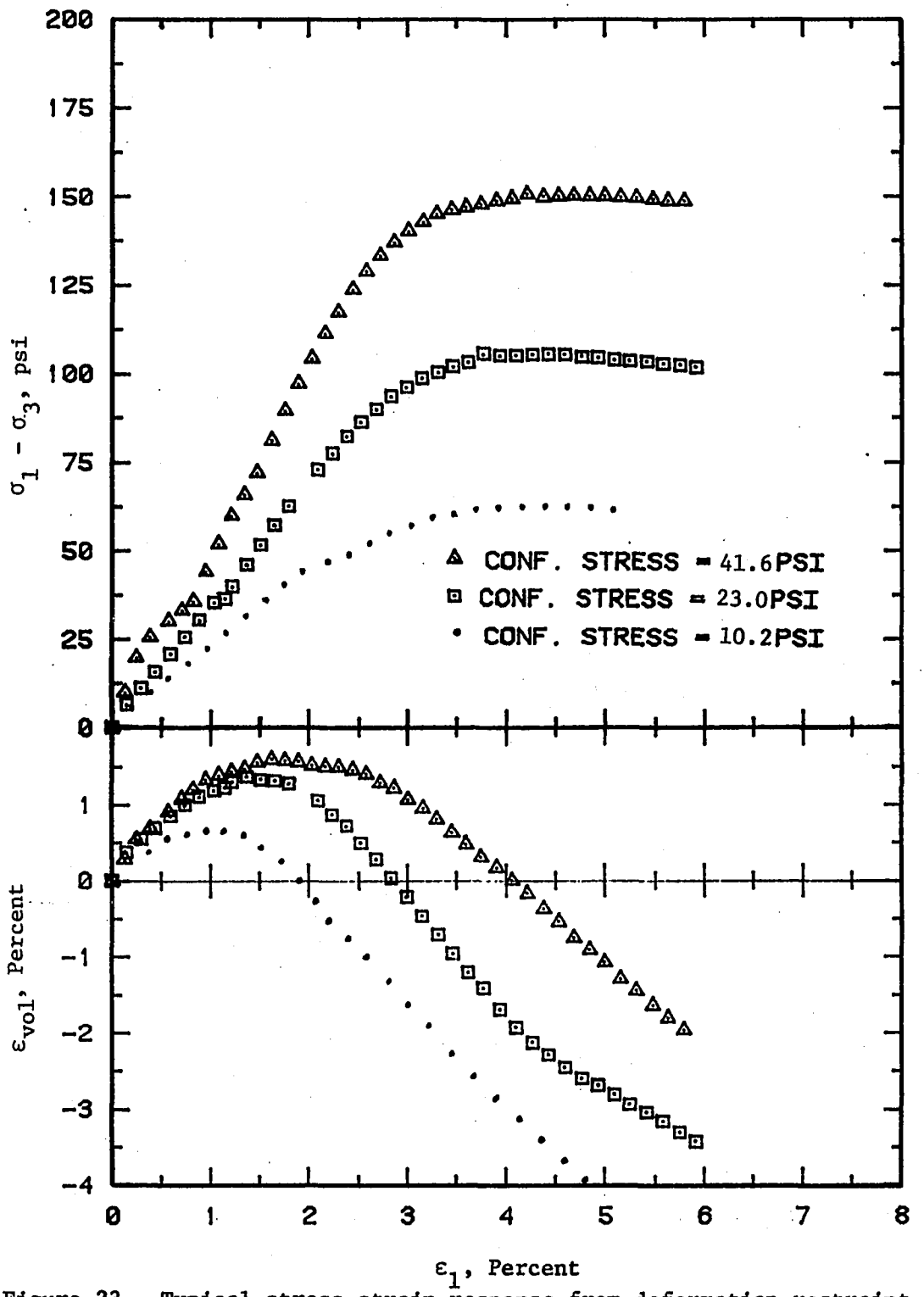


Figure 23. Typical stress-strain response from deformation restraint apparatus, $\sigma_3$ = constant

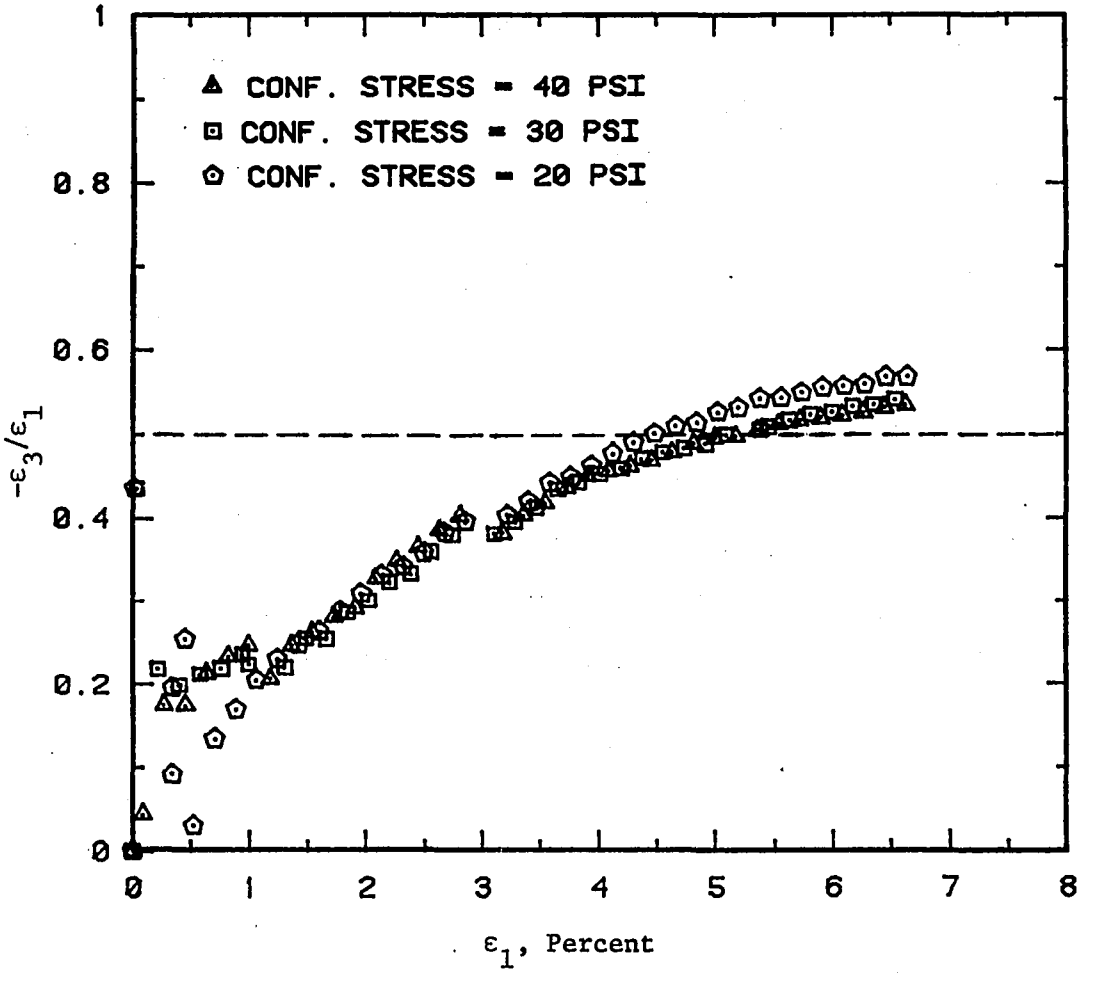


Figure 24. Strains from conventional triaxial tests, $\sigma_3$ = constant

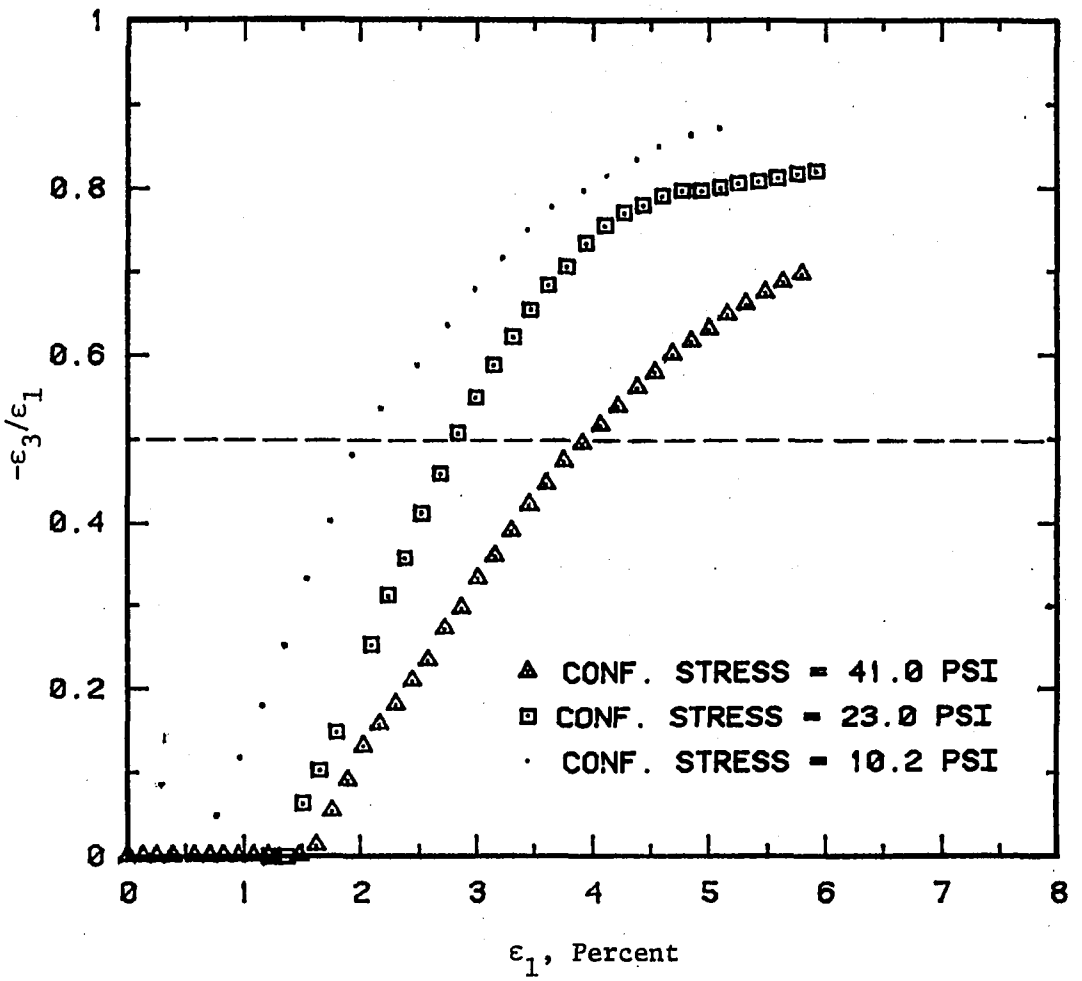


Figure 25. Strains from deformation restraint tests, $\sigma_3$ = constant

subsequent development of large strain ratios measured with the DR apparatus. Axial compression without radial strain is consistent with observations from unconfined tests, and the high strain ratios are representative of dilatant behavior. More radial strain being computed from DR apparatus data suggests that the physical averaging process and the computational assumptions used for triaxial data may lead to erroneous perception about material behavior. The fact that this soil is capable of undergoing axial compression without radial extension has been measured in the uncomplicated unconfined conditions. The same phenomenon occurs for specimens undergoing shear but subjected to constant confinement. A look at the erratic strain ratio results occurring for low axial strains in Figure 24 also makes the conventional triaxial test suspect.

The influence of rigid boundaries on deformation properties is illustrated by Figure 26 where the slopes of deviator stress versus major principal strain responses are plotted against confining stress. Pronounced scatter is common to data from both the triaxial and DR apparatus. A least squares regression summarized in Table 14 represents expected values for deviator stress modulus. The slope of the regression curves for the triaxial and rigid boundaries suggests that boundaries do influence deformation modulus. The difference becomes more pronounced as confinement is increased and for the upper $\sigma_1$ value evaluated, $E_D$ from the DR apparatus exceeds the equivalent triaxial result by about 10 percent. Kinematics of particulate motion can at least subjectively explain this observation. The DR apparatus should offer fewer options

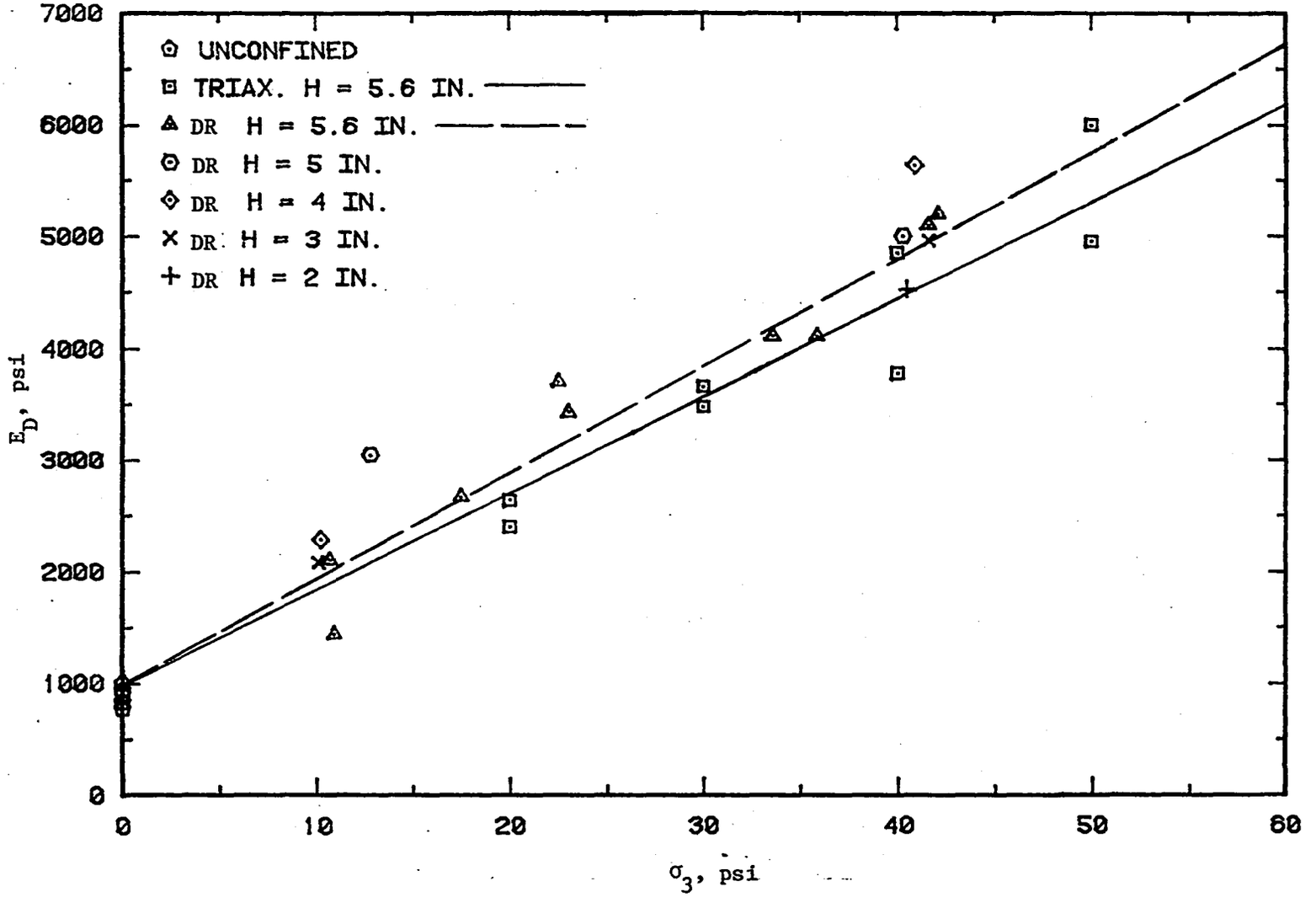


Figure 26. Influence of rigid boundary on modulus

or paths for particulate displacement than that allowed with triaxial boundary conditions. Elimination of some of the easy displacement paths means more energy is required for a bulk displacement, thus a higher modulus. The practical significance of this observation is not clear. It is unlikely that soil elements within a continuum are forced to maintain rigid geometries. Elastic theory, elastic-plastic finite element analysis, and model studies indicate that distortions occur continuously. It is just as unlikely, however, that the bulge in the middle of a triaxial specimen models this continuous distortion.

Deviator stress moduli for specimens of different lengths are also plotted in Figure 26, but scatter in the base data makes it difficult to assess whether specimen height makes a difference in modulus. Although the amount of data available are insufficient for a proper statistical analysis, residuals based on the expected values from the regression analysis may be useful in making a judgmental assessment. A look at residuals, summarized in Table 15, shows that maximum variation from the expected modulus occurred with 5.6 and 4.0 inch long specimens. The shorter specimens do show some scatter, but the magnitude does not appear to be inconsistent with that of the standard specimen length. Since the expected value comes from the 5.6 inch long specimens, the fact that individual points for the 5.6 inch specimens produced residuals as great or greater than the shorter specimens suggests that sample length may not influence $E_D$. Theoretically there is no reason to suspect that specimen length is a factor, but additional tests would be necessary to provide convincing experimental evidence.

Table 14. Regression for deviator stress modulus

| Test | n | Intercept psi | Slope | $R^2$ | CV |
|---|---|---|---|---|---|
| Triaxial | 14 | 875 ± 128 | 89.1 ± 4.6 | 0.9688 | 12.5 |
| DR | 14 | 903 ± 96 | 99.9 ± 4.3 | 0.9765 | 10.6 |
| Composite | 22 | 912 ± 126 | 92.8 ± 4.5 | 0.9538 | 12.1 |

Table 15. Residuals of deviator stress modulus for different specimen lengths

| Approximate Confining Stress, psi | Specimen Length inches | Residual, psi |
|---|---|---|
| 10 | 5.6 | -552 |
| | 5.6 | 129 |
| | 4.0 | 364 |
| | 3.0 | 175 |
| 40 | 5.6 | 90 |
| | 5.6 | 36 |
| | 5.0 | 71 |
| | 4.0 | 645 |
| | 3.0 | 18 |
| | 2.0 | -380 |

Using the DR apparatus results from Figures 23 and 25, $\nu$ was computed by equation 79, and the results are presented in Figure 27. The obvious difference between the strain ratio and $\nu$ is that values based on theory are far better behaved. Where the strain ratio is zero, $\nu$ ranges between 0.25 and 0.4 which is in essence the same values that would be derived from a constrained test. This is because $R = 0$ in equation 79, results in the equation for $\nu$ under constrained conditions. Another interesting feature evident in Figure 27 is that the relationship between $\nu$ and R is not dependent on $\sigma_3$. This feature should be useful if a variable parameter constitutive law for numerical analysis was desired. The fact that $\nu$ does not exceed 0.5 prior to failure also leads support to the legitimacy of adapting the elastic constitutive law to this soil.

The influence of appropriate values of $\nu$ on the parameter E can be seen in Figure 28. Here the ratio $E/E_D$ was formed using equation 78 and experimental values for $E_D$. The results are plotted against the ratio of principal stresses. Again when expressed in terms of normalized variables, the confining stress is not significant. Since $E_D$ for each specimen is constant, E is a variable dependent on the ratio of principal stress. In all cases, E takes on values less than the experimentally determined $E_D$. The nonlinear part of the relation described by the data in Figure 28 is attributed to the fact that $E_D$ in the region of low stress ratios is not linear as was assumed in the computations. Low stress ratios correspond to near failure conditions.

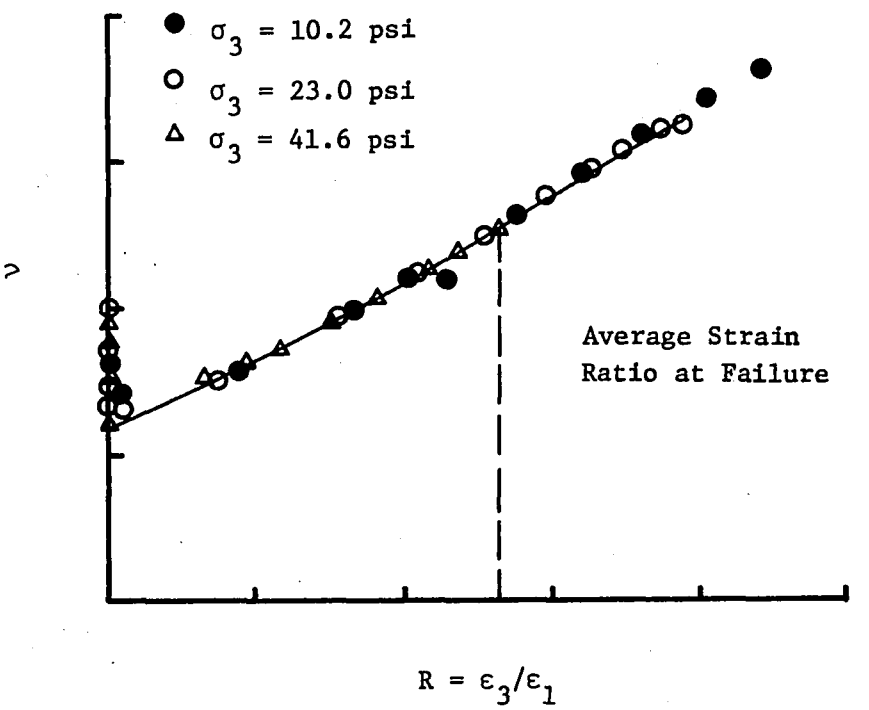


Figure 27. Poisson's ratio versus strain ratio

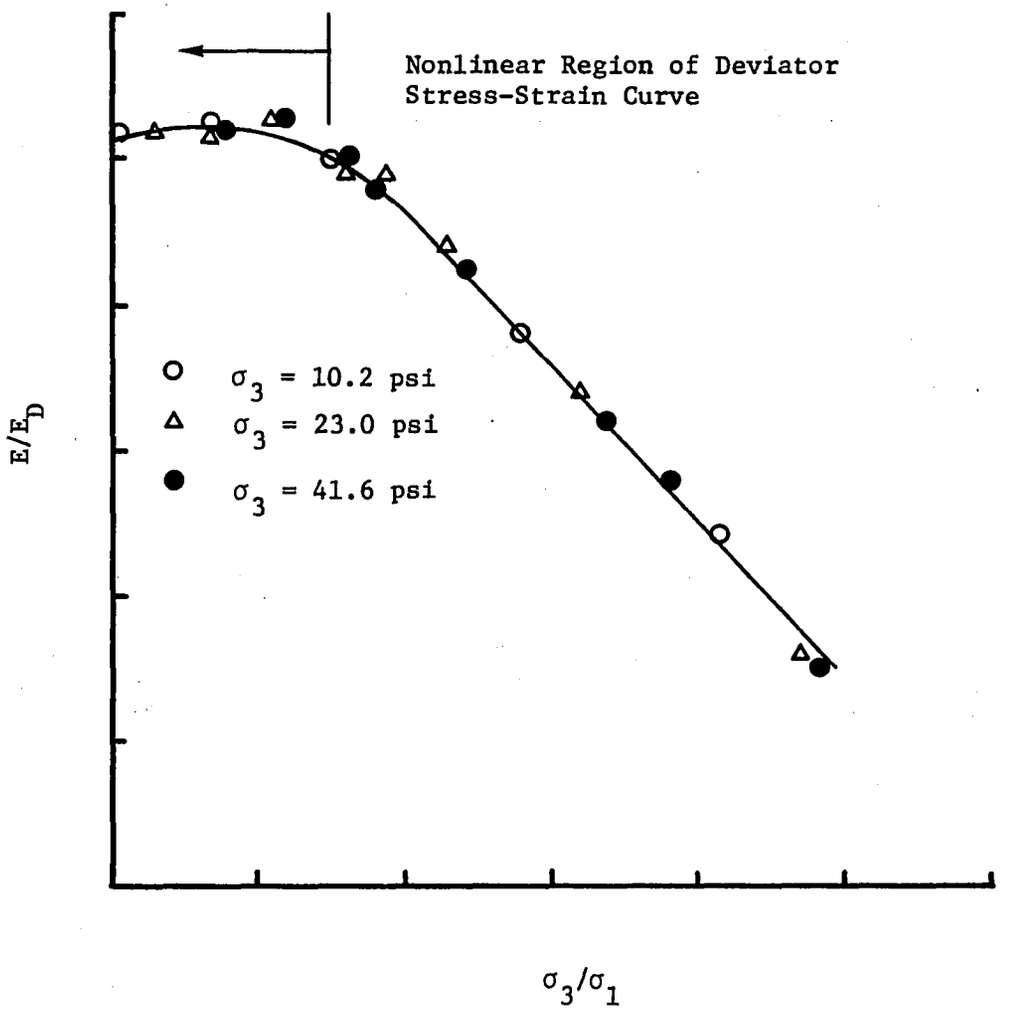


Figure 28. Theoretically derived deformation modulus

Constrained tests

$K_o$ or tests in which zero lateral strain is maintained were conducted using commercial consolidation and DR apparatus. The objective of these tests was to verify results from the experimental apparatus and determine whether deformation response is influenced by such factors as manner of load application and specimen treatment. The original 2.8 inch diameter specimen was prepared for the oedometer with a sharp trimming ring which sizes the specimen to fit the 2.5 inch diameter chamber. In the DR apparatus, the constrained test was performed by monitoring radial deformation and adjusting radial stress. Thus, the $\varepsilon_3 = 0$ condition was maintained within the limits of measurement precision or 0.02 percent radial strain.

Principal stress and strain from both tests are plotted in Figure 29. A first look at the oedometer data suggests a difference between the test modes. However, if the influence of time dependency is reduced, the results are comparable. With constant deformation rate loading of the DR apparatus, measurements relating stress to strain verge on representing an instantaneous connection between the two phenomena. In the oedometer apparatus, a constant stress is applied and deformations are monitored until they cease or become small. For this test, the first deformation was measured six seconds after increasing the load and within 10 minutes time dependent deflections ceased. Figure 29 shows what appears to be a relatively small degree of time dependency for the material. However, for the oedometer, this time dependency is accumulative and can be adjusted toward the instantaneous case by subtracting the time-dependent

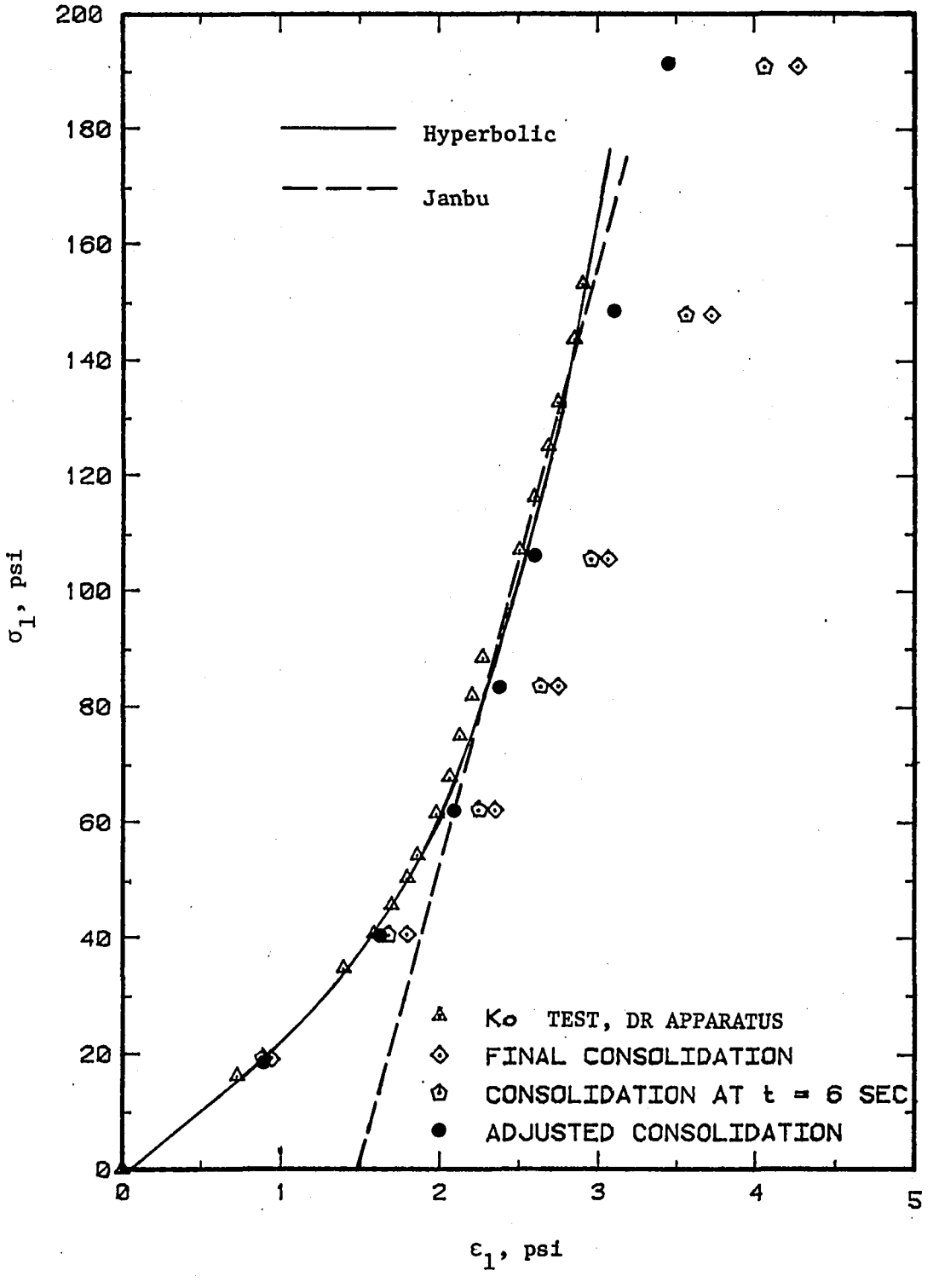


Figure 29. Constrained test results

strain components occurring at previous load levels. Such an adjustment is shown by the solid circles and agrees quite well with the stress-strain data resulting from the DR apparatus. A possible refinement in the adjustment technique would be to determine the instantaneous deformation by plotting strain versus time and extrapolating to zero time. Such a procedure should shift the consolidation data closer to the instantaneous DR results but would be as questionable as the extrapolation.

According to the system proposed by Janbu, this material would be categorized as constant modulus, $\omega = 1$, overconsolidated soil with the slope of the straight line part of the stress-strain curve defining m in equation 34 as being 10,000 psi. Since this soil has been subjected to an overconsolidation stress of about 1200 psi, this portion of Janbu's methodology seems valid. An inconsistency does arise in the interpretation of the curved part of the stress-strain plot. The stress at which the curve begins to run linear would be interpreted under the Janbu analysis as the point defining in situ vertical stress. For this soil, 70 psi represents such an in situ stress that has never occurred. Change in curvature probably has meaning relative to particulate behavior during loading. The stiffening occurring at low stress levels could be an indication of particle shifting and densification, while the constant modulus represents the influence of deformations within individual particles.

To obtain a functional relation between stress and strain, the constrained DR data were fit with a hyperbolic function proposed by Drnevich (16). The following hyperbolic relation is presumed to represent the data

$$\sigma_1 = \frac{M_i \varepsilon_1}{1 + \frac{\varepsilon_1}{\varepsilon_m}} \qquad \text{cf. Drnevich (16)} \tag{80}$$

where $M_i$ is a constant representing the initial slope of the hyperbolic curve and $\varepsilon_m$ is a constant defining the asymptotic limit. Equation 80 can be transformed to a form suitable for linear regression as

$$\frac{\sigma_1}{\varepsilon_1} = M_i + \frac{1}{\varepsilon_m} \sigma_1 \tag{81}$$

The constants $M_i$ and $\varepsilon_m$ can easily be evaluated and the constrained tangent modulus, $M_{ct}$, can be determined by taking the derivative of equation 80 with respect to $\varepsilon_1$. This results in

$$M_{ct} = M_i \frac{\varepsilon_m^2}{(\varepsilon_m - \varepsilon_1)^2} \tag{82}$$

For the work that follows, it is more convenient to express $M_{ct}$ in terms of stress rather than strain, and such a formulation can be achieved by solving equation 80 for $\varepsilon_1$ and substituting the result in equation 82. This manipulation results in

$$M_{ct} = M_i \left(\frac{\sigma_1}{M_i \varepsilon_m} + 1\right)^2 \tag{83}$$

For the constrained DR data, the regression of $\sigma_1/\varepsilon_1$ on $\sigma_1$ produced the

constants: $M_1$ = 16.88 and $\varepsilon_m$ = 4.22. $R^2$ was 0.9931 and CV was 2.2 percent. Results of the hyperbolic fit are drawn in Figure 29.

An alternative way of viewing the results of the constrained test is through the relations occurring between major and minor principal stresses on a p-q plot. Results of the DR apparatus constrained test are presented in Figure 30. A linear regression for the data with the point at the origin being omitted, resulted in an intercept of 3.3 psi and a slope of 0.5278. For comparison, the empirical relations for at-rest earth pressure proposed by Jaky (equation 35) and Brooker and Ireland (equation 36) are also plotted for $\phi$ = 34.8 degrees. At first glance, there appears to be a sizeable disparity between the results obtained from this research and previous work. The $K_o$ line for the loess has a steeper slope, and the regression suggests an intercept or an upward positional translation. In terms of stress transfer capacity, the position of the experimental $K_o$ line means the loess is capable of transferring a smaller proportion of its axial stress to the radial direction than materials described by the classical relations. Actually, the regression intercept probably represents nothing more than an operational parameter, useful for describing the data points occurring beyond the first measurement. The dashed line in Figure 27 seems a more logical stress path.

One way to evaluate the results shown in Figure 30 is to presume that particulate displacement occurring during constrained loading is resisted by inter-particulate sliding friction and not dilation. Using energy principles, Newland and Allely (48) showed that the internal

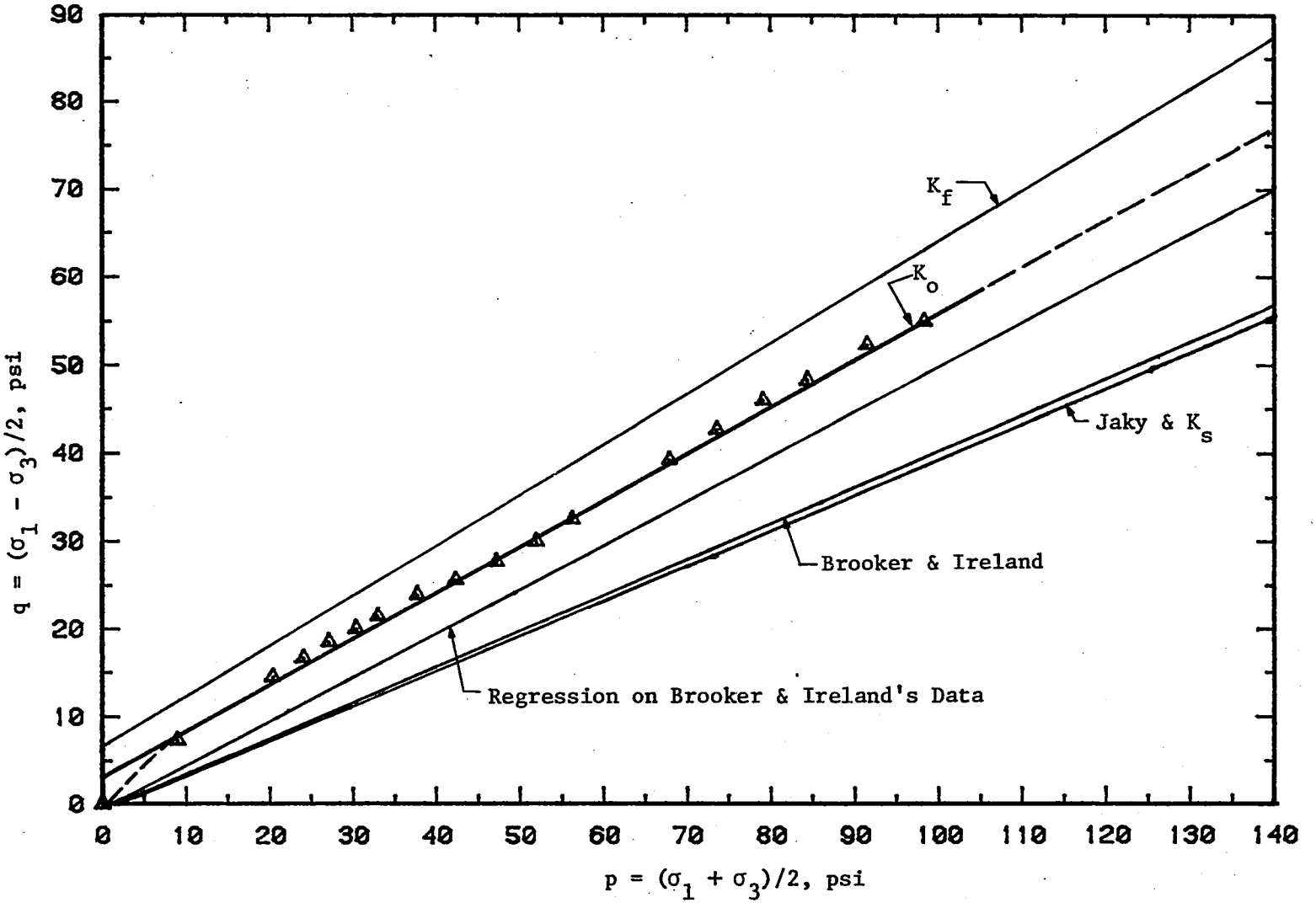


Figure 30. Analysis of at-rest earth pressure

friction angle of a dilatant soil could be separated into a sliding friction component, $\phi_s$, and an overriding component, $\theta$ which relate to friction angle by

$$\phi = \phi_s + \theta \quad \text{cf. Spangler and Handy (58)} \tag{84}$$

where

$$\tan \theta = \frac{dV}{d\Delta} \quad \text{cf. Spangler and Handy (58)} \tag{85}$$

in which $dV/d\Delta$ represents the slope of the height-displacement curve from a direct shear test. For the 1.73 inch high specimens used in the direct shear results presented in Figure 21 an average value for $dV/d\Delta$ is 0.190. This means $\theta = 10.8^{\circ}$ and $\phi_s = 24^{\circ}$. Lambe and Whitman (41) report sliding friction angles for soil components as ranging between 8 to 34 degrees, depending on surface moisture conditions and mineralogical composition. Thus,the 24° measured for this material is not unreasonable. Transformation of the sliding friction angle to the p-q plot can be accomplished with equation 5a producing the following result

$$\tan \alpha = \sin 24^{\circ} = 0.41$$

When plotted on Figure 30, the sliding friction slope, designated as the $K_s$ line, coincides with Jaky relation. Thus,if separation of frictional and overriding components by Newland and Allely's method is valid, the Jaky relation used for this material represents stress transfer by

sliding friction.

Jaky's relation as presented in the English language literature was taken from a 1948 publication (34) devoted to pressure in silos where equation 35 is presented without proof. Thus, many have apparently taken the equation to be of empirical origin. The actual development is presented in an earlier paper (33) written in Hungarian. Although the development was difficult to follow, it seems that 1 - sin $\phi$ represents an approximation to a theoretical derivation based on the angle of repose for granular materials. Since $\phi$ is known to be very much a function of void ratio and since granular materials when dumped into a pile defining the angle of repose usually find themselves in a loose state, the shear strength under such conditions should not include a dilatant component. Thus, the essence of Jaky's relation is stress transfer in a medium characterized by sliding friction.

The truly empirical relation proposed by Brooker and Ireland for cohesive soils should be more consistent with the loess used in this study. As can be seen in Figure 30, there is actually very little difference between the Brooker and Ireland and Jaky relations. The suitability of Brooker and Ireland's equation was questioned because it was developed from tests on materials having much lower friction angles than the loess. Also,there seemed to be considerable amount of scatter in the data presented in reference 6. Thus,as a matter of interest, a regression of $K_o$ on sin $\phi$ was performed with the original data to determine whether variability could be an explanation for difference between the

two sets of data. The surprising result obtained from Brooker and Ireland's data is that a regression produced the relation

$$K_o = 1 - 1.17 \sin \phi \tag{86}$$

which plotted in terms of p and q is significantly different than the original equation. In fact, if the intercept were excluded, the experimental results obtained from the present research is in close agreement with the results obtained by Brooker and Ireland. The data used in the regression for equation 86 are presented in Table 16. The squared correlation coefficient was found to be 0.9412, which is much higher than expected.

Table 16. At rest earth pressure data after Brooker and Ireland (6)

| Material | $K_o$ | $\phi$, degrees | sin $\phi$ |
|---|---|---|---|
| Bearpaw shale | .70 | 15.5 | 0.2672 |
| London Clay | .67 | 17.5 | 0.3000 |
| Weald Clay | .54 | 22.0 | 0.3746 |
| Chicago Clay | .47 | 26.3 | 0.4431 |
| Goose Lake Flour | .50 | 27.5 | 0.4617 |

Inter-particulate cohesive shear resistance which would be additive to sliding shear components is at least one reason why cohesive soils display an ability to transmit less axial stress in the radial direction than do materials possessing sliding friction alone. Cohesion in the

materials used by Brooker and Ireland was destroyed by pulverization, and the field conditions simulated by their tests should be the natural deposition process for normally consolidated materials. It may be postulated that as stress was applied to the cohesive soil, bonds at particle contacts were created as a result of high localized normal stress. These bonds were then available to resist stress transfer by mechanisms similar to that of sliding friction. The material used in this research possessed an intrinsic strength which might be thought of as an additional constant additive component to shear resistance which operates in conjunction with new bonds, created during the reloading process. The constant cohesive component is manifested as the intercept observed in the p-q plot. The fact that the constrained intercept is less than that for maximum strength can be attributed to limited relative particulate displacement allowed under constrained conditions.

An accurate assessment of at-rest earth pressure is important to many aspects of geotechnical design. As previously described, the stress path method depends on $K_o$ relations to reestablish in situ stress. Also, application of the finite element method requires an initial stress definition as a starting point for incremental analysis. It seems that the empirical relation previously established for cohesive soil could be a partial cause for prediction errors for methods depending on $K_o$. For this research, definition of the $K_o$ line is important because it places limits on the results of deformation restraint tests. Since $k = \infty$ in the restraint function also represents the $K_o$ line, and if the soil being

tested cannot achieve strengths greater than that defined by conventional tests, the results of deformation restraint tests should fall within the rather narrow band established by the $K_f$ and $K_o$ lines.

As for stress and strain, an empirical functional relation for stresses occurring under constrained conditions will be useful for analysis of k-path results. Figure 31 represents the results of a slightly different form of a hyperbolic fit suggested by Duncan and Chang (19). In this case, the ratio of at-rest earth pressures, $K_o = \sigma_3/\sigma_1$ is expressed as a function of $\sigma_1$ in the following manner

$$K_o = \frac{\sigma_1}{g + h\,\sigma_1} \qquad \text{cf. Duncan and Chang (19)} \qquad (87)$$

Equation 87 can be rewritten in a linear form as

$$\frac{\sigma_1}{K_o} = g + h\,\sigma_1 \qquad (88)$$

which is conducive to linear regression. Results of such a regression defined the constants g = 97.8 and h = 2.88. Statistical measures on the regression are: $R^2 = 0.9891$ and CV = 4.8 percent.

## Deformation Restraint Tests

Having established standards for ultimate strength, deformation properties, and volumetric behavior under the influence of constant confining stress, this portion of the experimental evaluation is devoted to

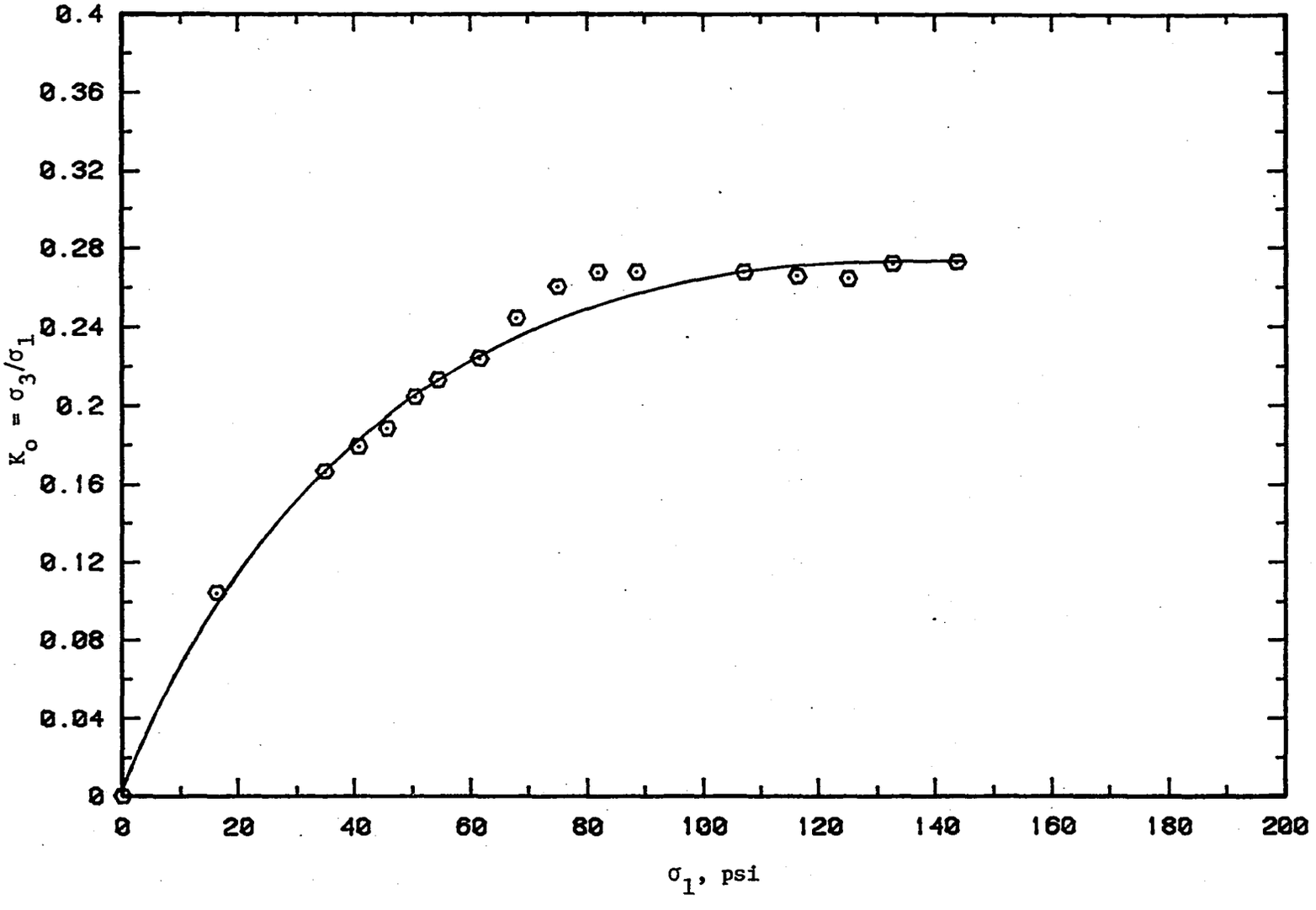


Figure 31. Hyperbolic fit for stresses measured under constrained conditions

observing soil behavior subjected to boundary conditions defined by the restraint function given in equation 54. First, an attempt is made to experimentally define a restraint constant, k, which produces ultimate strength. With a yield strength k established, the significance of restraint can be evaluated by systematically changing its value.

Shear strength

Figure 32 shows the results of a test performed such that failure stress conditions defined by conventional procedures were forced to prevail. The specimen was hydrostatically consolidated, taken to ultimate strength by reducing confining stress, and then forced along the $K_f$ line. This test is similar to a staged test but has the distinction of not developing excessive strain thought to influence cohesion. Since this $K_f$ test defines limiting strength, the radial stress-strain relation could represent a unique restraint function. Figure 33 is a plot of the radial stress-strain relation resulting from the $K_f$ portion of the test. The curve is linear up to $\sigma_3$ = 20 psi and is strikingly similar to the axial stress-strain response for two of the unconfined tests. The slope of linear portion of the radial stress-strain response was determined to be 1159 psi, and this value will be taken to define k in the single parameter restraint function.

Results of tests in which k was arbitrarily set between 200 and 12,000 psi are shown in Figures 34 a-f. A comparative reference is provided through the $K_f$ and $K_o$ lines, and the position for average unconfined strength is shown with the large dot. Within reasonable bounds of

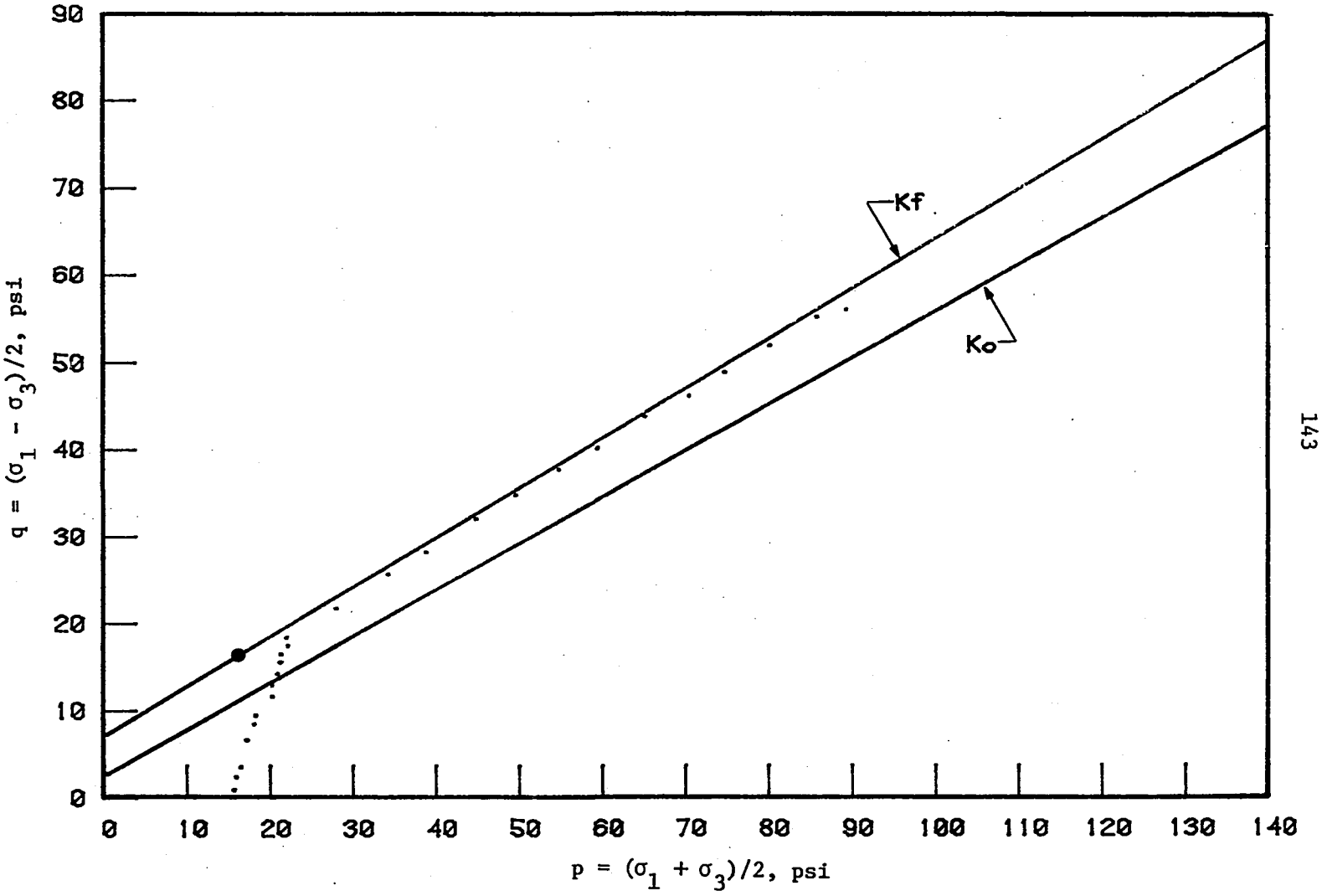


Figure 32. Ultimate strength stress path

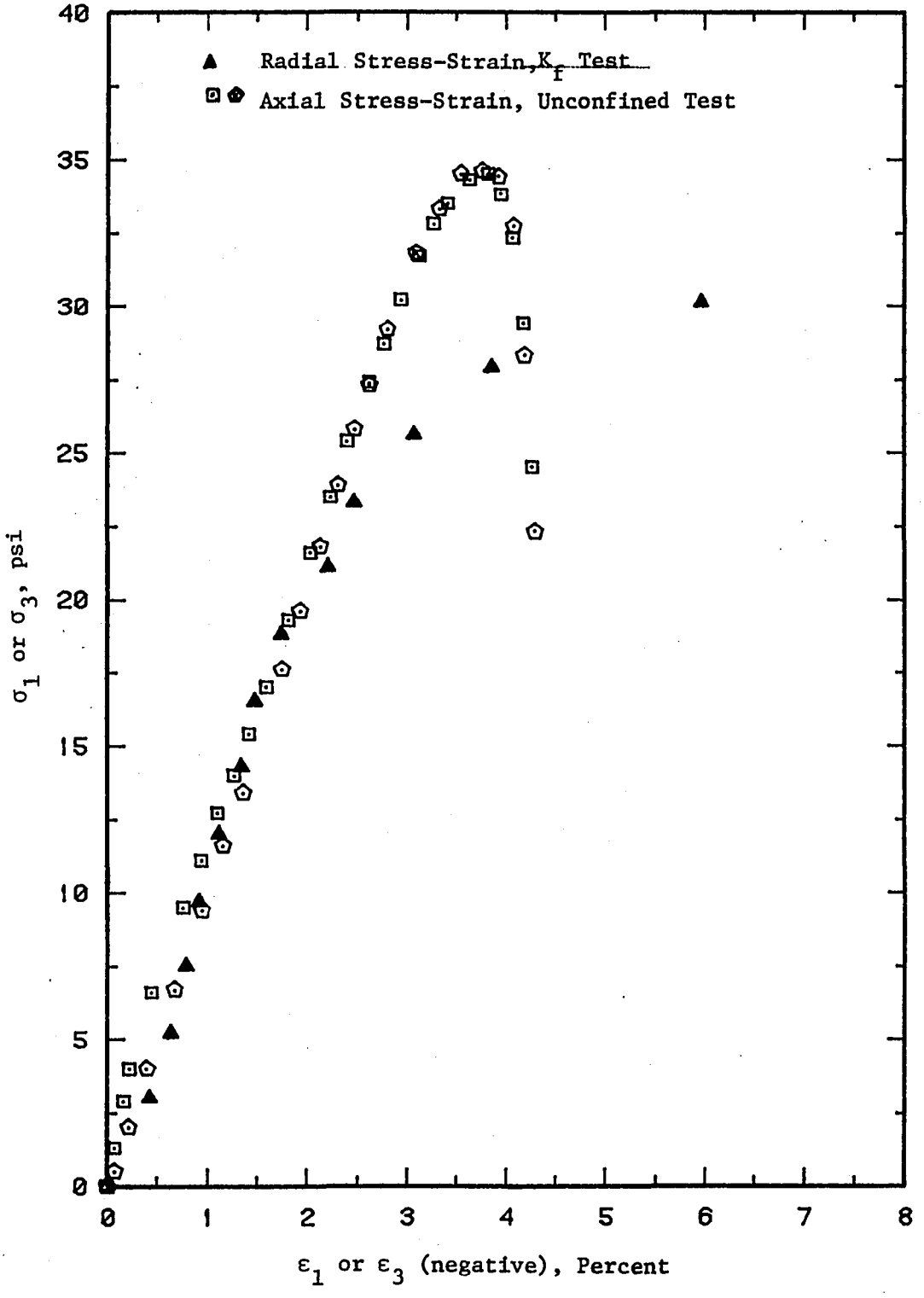


Figure 33. Restraint relation from $K_f$ test

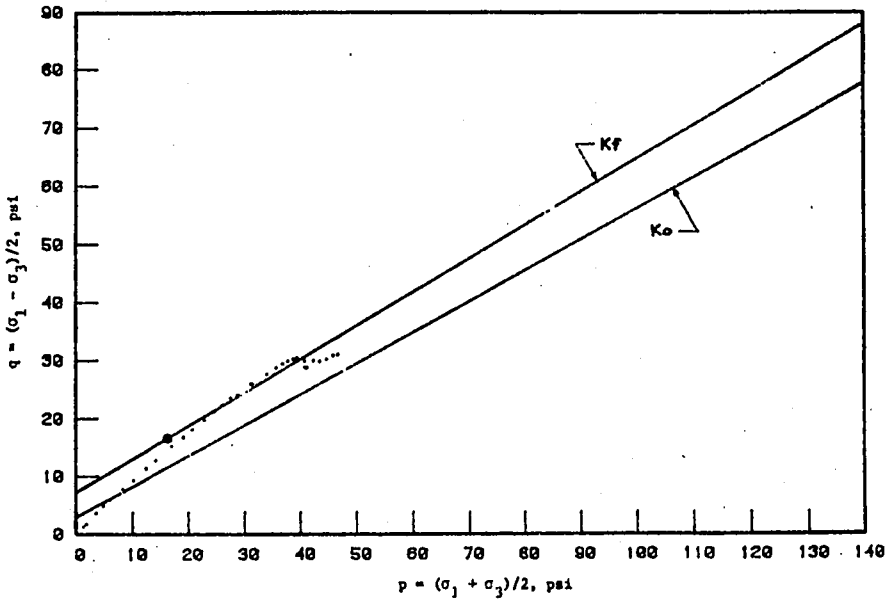


Figure 34a. Deformation restraint test, k = 200 psi

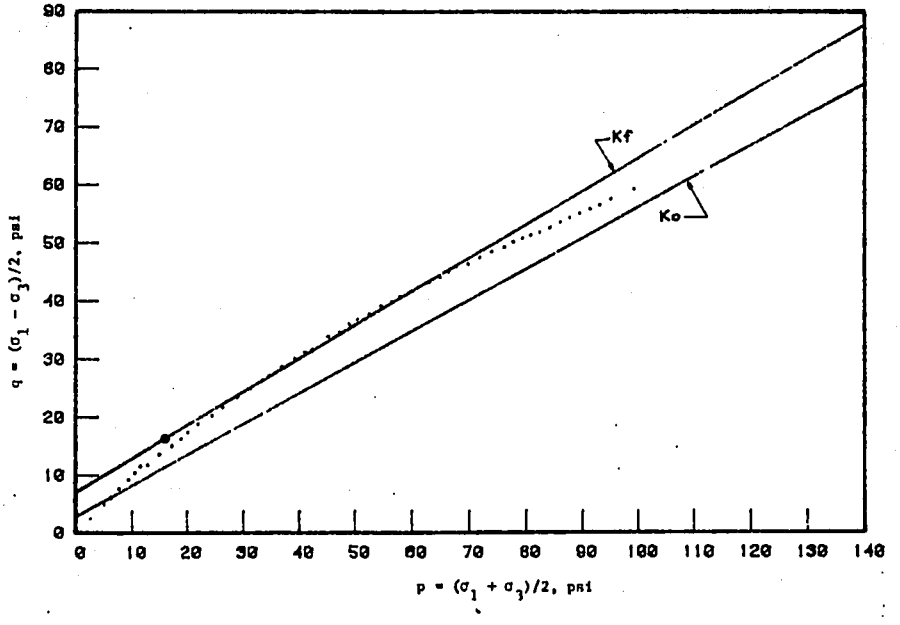


Figure 34b. Deformation restraint test k = 600 psi

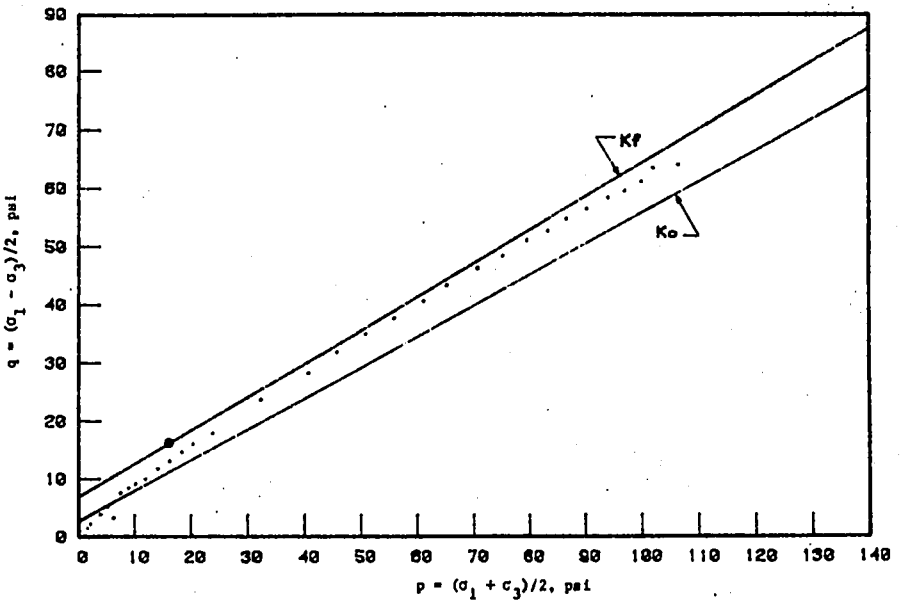


Figure 34c. Deformation restraint test, k = 1159 psi

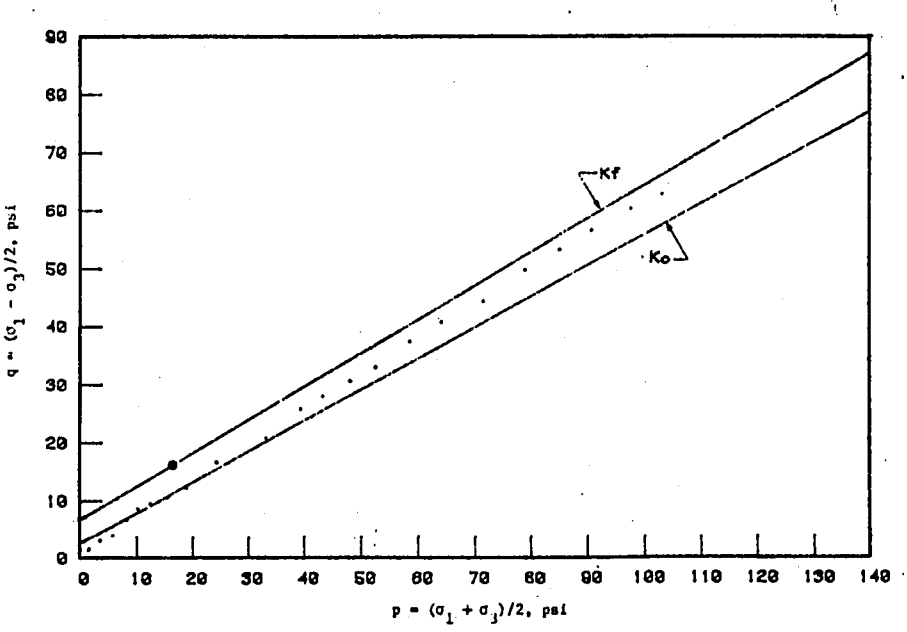


Figure 34d. Deformation restraint test, k = 3000 psi

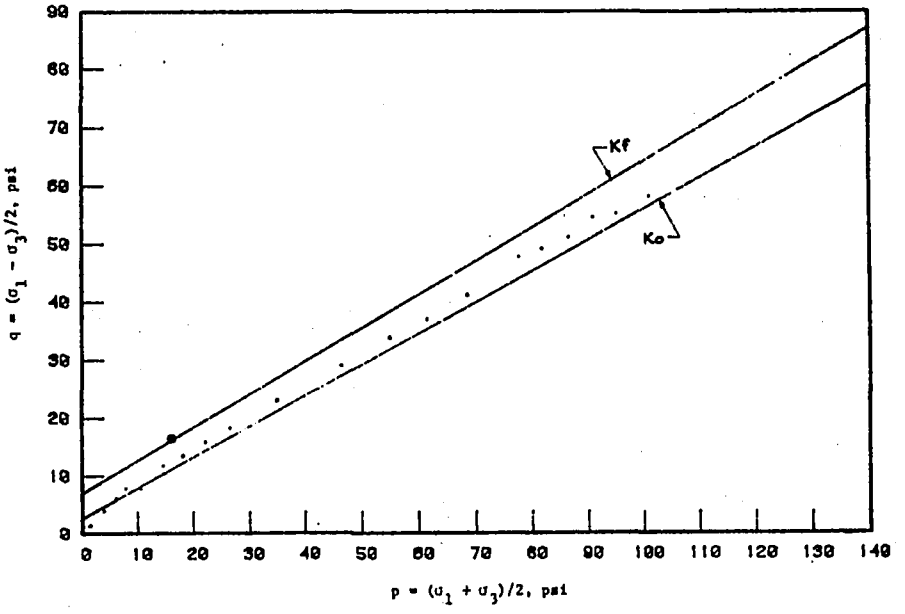


Figure 34e. Deformation restraint test, k = 5,000 psi

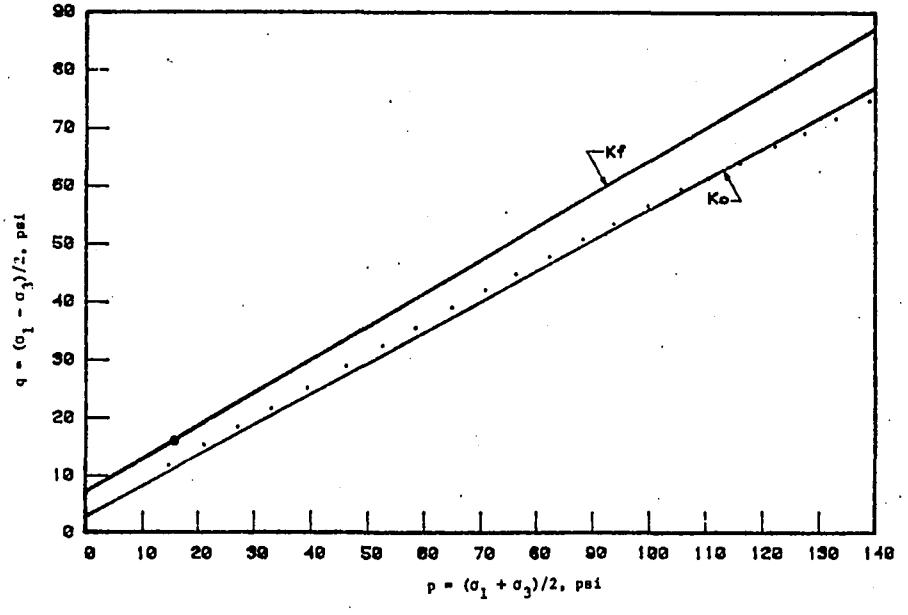


Figure 34f. Deformation restraint test, k = 12,000 psi

experimental error, the stress paths developed for all k values selected were confined to the region defined by $K_f$ and $K_o$ lines. For k = 200 psi and 600 psi, the stress path ran along a 45 degree line until the unconfined strength was reached, followed the $K_f$ line, and then fell below the limit for conventionally defined ultimate strength. In view of the observation that this soil is sensitive to loss of cohesion during staged testing, divergence from the $K_f$ line could also be the result of cohesion loss due to the excessive strain permitted by small restraint constants. As k was increased, the resulting stress paths shifted from the $K_f$ to the $K_o$ line with results from the k = 12,000 psi test falling on the constrained stress path. The restraint constant for the stiff Iowa K-Test mold happens to be 12,000 psi and k for the commercial model is about 230 psi.

Although the stress path fell slightly below the $K_f$ line, the test where k was set at 1159 psi produced the best estimate of ultimate shear strength of the entire set of tests. Slight disagreement with the $K_f$ line could easily be due to sample variation, but the important result is that the stress path did not systematically diverge below the $K_f$ line as the test progressed. This suggests that there may exist a unique restraint constant which limits radial strain such that the net loss in cohesion is not measurable.

Accuracy of the deformation restraint tests in predicting ultimate strength of the soil can be evaluated by performing a least squares regression on the p-q data. The regression coefficient can then be

transformed to c and $\phi$ as was done for the constant $\sigma_3$ tests. Table 17 is a summary of these regressions performed after deleting data points which are not pertinent to the failure criterion. For example, points occurring at stresses below the unconfined strength should not be included because the material has not failed. Also, the points falling below the $K_f$ line in the k = 200 test, Figure 34a, could logically be omitted on the basis of recognizing the mechanism of lost cohesion.

Table 17. Summary of strength parameters from deformation resistent tests

| Test Description | n | a psi | tan $\alpha$ | c $\pm$ s psi | $\phi \pm$ s degrees | $R^2$ | CV |
|---|---|---|---|---|---|---|---|
| k = 200 psi | 13 | 5.6 | 0.6410 | 7.3±0.4 | 39.9±0.8 | 0.9951 | 1.0 |
| k = 600 psi | 40 | 10.0 | 0.5109 | 11.6±0.5 | 30.7±0.4 | 0.9927 | 2.3 |
| k = 1,159 psi | 18 | 6.8 | 0.5485 | 8.2±0.5 | 33.3±0.4 | 0.9976 | 1.3 |
| k = 3,000 psi | 13 | 2.0 | 0.5328 | 2.4±0.5 | 32.7±0.4 | 0.9986 | 1.3 |
| k = 5,000 psi | 11 | 6.5 | 0.5148 | 7.6±1.4 | 31.0±1.0 | 0.9880 | 2.3 |
| k = 12,000 psi | 23 | 5.6 | 0.5043 | 6.4±0.3 | 30.3±0.5 | 0.9988 | 1.5 |

The regression statistics, $R^2$ and CV in Table 17, look good for all of the tests but there obviously exists quite a range in c - $\phi$ parameters. Although c and $\phi$ are used to determine strength in design equations, their ultimate purpose is to define shear strength at specific normal stress levels. Thus, a more direct way of assessing the accuracy of deformation restraint tests is to compare shear strengths as expressed in equation 4.

Using composite conventional test c - $\phi$ values from Table 13 to determine a base strength, $\tau_b$, and computing the ratio $\tau/\tau_b$ where $\tau$ is the shear strength based on deformation restraint test parameters, a relative measure of shear strength varying with normal stress can be established. The results of such computations are shown in Figure 35. The limiting boundaries are established by $\tau/\tau_b = 1$ and the line labeled as $K_o$. One observation which can be made from Figure 35 is that shear strength can be overestimated by a factor of about 1.2 when k is set at 600 psi or less. This rather significant error can be due to two causes. First, in the k = 200 psi test, Figure 34a, few points actually fell on the $K_f$ line, and the regression interpretation was significantly influenced by points occurring between the unconfined cutoff and the $K_f$ line. For the k = 600 psi test, Figure 34b, the gradual loss of strength occurring when p was greater than 70 psi produced a high c and low $\phi$ which resulted in strength overestimated for $\sigma_n$ less than 30 psi.

When k was 1159 psi or greater, estimates on strength were conservative, and with the exception of the k = 3000 psi test, the results were consistent with the $K_o$ limit. Obviously, a conservative strength estimate for this soil could be achieved by arbitrarily setting k at a large value and as long as normal stress is also large, the conservatism for this soil should be limited to about 0.8 times the base strength. However, in many geotechnical applications, the appropriate normal stress range is determined by the unit weight and depth of the soil. To illustrate, from the geometry of the classic bearing capacity solution,

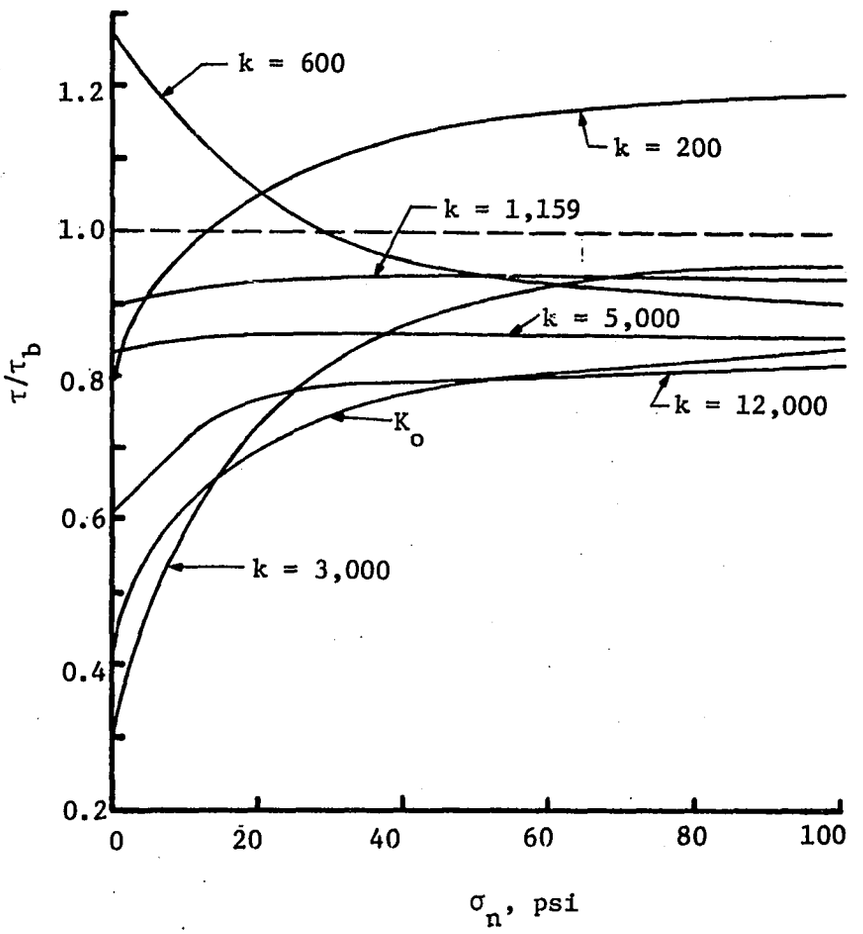


Figure 35. Shear strength comparison

the maximum depth of influence is roughly the width of the footing. Thus, for a 20 foot wide footing on 100 pcf soil, normal stress on portions of the rupture surface would be on the order of 15 to 20 psi. The only test results providing consistently reasonable estimates at low normal stress levels are from the k = 5000 and k = 1159 psi tests. Obviously the restraint function corresponding to the unconfined stiffness, k = 1159 psi, provides the best estimate for shear strength. At $\sigma_m$ = 20 psi shear strength is within 6 percent of the base value.

Use of the unconfined deformation properties of a soil to establish a restraint function, which produces acceptable measures of shear strength, has important practical significance. If such a procedure were valid, it should be possible to define the appropriate restraint constant for a specimen by evaluating the slope of the axial stress-strain data prior to failure, and then applying the stiffness defined by $E_u$ as restraint. As an additional experimental check on the validity of using axial unconfined deformation properties to define restraint functions, a second test was performed. In this test, however, an attempt was made to include the influence of minor loading nonlinearity and decrease in strength occurring after yield as typically displayed in Figure 18. The composite axial stress-strain data was regressed on all possible iterations of a third order polynomial with the best fit based on $R^2$ being the equation

$$\sigma_1 = 7.39\ \varepsilon_1 + 1.76\ \varepsilon_1^2 - 0.43\ \varepsilon_1^3 \qquad (89)$$

By arbitrarily setting $\sigma_3 = \sigma_1$ and $\varepsilon_3 = \varepsilon_1$, in equation 89, and treating expansive radial strains as positive, the unconfined restraint stress path results shown in Figure 36 were obtained. The results are slightly better than the k = 1159 psi test. The cluster of points occurring at the end of the test resulted from the restraint decrease resulted from the unstable portion of the unconfined tests.

To evaluate the performance of the stiff Iowa K-Test mold, a Proctor sized specimen of loess was tested. The results of this test are also shown in Figure 36. Obviously, the k = 12,000 psi mold provides a good estimate of a $K_o$ stress path.

Deformation properties

Stress-strain results for selected deformation restraint tests are shown in Figure 37. As both the elastic and plastic theories predict, deformation is systematically and significantly influenced by the degree of restraint. As might be expected, the experimental results support the theoretical contention that as radial restraint increases, so do axial deformation properties. For the soil tested and the range of restraint constants used, estimates of $E_D$ for the straight line portion of the deviator stress versus axial strain curves range from 1250 to 6650 psi. Since deformation predictions are linearly related to the modulus, arbitrary selection of a restraint function could result in more than a fivefold difference in predictions.

An interesting feature of the fan-shaped curves in Figure 37 is that for deviator stresses less than 25 psi, the stress-strain behavior for

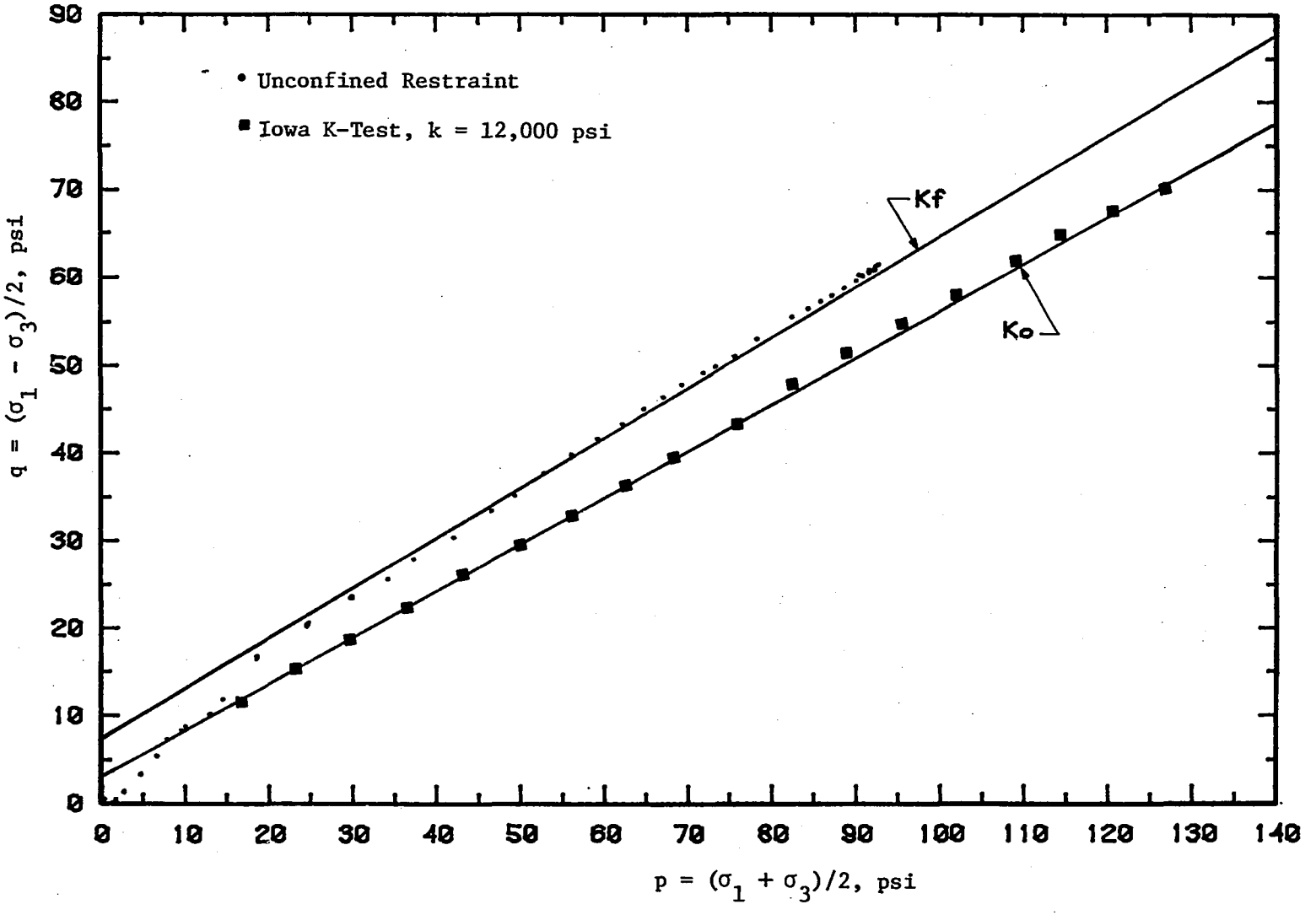


Figure 36. Unconfined restraint and Iowa K-Test

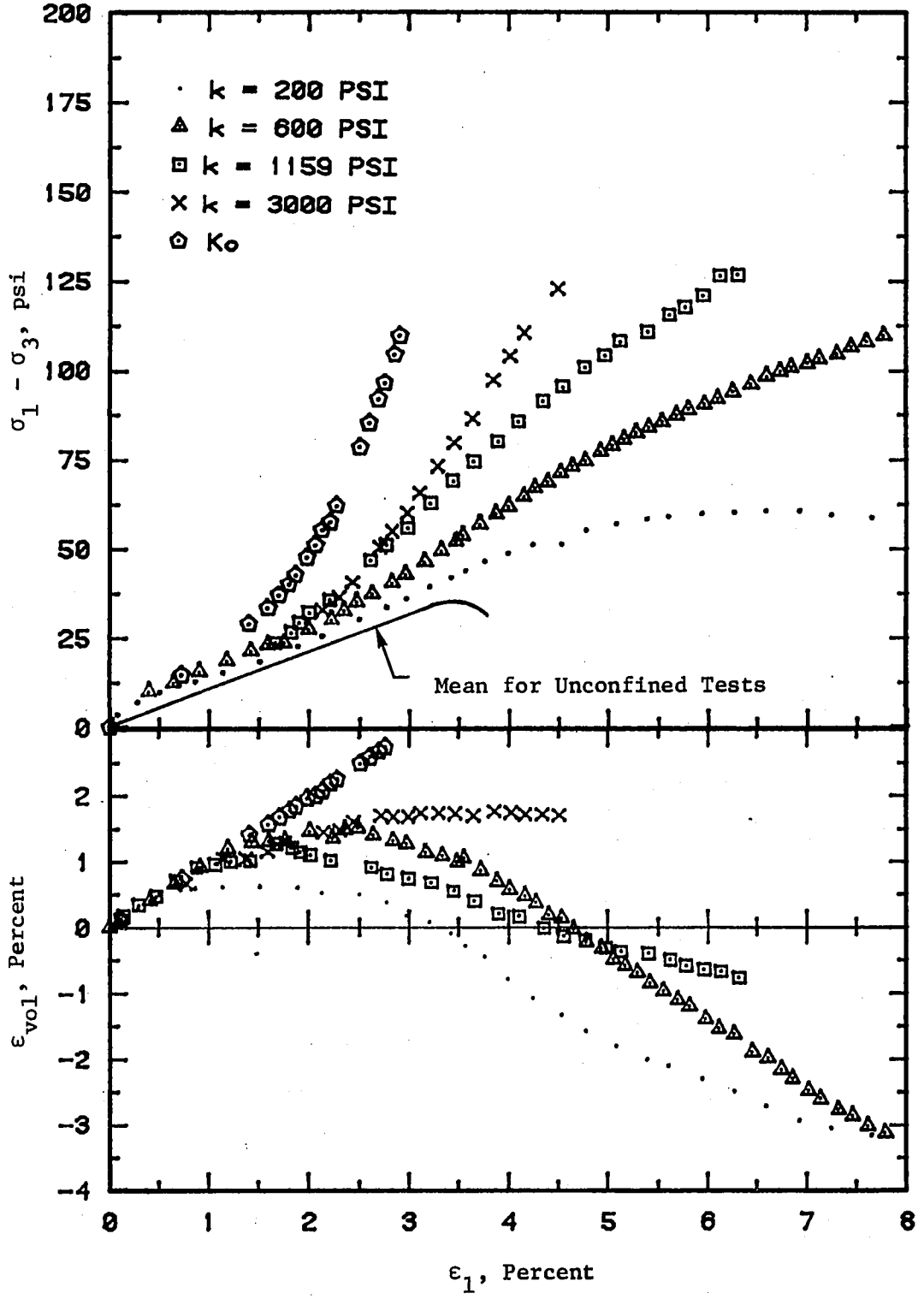


Figure 37. Typical stress-strain response for deformation restraint tests

all specimens is nearly identical and close to that for the average unconfined tests. This is because lateral displacement during the early phases of the test were either zero or very small, producing no requirement for radial stress as stipulated by the restraint function. This is consistent with the zero or small lateral strains measured in the unconfined tests at low axial loads.

Volumetric behavior displayed in the lower part of Figure 37, shows that degree of restraint dictates whether the material undergoes compression or dilation. Total restraint produced volumetric compression while k = 3000 psi produced volumetric compression until axial strain reached 2 percent. Beyond this value, volume was constant. Restraint constants at levels less than what have previously been determined as allowing failure (e.g. k = 1159 psi) produced initial compression followed by dilation.

The initial compression can be explained by the specimen capacity of undergoing axial strain without appreciable radial expansion. However, the dilatant or negative sloped portions of the curves could be significant in defining the restraint constant which produces the best estimate for limit strength conditions. The k = 200 and k = 600 psi dilational slopes are approximately the same at 0.8, but when k was 1159 psi, the resulting slope was about 0.40. Since the theory proposed by Drucker stipulates a relation between volumetric strain and failure criterion, the fact that dilation is different for the k = 1159 psi case might be useful in defining restraint conditions producing an ultimate

strength stress path not influenced by loss of cohesion. Intuitively, this seems possible because excessive dilation could cause disruption of cohesive bonds.

Strain ratios measured from the deformation restraint tests are plotted in Figure 38. Many features evident in this representation are corollary to observations from the volumetric strain plot. However, it is interesting to note that strain ratios for the k = 200 psi and k = 600 psi deformation restraint tests are of about the same magnitude as occurred in the constant confining stress tests, using the same apparatus. Suppression of radial strain with increasing k is also evident.

Theory and experimental results

Since the elastic and plastic theories have been developed in terms of major principal stress and strain, the deformation restraint data are plotted in this format in Figure 39, to facilitate a comparison to theory. An obvious difference between the experimental results and the stress-strain relation developed from the elastic constitutive law is the inflection point occurring near $\sigma_1$ = 25 psi. Equation 58 predicts an increase in apparent modulus with an increase in k, but it also infers straight radial lines passing through the origin.

Computed values of $\nu$ and E resulting from selected deformation restraint tests are plotted in Figures 40 and 41. Poisson's ratio was computed from equation 79 and shows a systematic dependence on k when plotted against the ratio of principal stresses. As with the constant confining stress tests, theoretical values for Poisson's ratio are not

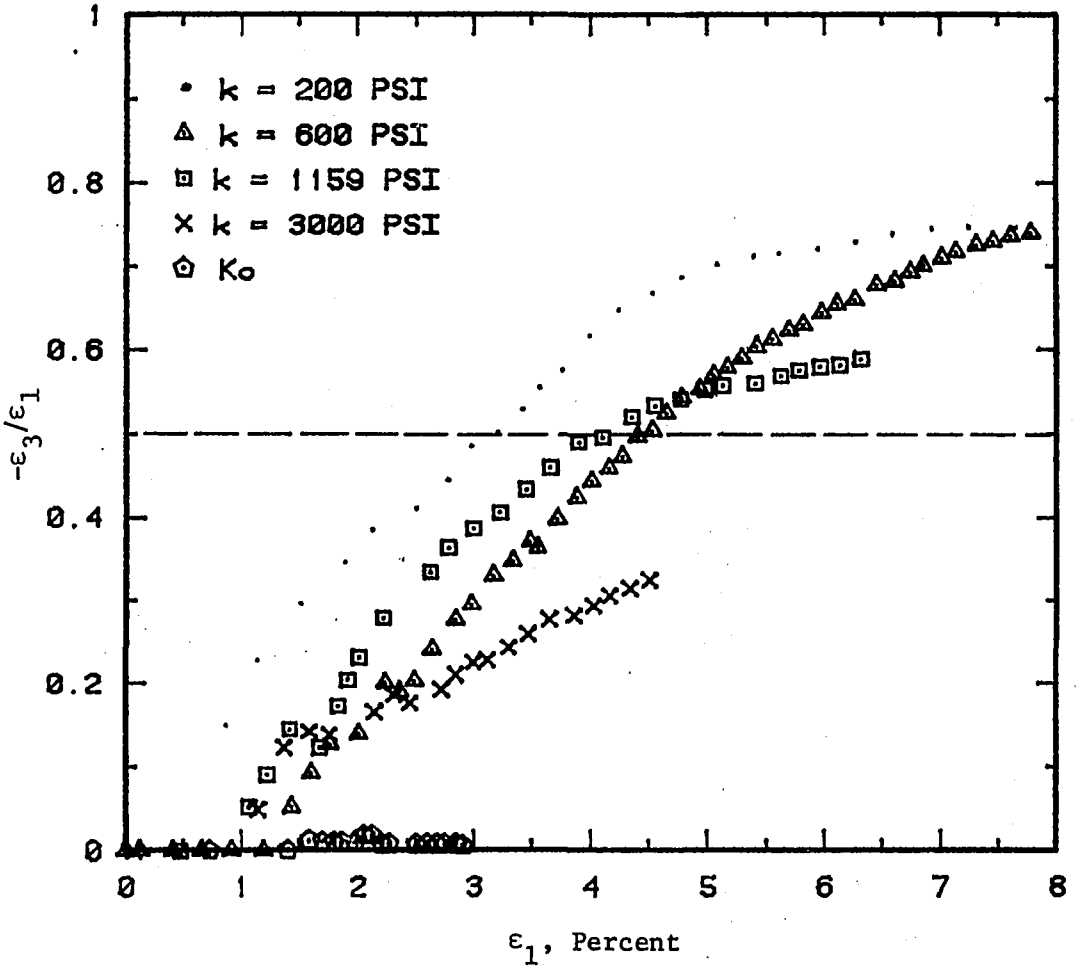


Figure 38. Strain from deformation restraint tests

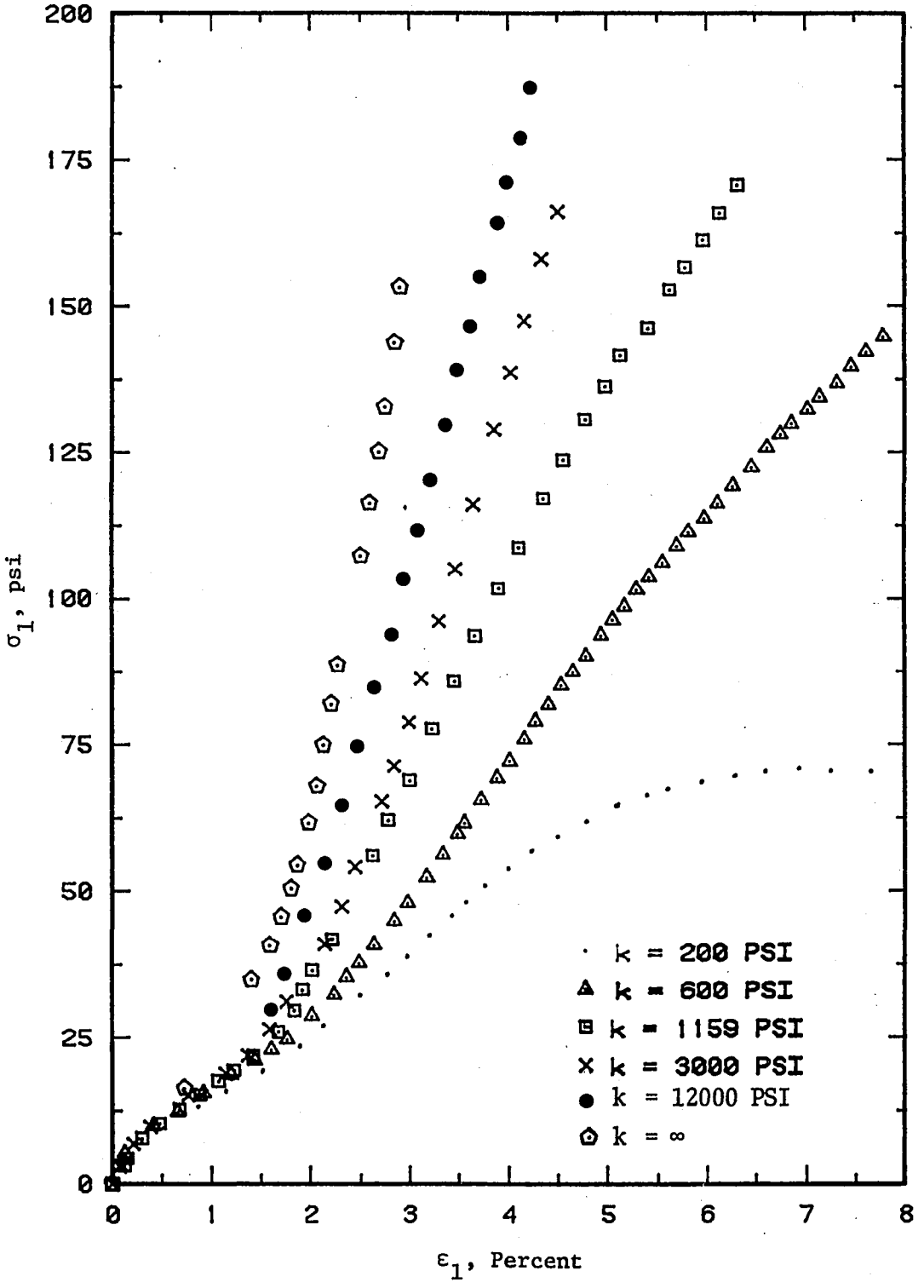


Figure 39. Axial stress-strain for deformation restraint tests

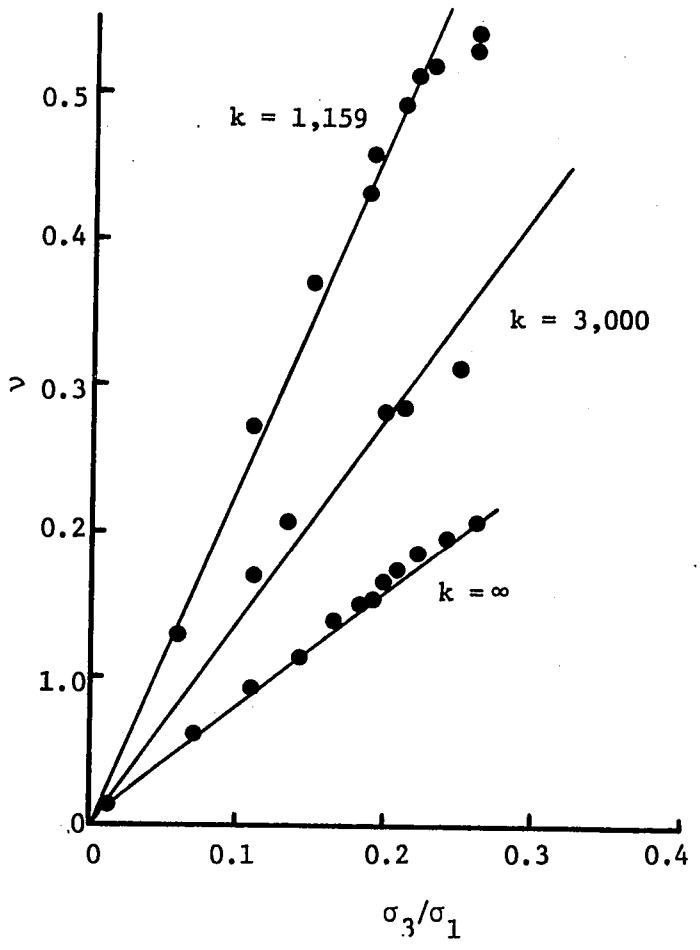


Figure 40. Poisson's ratio from deformation restraint tests

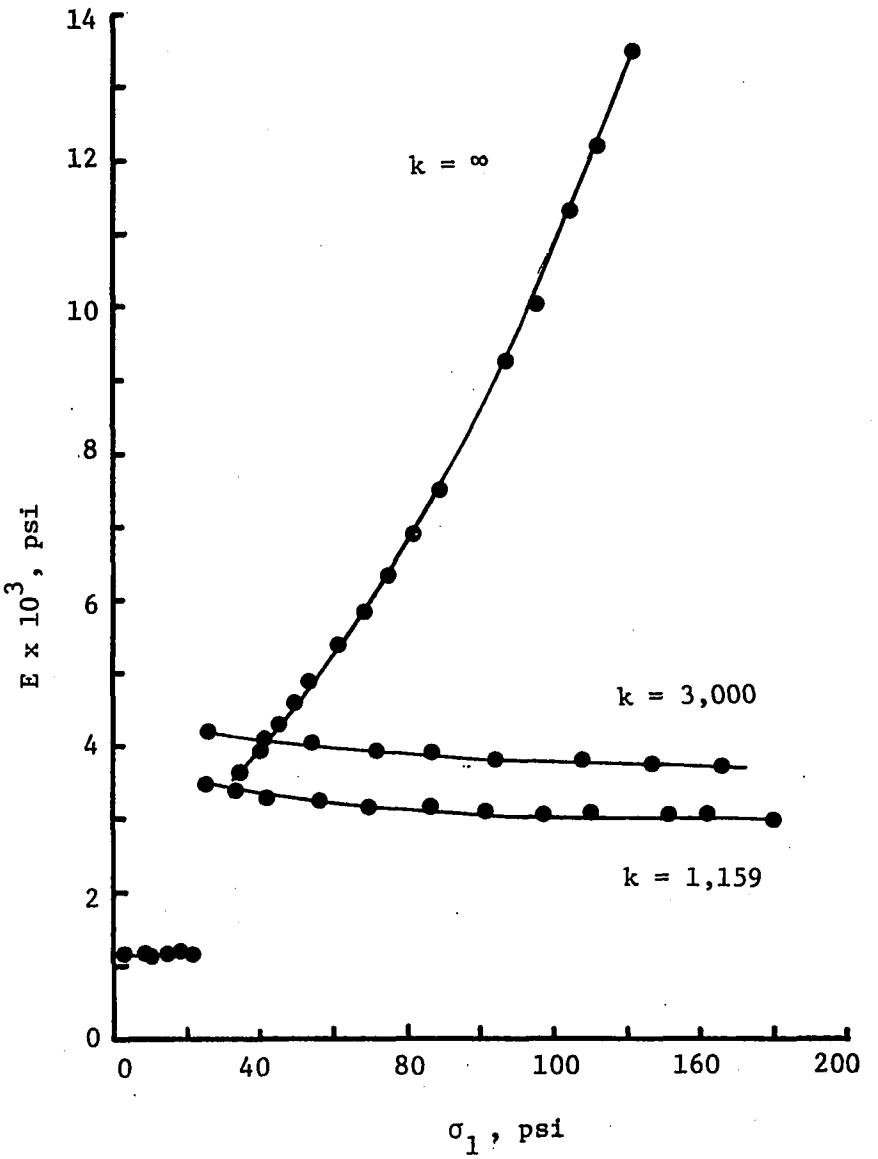


Figure 41. Theoretical modulus from deformation restraint tests

in excessive violation of the $\nu \leq 0.5$ requirement of elastic theory. Values for E were computed by extracting the positive root of the bracketed term of equation 58 which was set equal to the restrained moduli measured from Figure 39. Common for all k's is a constant E when $\sigma_1$ was less than 25 psi. This is a reflection of $\varepsilon_3$ thus k and $\sigma_3$ being equal to zero during early stages of the tests. Under these conditions, the computed restrained modulus is identical to the slope of the axial stress-strain relation. For stresses above 25 psi, it is obvious that E is highly dependent on k with the greatest values occurring for constrained conditions. If the material were truly elastic, E would be constant at a value defined by unconfined tests. Thus,the results shown in Figures 40 and 41 verify the stress dependency of the deformation parameters, and the need for associating these parameters with the appropriate stresses if elastic theory is to be used to approximate soil behavior. This factor has been recognized in the formulation of constitutive laws from numerical solutions such as the finite element method and should also be important to the application of less rigorous prediction techniques such as stress path and the proposed k-path.

At least in concept, the stress-strain relation developed from Drucker's hypothesis is consistent with the experimental results in Figure 39 in that it allows a bilinear deformation response. Plastic strain occurring after yield is defined by the second term in equation 64. The axial stress-strain relation occurring prior to yield should be that of an unconfined specimen. The common initial slope in Figure 39 is about

1170 psi while the average unconfined modulus is 909 psi. In part, the difference in slopes can be explained by a 2 psi radial seating stress applied to the specimens prior to conducting the deformation restraint tests. The influence of radial stress on modulus, summarized in Table 14, indicates that 2 psi confinement results in a 200 psi increase in stiffness. Thus, the initial part of the deformation restraint tests should be on the order of 1109 psi. Specimen variability could account for the remaining difference.

If Drucker's postulate is correct, the relationship established by equation 64 should hold when the material has failed but undergoes plastic deformation under the influence of elastic restraint. The stress path representation for deformation restraint results in Figure 34 and Table 17 suggest that a unique restraint value defining failure conditions may exist when k = 1159 psi. If this restraint is unique, equation 64 states a relationship exists among k, $\alpha_f$ or $\phi$, and the slope of the plastic stress-strain curve. To check the validity of this hypothesis, $\alpha_f$ and the theoretical slope can be computed from equations 9 and 64 for each restraint and $\phi$ parameter established for the deformation restraint tests. If the material undergoes constrained plastic flow under the conditions established by Drucker's hypothesis, computed slopes should be the same as those resulting from the experiments. Results of such an analysis are in Table 18 where the measured slopes were taken from Figure 39. For the k = 200 psi test, a linear approximation representing the portion of the curve between 2 and 5 percent axial strain was used. The last

column of Table 18 shows the best agreement between computed and actual slopes does occur when k = 1159 psi, suggesting that $\phi$ = 33.3° and k = 1159 psi are the best parameter combinations producing results consistent with the theory.

It is not surprising that results from the k = 3,000 and k = 12,000 psi tests were not in agreement with the theory because the material is not in failure. However, the p-q representations in Figures 34a and b suggest that at least for part of these tests, specimens subjected to

Table 18. Analysis of plastic theory

| k (psi) | $\phi$ (degrees) | $\alpha_f$ | Computed Slope (psi) | Measured Slope (psi) | Actual Slope / Measured Slope |
|---|---|---|---|---|---|
| 200 | 39.9 | 0.2005 | 674 | 1167 | 1.73 |
| 600 | 30.7 | 0.1632 | 1428 | 1920 | 1.34 |
| 1159 | 33.3 | 0.1744 | 3059 | 3225 | 1.05 |
| 3000 | 32.2 | 0.1697 | 7590 | 4760 | 0.63 |
| 12,000 | 30.3 | 0.1614 | 28,080 | 6250 | 0.22 |

200 and 600 psi restraint constants did achieve failure stress conditions. However, these tests did not satisfy the criterion established by the Drucker hypothesis. Since the theory is based on energy principles, this could suggest that there exists a unique energy input which corresponds to the limiting strength of the material.

If Drucker's hypothesis were valid for all soils, equation 64 could represent a tool by which the restraint constant unique to the failure conditions could be estimated. The $\alpha_f$ values in Table 18 vary only slightly when compared to k. Since the two bracketed components of the slope term in equation 64 depend on $\alpha_f$, it would be possible to run a test with an estimated value, and by monitoring the resulting axial stress-strain relation, make adjustments to k meeting the equality established by equation 64. An obvious disadvantage of this approach is the requirement for continuous monitoring and feedback. Another potential difficulty could be that equation 64 does not apply to all soils. The Drucker hypothesis requires dilation if $\alpha_f$ or $\phi$ is greater than zero. Soils displaying frictional strength without dilation are certainly a possibility. Nonetheless, the compacted loess used in these experiments is one example of the suitability of Drucker's hypothesis.

Probably the most important evidence resulting from the experiments of this research is the unique role played by unconfined deformation properties when used as restraint function. Theory as thus far developed does little to explain this observation, but its experimental consistency can also be viewed in terms of the Drucker hypothesis. Axial stress-strain results for three tests resulting in failure stress paths induced either by direct stress control or through unconfined restraint are shown in Figure 42. Obviously, the phenomenon expressed in terms of axial stress-strain is reproducible and consistent with the Drucker postulate.

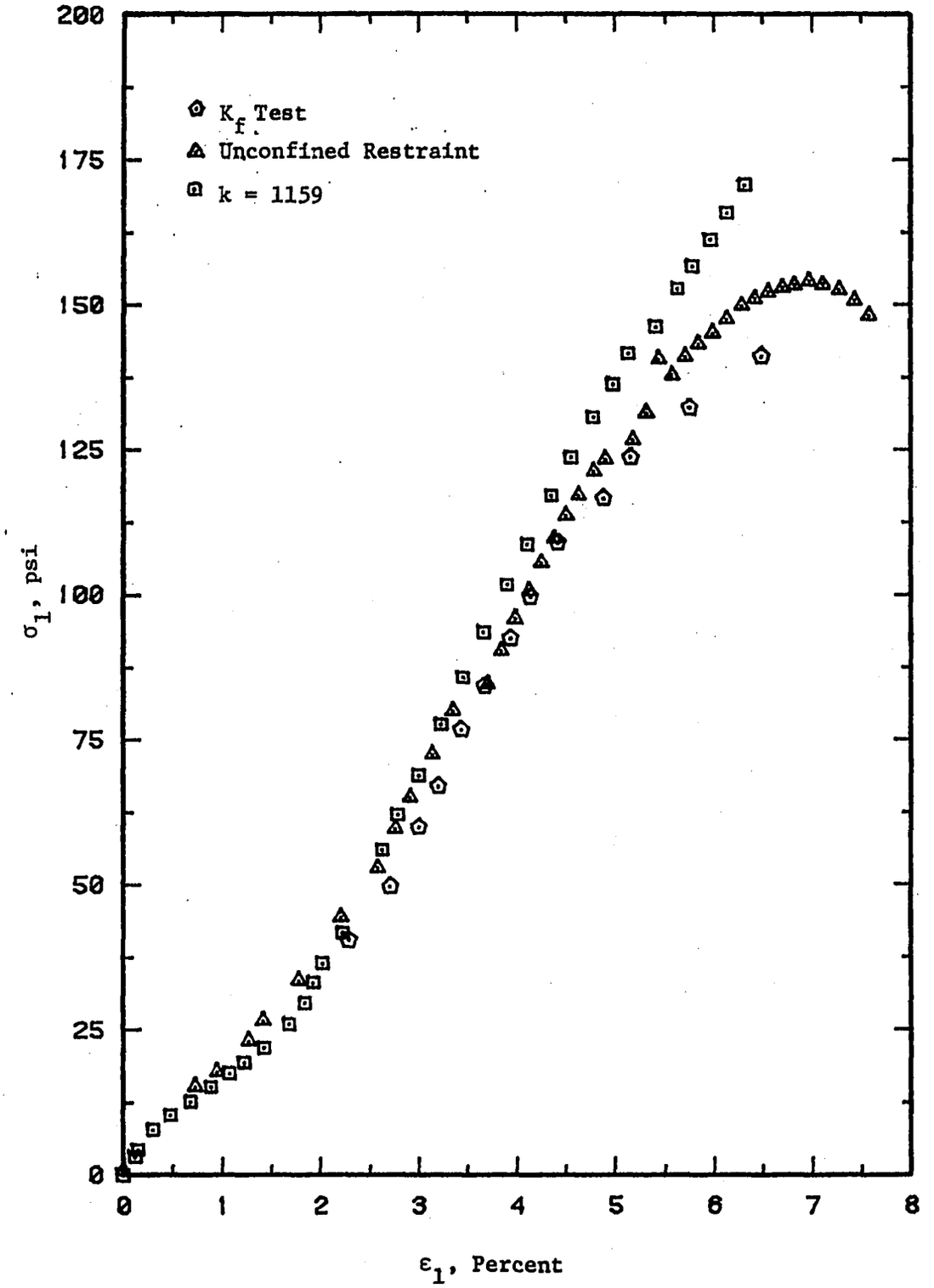


Figure 42. Axial stress-strain for ultimate strength tests

An alternative way of visualizing the significance of unconfined restraint is in terms of the geometry of the bearing capacity problem. If the block shown by the dashed line in Figure 5 is taken as a reactive element to the column of soil lying immediately beneath the loaded area, under circumstances where the surcharge is zero, this reactive block might be taken as an unconfined specimen lying on its side. This model suggests that the minimum possible restraint available to a primary element is the unconfined restraint.

## Settlement Predictions

The objective of this phase of the research is to compare k-path methodology to existing settlement prediction techniques. To accomplish this goal, settlements will be estimated for a hypothetical problem involving a 64 foot diameter, circular loaded area resting on a thick layer of soil possessing the same properties as the material used in this research. The oedometer and Lambe's stress path tests are used for comparison.

### Stress path

With exception of being privy to a predefined $K_o$ stress path, the Lambe stress path evaluation was conducted under the constraints common to practical application of the method. This means nothing is known about $\nu$ so it is presumed to be 0.5. The resulting stress control parameters for superposition on the in situ stresses are given in the second column of Table 19. These ratios were computed from equations 30

and 31 and the ratio, z/a, represents the depth, z, expressed as a fraction of the load over radius, a. Rigorous application of stress path methods would involve testing several specimens from various positions within the profile. However, to reduce the amount of testing and offer a look at the influence of different boundary conditions, tests were performed at the z/a positions, 0.8 and 3.0. The 0.8 position approximates Lambe's average element while z/a = 3.0 represents a deep-seated specimen. The superimposed stress ratios for the selected positions are 0.24 and 0.02. The latter stress ratio means the increase in lateral stress is nearly zero or the test is conducted under constant confining stress.

Table 19. Settlement test control parameters

| (1) z/a | (2) $k = \sigma_3/\sigma_1$ | (3) $\sigma_{zo}$, psi | (4) $\nu$ | (5) $M_{ct}$, psi | (6) E, psi | (7) k, psi |
|---|---|---|---|---|---|---|
| 0 | 1.00 | 0 | 0 | 1688 | 1688 | 1688 |
| 0.2 | 0.71 | 5.4 | 0.05 | 1952 | 1944 | 2552 |
| 0.4 | 0.49 | 10.8 | 0.06 | 2236 | 2207 | 3902 |
| 0.6 | 0.34 | 16.1 | 0.10 | 3539 | 2482 | $\infty$ |
| 0.8 | 0.24 | 21.5 | 0.12 | 2861 | 2770 | -2188 |
| 1.0 | 0.18 | 26.9 | 0.13 | 3202 | 3072 | - 338 |
| 1.5 | 0.09 | 40.3 | 0.16 | 4139 | 3894 | - 312 |
| 2.0 | 0.05 | 53.6 | 0.17 | 5197 | 4811 | 0 |
| 3.0 | 0.02 | 80.6 | 0.20 | 7673 | 6940 | 0 |

k-path

Control parameters for the k-path analysis are listed in columns 4 through 7, Table 19. Poisson's ratio for the appropriate vertical geostatic stress, $\sigma_{zo}$, was computed from equation 87, the hyperbolic fit of $K_o$ versus $\sigma_1$ for constrained test results. Tangent values for the constrained modulus, $M_{ct}$, are also dependent on $\sigma_{zo}$ and were computed from equation 83, and E was computed from equation 70. The restraint constant as defined in equation 68 is listed in column 7. By elastic theory, restraint should be posed by an active spring until z/a approaches 0.6, at which point the test could be performed under constrained conditions. For z/a ranging from 0.8 to 1.5, a reactive spring is appropriate and for z/a greater than 2, the superimposed radial stress is zero as with the stress path test. k-path tests were performed at the same z/a positions as were used in the stress path analysis. The z/a = 3.0 position represents identical tests.

Test results

A p-q representation of the results is shown in Figure 43. Although the theories supporting both the k-path and stress path methods are identical, the stress paths resulting from the z/a = 0.8 tests were different. The k-path produced a stress path lying closer to the $K_o$ line and did not converge on the $K_f$ line as did the result from Lambe's method. Under constant confinement (z/a = 3.0), failure was expected. Figure 44 is a plot of radial stress-strain data resulting from the three

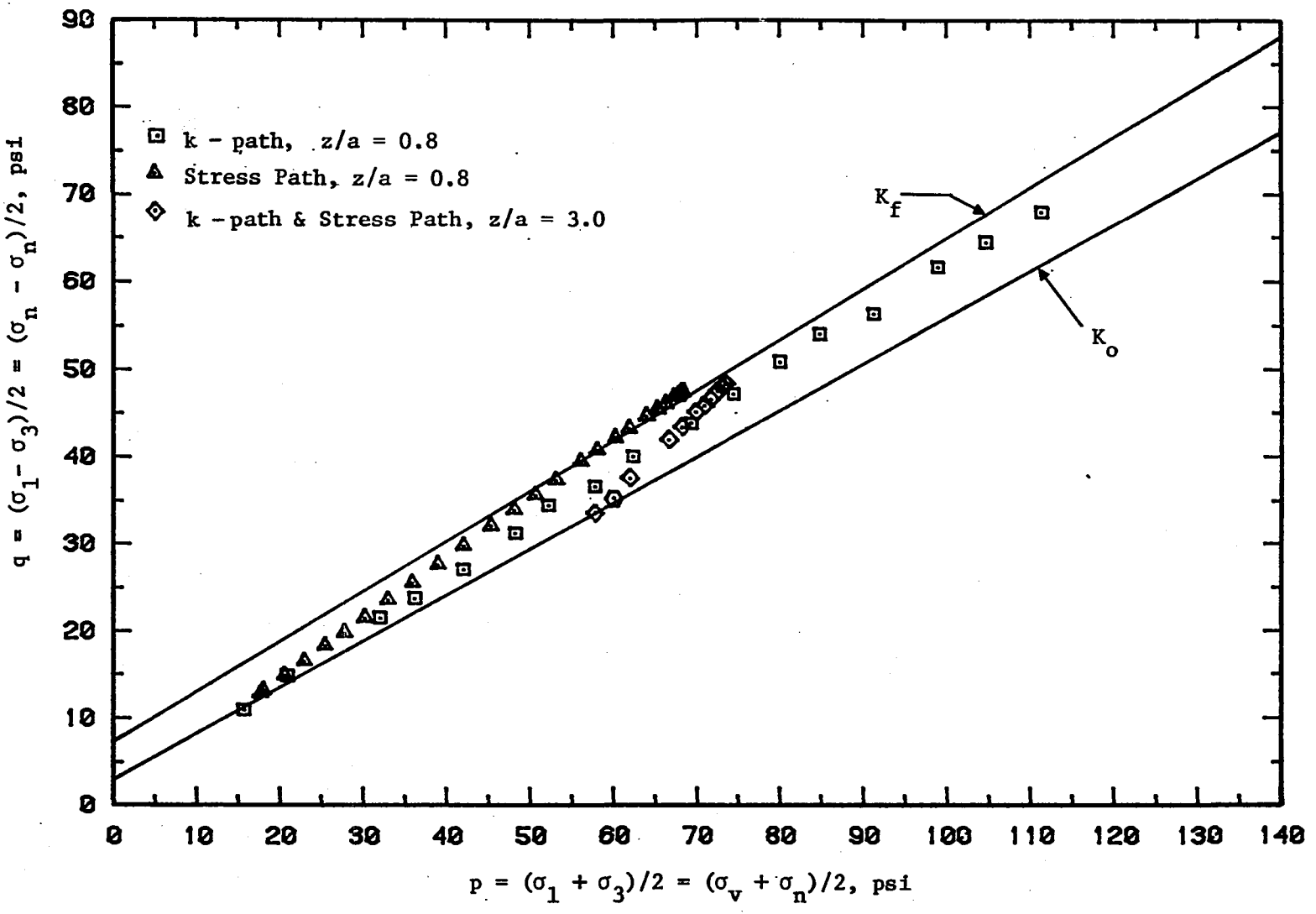


Figure 43. Stress ratios for settlement predictions

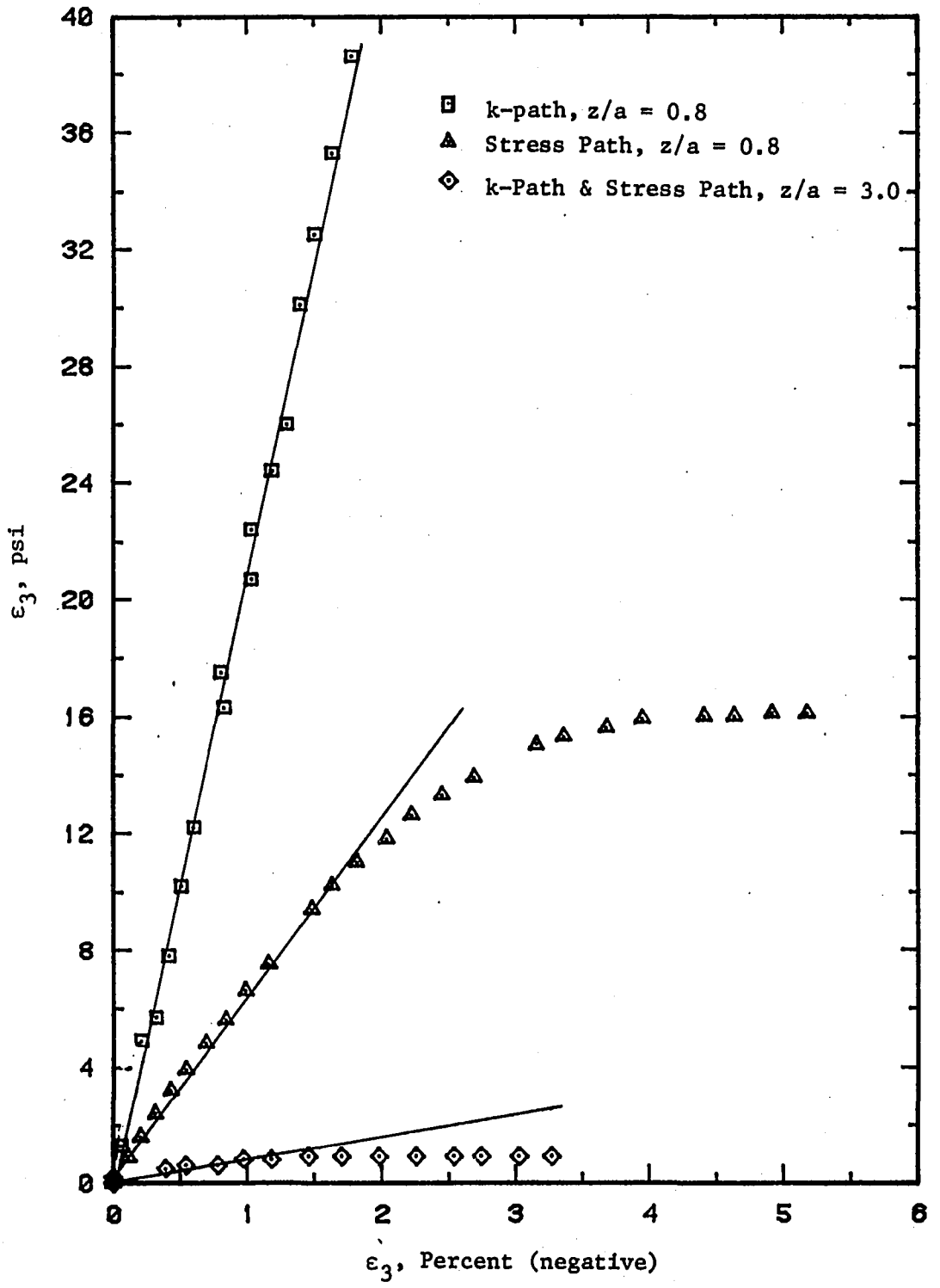


Figure 44. Radial stress-strain relation for settlement prediction tests

tests. Obviously for the k-path tests, this plot represents nothing more than a representation of the functional restraint applied during the test. This does, however, serve as a check on the ability of the incremental test procedure to apply a specified restraint. For the $z/a = 0.8$ k-path, the specified slope is -2188 psi while the measured slope from Figure 44 is -2153 psi. Slopes and shapes of the curve for the equivalent stress path test bear no resemblance to the k-path restraint function. Much more radial strain was permitted by Lambe's method.

Axial stress strain relations resulting from the k-path, stress path, and one-dimensional compression tests are presented in Figure 45, where the data have been adjusted to reflect deformations occurring for vertical stress superimposed on in situ stresses. For superimposed stress levels less than 30 psi, both the $z/a = 0.8$ k-path and stress path tests produced nearly identical results. However, beyond this level, the results diverged with the stress path result displaying an ultimate strength and the k-path a linear stress-strain relation. Both methods allowed more strain than the equivalent constrained test. At stress levels below 10 psi, the $z/a = 3.0$ k-path and stress path tests resulted in axial strain roughly equivalent to that of the constrained test. As would be expected, this consistency does not hold as the constant $\sigma_3$ specimen continues on a 45 degree stress path, intersecting the $K_f$ line. In a practical sense, the superimposed stress acting on a deep-seated element may be below the 10 psi level, making the difference unimportant.

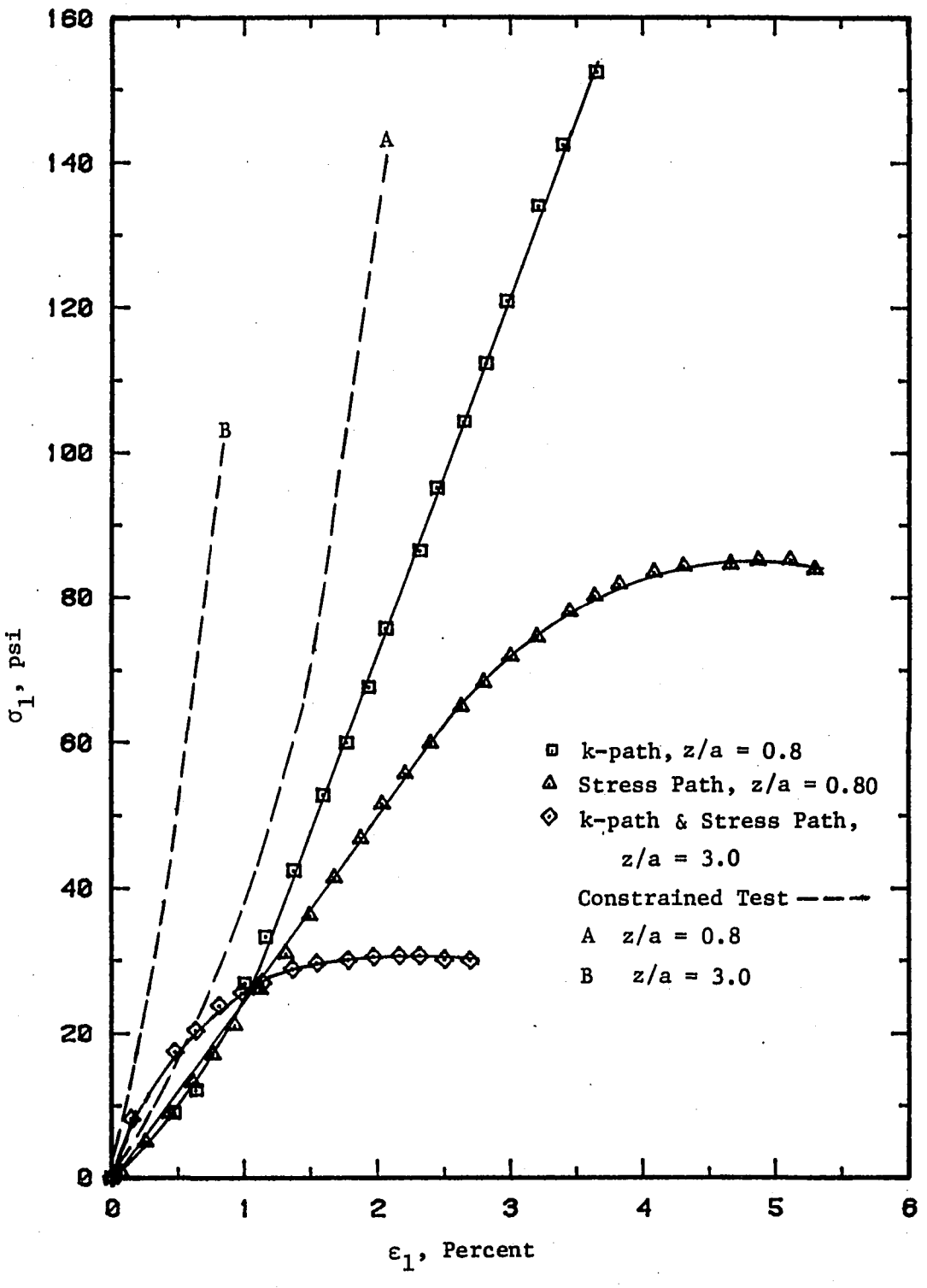


Figure 45. Axial stress and strain occurring beyond in situ stress levels

The stress-strain response in Figure 45 supports the logic of permitting lateral deformation in settlement prediction tests. Regardless of whether boundary conditions are applied through Lambe's stress path or the proposed k-path methods, the resulting stress-strain relations when applied to a settlement prediction will produce more settlement than the corresponding constrained test. The statistical analysis of predictions from constrained tests indicates that greater settlement predictions are necessary for consistency with prototype observations. The important question is whether the k-path or stress path predictions are accurate representations of field performance. Since large scale settlement data are not available for the material used in this research, the only method for gauging the suitability of the proposed test is by comparison to established procedures. As the single stress path experience reported in the literature is of little statistical value, constrained or consolidation testing must serve as the benchmark. If for comparative purposes the constrained tests performed for this research are thought to represent a time-independent consolidation process by virtue of air rather than water occupying the voids, the statistical treatment of the consolidation prediction record should represent a valid comparative base. Applied stress versus settlement relations for the constrained, stress path, and k-path methods are shown in Figure 46. Computations were based on presuming the $z/a = 0.8$ specimen represents the mid-depth of a 51.2 foot thick compressible layer and settlements were computed from strains in Figure 45. This approximates the average

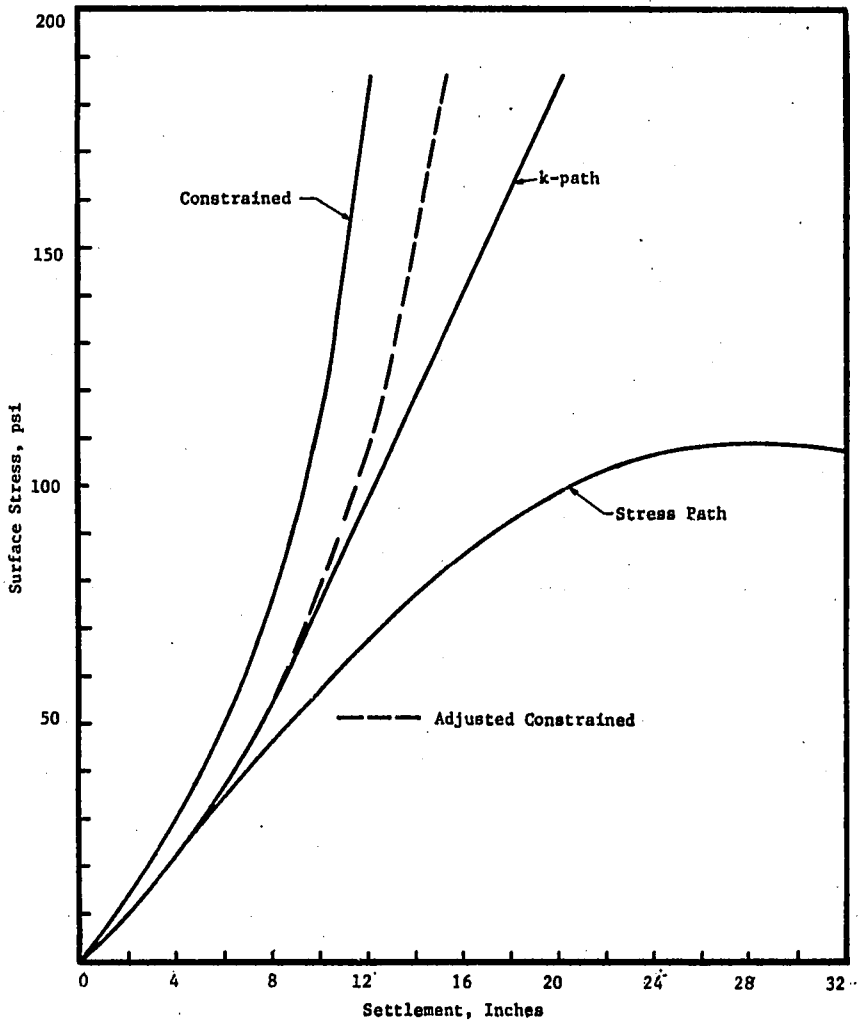


Figure 46. Settlement prediction results

element concept for the stress path analysis, represents common treatment of consolidation data, and presumes that the z/a = 3.0 specimens contribute little to the overall settlement problem. The latter presumption is fairly accurate because vertical stress 96 feet below the surface is only about 10 percent of the applied surface stress.

It is obvious from Figure 46 that a large variation in settlement predictions, dependent upon the applied stress level, is possible. When the surface stress is less than 30 psi, k-path and stress path methods produce identical results and above this stress level their predictions differ significantly with the stress path and constrained test results defining limits. Applying the knowledge that the constrained test mechanism statistically underpredicts true settlement by about 22 percent, appropriately factored laboratory results shown as a dashed line in Figure 46 should represent the best available estimate for field settlements. For the stress range included in the experimentation, the k-path method offers the best approximation.

The 105 psi limiting bearing capacity predicted by the stress path is difficult to justify when the ultimate bearing capacity computed according to equations 23 through 29 is 720 psi. This could reflect the inadequacy of keying settlement predictions to laboratory tests on specimens subjected to theoretical boundary stress conditions for small elements located directly beneath the center line of the loaded area. Finite element evaluations of the bearing capacity problem (9) for an elastic-plastic material have shown that localized yield first occurs

along the line of symmetry, at about one radius beneath the footing, and at load levels far less than those producing general failure in the supporting material. This localized yield may be reflected in the stress path result, and portions of the stress settlement curve may not reflect overall performance of the structure.

Another question arising from the results in Figure 46 is that if both the stress path and k-path methods are dependent on the same theory to establish boundary conditions, why is there such a difference in the results? A partial explanation may be in the assessment of $\nu$ used to determine the superimposed stress ratio for the stress path method. $\nu$ at the $K_o$ stress conditions corresponding to the $z/a = 0.8$ position was experimentally determined to be 0.12. Had this value been used to assess the superimposed stress ratio, $K = \sigma_3/\sigma_1$, would have been 0.81 rather than the 0.24 as used in the test. This threefold increase in confining stress would certainly stiffen the axial stress-strain response, resulting in better agreement with the k-path results. Inability of assessing $\nu$ under the limitations of common triaxial apparatus makes the theoretical validity of practical stress path testing suspect. When viewed in the context of predictions commensurate with building design, this problem is somewhat diminished because total settlement limitations for many structures are in the range of 3 to 6 inches (Table 5), a region for which k-path and stress path predictions are identical. For the upper design limit of 12 inches, stress path in this example would result in gross error while the k-path would overpredict by perhaps 9 percent.

Lastly, there remains one nagging problem regarding the need for an improved test. The entire analysis of settlement predictions is based on the statistical adjustment of constrained test results, and this adjustment produces results in exceptionally good agreement with the k-path results. If the factored constrained results are truly representative of a prototype response on the material used in these tests, an equally strong argument can be mustered for simply using factored oedometer predictions and alleviating the necessity of either k-path and stress path tests. Since true prototype performance is not available, the only statement that can be made about the k-path method is that it tends to result in 22 percent greater settlement predictions than constrained testing.

# SUMMARY AND CONCLUSIONS

An analysis of information from the literature showed that soil variability and inaccuracy of consolidation settlement prediction techniques are factors which can adversely influence geotechnical predictions for shallow building foundations. The need for improvement in these areas substantiates the value of investigating the deformation restraint test in the context of providing a quick, inexpensive method for evaluating ultimate strength parameters and better settlement predictions.

The experimental test program was conducted in phases so that a link could be provided between conventional test results, and the transition to a deformation restraint apparatus which enforces cylindrical geometry on a specimen. Under constant radial stress, imposition of cylindrical geometric boundaries had no influence on ultimate strength parameters of the soil tested. However, a slight increase in deformation moduli was observed. Specimen length was evaluated in the DR apparatus and was found not to be a significant factor in determining ultimate strength parameters.

An evaluation of specimen length and deformation properties was not conclusive. Also, a difference was found when direct radial deformation measurements from the DR apparatus were compared to equivalent computed values from triaxial volumetric measurements. Different radial and volumetric strain patterns and magnitudes for similar specimens under equivalent stress conditions were evident, and logic suggests the more

direct measure may be appropriate.

A series of deformation restraint tests shows that for the soil tested the degree of reactive radial restraint provided to a specimen dictates the resulting stress path. The upper restraint limit, being $k = \infty$, represents a $K_o$ stress path, and as k was reduced, the resulting stress path shifted toward one defining the limiting strength of the material. It was also found that accurate definition of ultimate strength was sensitive to selection of the restraint constant. For the compacted loess, the appropriate radial restraint constant was experimentally determined to be the restraint defined by the axial deformation moduli of unconfined specimens. This observation was experimentally verified on three occasions and supported by agreement between a theoretical stress-strain relation developed from the Drucker postulate and experimental stress-strain results. This experimentation also illustrates that arbitrary selection of restraint constant can result in significant strength over-estimates when k is too large. Feedback control systems, based on early phases of deformation restraint tests or a theoretical plastic strain equation were suggested but not attempted.

The influence of k on deformation response of the compacted loess was even more significant than its effect on the stress path. Use of deformation restraint testing to predict settlements requires some logical means for stipulating the appropriate boundary condition, and a methodology consistent with Lambe's stress-path method was developed. Results of the proposed k-path technique were compared to those of

constrained and stress path tests. The proposed method was found to predict greater settlement than constrained tests and equivalent or less settlement than stress path, depending on stress level. An adjustment based on statistical evaluation of field consolidation predictions showed excellent agreement to the k-path method.

# RECOMMENDATIONS FOR FURTHER RESEARCH

This research undoubtedly raises more questions than it provides solutions. It was found that c - $\phi$ parameters for a relatively incompressible compacted loess could be accurately defined by deformation restraint tests. Based on volumetric behavior, this class of soil represents a wide variety of natural and artifically compacted deposits; however, deformation restraint testing of highly compressible and cohesionless soils is still subject to question. It seems that answers to these problems might best be resolved by careful experimentation on a material representing the other extreme in volumetric compressibility and a cohesionless soil. Existing theories would reveal very little.

A comparative evaluation of the k-path method should also be considered. However, the case study approach to validating settlement prediction methods which seems to prevail in the literature would be of little value unless enough tests could be performed to assess the influence of variability. Experience with soil variability and the hundreds of tests which could be required for variability definition suggests that a few case studies would resolve nothing. Thus, a better validation might be achieved through model studies where soil properties can be controlled and variability reduced to a manageable level. This is in essence the same approach used to validate the bearing capacity equation.

Although the versatility incorporated in the apparatus used for this work makes it an excellent research tool, its complexity and cost

renders it unsuitable for practical application. Since definition of both ultimate strength and deformation parameters is dependent on k, and because possible forms of practical tests leading to both types of parameters call for definition of k during initial phases of a test, an apparatus of the form shown in Figure 47 is proposed.

The device consists of a segmented mold restrained by a hinged band making contact with mold segments at the hinge points. The reactive restraint is provided by a hinged, U-shaped restraint spring incased in a stiff housing. The housing can be moved along the spring with a screw causing the spring to protrude different amounts, thus providing adjustable spring constants. The position nearest the mold should represent a $K_o$ test. To allow application of initial stress or take slack out of the restraint band, a stress control adjustment forcing the hinged restraint spring inward should be provided. The threaded adjustment could be replaced with a small air cylinder to allow for stress controlled tests. The apparatus could be calibrated to provide a relation between spring housing position, restraint constant, radial strain, and radial stress monitored from calibrated strain gage readings. Since ultimate strength parameters were found to be independent of specimen height, it is envisioned that the apparatus length be limited such that consolidation as well as ultimate strength can be measured. Axial loading could be accomplished either in conventional consolidation or constant deformation rate load frames.

Although the adjustable constant restraint mechanism could be attached to the existing thin-walled Iowa K-Test, the segmented mold and

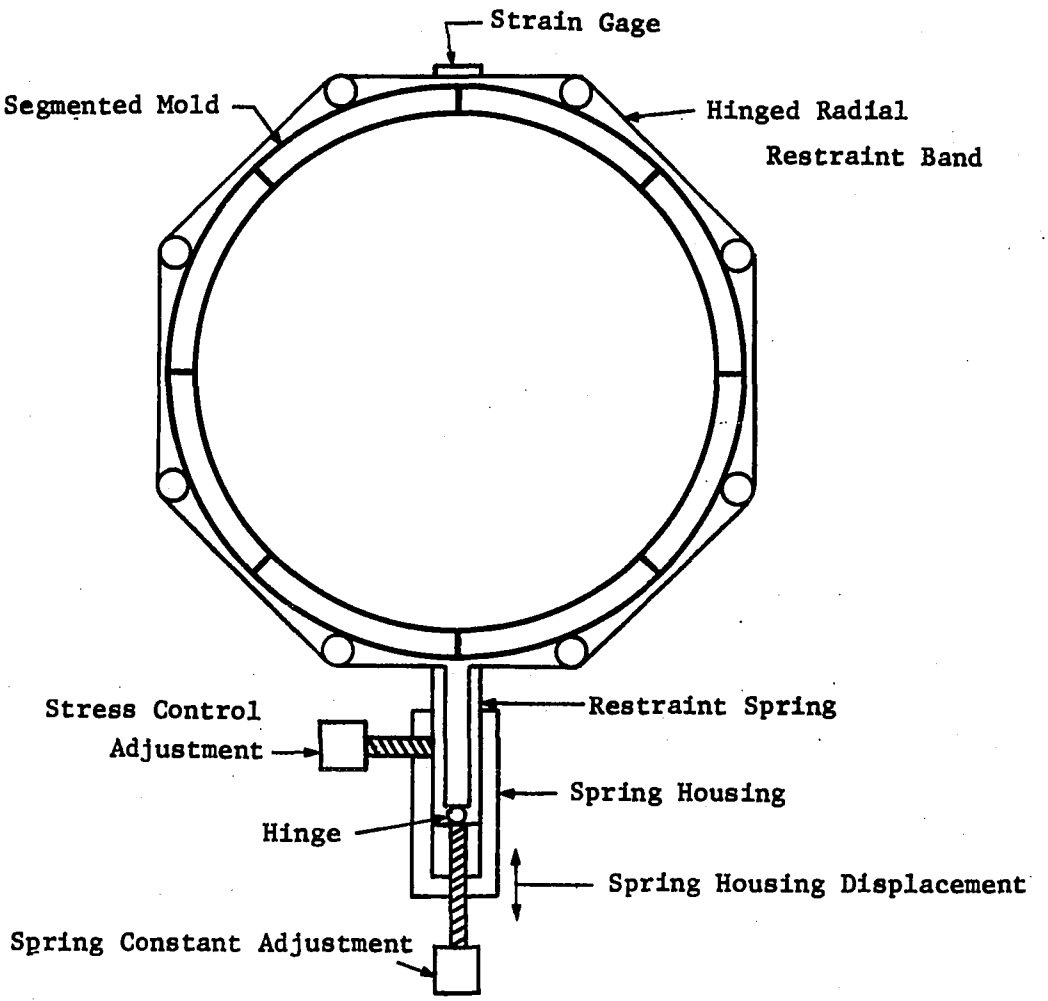


Figure 47. Proposed adjustable deformation restraint apparatus

restraint band is recommended to achieve a better approximation of axisymmetric conditions. Some practical considerations of the apparatus would be the need for a frictionless boundary on the interior of the mold. This could be accomplished with overlapping teflon as was used with the experimental apparatus, and a possible alternative to the rubber membrane might be wrapping specimens in PARAFILM M. This is a low tensile strength plastic film which appears to have the near frictionless properties when interfaced with a lubricated teflon surface. Rubber membrane application is sometimes tedious, whereas wrapping specimens in a film to prevent moisture loss is easy and something that must be done anyway.

Even though deformation restraint testing by defining strength parameters from single specimens has the potential of increasing the speed of limit strength testing and improving settlement predictions, the statistical testing demands given in Table 9 strongly suggest that this improvement in many instances still will not solve the variability problem. Determination of eleven friction angles is feasible but 57 is not. The least variable of settlement conditions calls for 31 samples while the most variable condition calls for an impossible 111. However, there may be a way to couple the improvements offered by deformation restraint testing to the speed and cost effectiveness of some of the field tests through statistical theory.

A requirement for including variability in reliability analysis is parameters consistent with prediction techniques. Also, logical

analysis of performance is not through statistical analysis of parameters, but of performance factors such as load capacity or settlement. Defining performance factors is the value of deformation restraint testing. On the other hand, field tests such as the cone penetrometer, wave velocity measurements, vane shear test, or pocket penetrometer have the potential of providing sufficient amounts of data to allow an evaluation of variability, but the results of these tests are usually incompatible with prediction theories. Thus, the proposed scheme involves taking advantage of the strengths of both types of tests.

Figure 48 is a graphic representation of a statistical technique of derived distributions. The mathematical details will not be presented here, but they can be found in reference 5. If a probability distribution function (pdf) can be defined for one variate, x, and if a functional relation exists between x and a second variate, y, it is then possible to define the probability distribution function via a $y = g(x)$ transformation for the second variate. Application to geotechnical problems would involve defining the pdf for x with a simple fast test. Such data are represented by the dots under the $f_x(x)$ curve in Figure 48 and provide a statement about variability in terms of meaningless parameters. The second step would involve selecting equivalent specimens at various x positions under the $f_x(x)$ pdf curve and perform the appropriate test allowing definition of desired prediction variate. Examples of this are ultimate load or settlement. For bearing capacity analysis, deformation restraint tests would be ideal because they

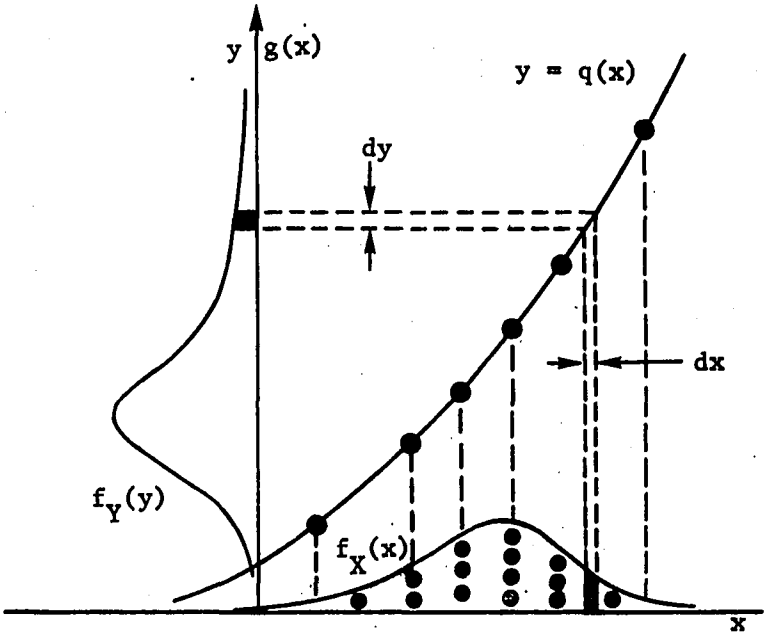


Figure 48. Derived distribution (after Box, Hunter and Hunter (5))

provide both c and $\phi$ from a single specimen. Bearing capacities could be completely defined from a single specimen and several tests are possible. The value of deformation restraint tests to settlement prediction could be better accuracy at about the same expense as oedometer testing. The third step in the analysis would be definition of the function $y = g(x)$ through curve fitting which allows definition of the desired $f_y(y)$ pdf, useful to reliability analysis.

## ACKNOWLEDGMENTS

The author wishes to acknowledge the Engineering Research Institute for sponsoring this research project.

A great indebtedness is extended to Dr. R. L. Handy and Professor J. M. Hoover, my Major Professors. Not only was academic latitude given to the author but also guidance and inspiration.

The writer extends thanks to Mr. Leon Girard and the E.R.I. Machine Shop for their persistence in dealing with this project. Dr. Turgut Demirel, Dr. Darwin Fox, and Dr. Alan J. Lutenegger are to be acknowledged for their interest and assistance given during this research.

The writer is also grateful to his devoted wife, Marytha. Her encouragement and understanding through this research has been appreciated. Finally, thanks goes to my in-laws, Mr. and Mrs. Wendell Cook for their assistance.

BIBLIOGRAPHY

1. American Concrete Institute. Building Code Requirements for Reinforced Concrete. ACI Standard 318-77, August, 1979.

2. Baker, C. N., Jr. Discussion in Design of Foundations for Control of Settlement. New York: American Society of Civil Engineers, 1964, pp. 517-519.

3. Bishop, A. W. and D. J. Henkel. The Measurement of Soil Properties in the Triaxial Test. London: Edward Arnold Publishers, 1962.

4. Bjerrum, L. "Allowable Settlements of Structures." Norwegian Geotechnical Institute, 98 (1973), 1-4.

5. Box, G. E. P., W. G. Hunter, and J. S. Hunter. Statistics for Engineers. New York, N.Y.: John Wiley and Sons, 1978.

6. Brooker, E. W. and H. O. Ireland. "Earth Pressures at Rest Related to Stress History." Canadian Geotechnical Journal, 1 (1965), 1 - 15.

7. Butler, F. G. "Heavily Over-Consolidated Clays." In Settlement of Structures. Review Paper: Session III. London: Penteck Press, 1975, 531-578.

8. Chatfield, C. Statistics for Technology. London: Hallsted Press, 1978.

9. Christian, J. T. "Shallow Foundations." In Numberical Methods in Geotechnical Engineering. Ed. C. S. Desai and J. T. Christian. New York: McGraw-Hill, 1977, pp. 211-234.

10. Corotis, R. B., R. J. Krizek, and H. H. El-Moussi. "Probabilistic approach to prediction of consolidation settlement." Soil and Rock Mechanics. Transportation Research Record, 548 (1975), 47-61.

11. Cowley, B. E., E. G. Haggar, and W. J. Larnack. "A Comparison Between the Observed and Estimated Settlements of Three Large Cold Stores in Grimsby." In Settlement of Structures. London: Penteck Press, 1975, 79-90.

12. D'Appolonia, D. J., H. G. Poulos, and C. C. Ladd. "Initial Settlement of Structures on Clay." ASCE Journal of the Soil Mechanics and Foundations Division, 97, SM 10 (October, 1971), 1359-1377.

13. De Beer, E. E. "Experimental Determination of the Shape Factors and the Bearing Capacity Factors of Sand." Geotechnique, 20, No. 4 (1970), 387-411.

14. D'Elia, B. D. and M. Grisolia. "On the Behavior of a Partially Floating Foundation on Normally Consolidated Silty Clays." Settlement of Structures. London: Penteck Press, 1975, 91-98.

15. Desai, C. S. and J. T. Christian. Numerical Methods in Geotechnical Engineering. New York, N.Y.: McGraw-Hill Publishing, 1977.

16. Drnevich, V. P. "Constrained and Shear Moduli for Finite Elements." ASCE Journal of the Geotechnical Engineering Division, GT 5 (1975), 459-473.

17. Drucker, D. C. "A more fundamental approach to plastic stress-strain relations." Proceedings of the U.S. National Congress on Applied Mechanics, 1 (1951), 487-491.

18. Drucker, D. C. and W. Prager. "Soil mechanics and plastic analysis or limit design." Quarterly of Applied Math, 10 (1952), 157-165.

19. Duncan, J. M. and C. Chang. "Nonlinear Analysis of Stress and Strain in Soils." ASCE Journal of the Soil Mechanics and Foundations Division, 96, SM 5 (September, 1970), 1629-1653.

20. Ehrgot, J. Q. "Calculation of Stress and Strain from Triaxial Test Data on Undrained Soil Specimens." U.S. Army Engineer Waterways Experiment Station (Vicksburg, Miss.) M.P. 5-71-9, 1971.

21. Flemming, H. D. "Undrained Triaxial Compression Tests." Proceedings of the First Australia-New Zealand Conference on Soil Mechanics and Foundation Engineering, Melbourne: University of Melbourne, 1952, 112-122.

22. Foster, C. R. and S. M. Fergus. "Stress Distribution in a Homogeneous Soil." Highway Research Board Report No. 12-F, January, 1951.

23. Freudenthal, A. M. "The Safety of Structures." Transactions, American Society of Civil Engineers, 2 (1947), 125-180.

24. Hahn, G. J. and S. S. Shapiro. Statistical Models in Engineering. New York, N.Y.: John Wiley and Sons, Inc., 1967.

25. Handy, R. L. and J. M. Hoover. "Testing Device for Measuring Lateral Pressure Induced on a Material by a Vertical Applied Pressure." Patent Application S.N. 641545, December, 1975.

26. Handy, R. L., A. J. Lutenegger, and J. M. Hoover. "The Iowa K-Test." Transportation Research Record, No. 678 (1978), 42-49.

27. Harr, M. E. Foundations of Theoretical Soil Mechanics. New York, N.Y.: McGraw-Hill, 1966.

28. Harr, M. E. Mechanics of Particulate Media. New York, N.Y.: McGraw-Hill, 1977.

29. Hoeg, K. and R. P. Murarka. "Probabilistic Analysis and Design of a Retaining Wall." Journal of Geotechnical Division, American Society of Civil Engineers, GT 3 (March, 1974), 349-366.

30. Holtz, R. D. and W. D. Kovacs. An Introduction to Geotechnical Engineering. Englewood Cliffs, N.J.: Prentice-Hall, 1981.

31. Hoover, J. M. and R. L. Handy. "Chemical Compaction Aids for Fine-Grained Soils." Federal Highway Administration Report No. FHWA-RD-79-63, Vol. 1, June, 1978.

32. Hveem, F. N. and H. E. Davis. "Some Concepts Concerning Triaxial Compression Testing of Asphaltic Paving Mixtures and Subgrade Materials." Triaxial Testing of Soils and Bituminous Mixture. ASTM Special Technical Publication No. 116 (1950), 25-45.

33. Jaky, J. "The Coefficient of Earth Pressure at Rest." (Hungarian) Magyar Mernak es Epitesz Egylet Kozlone, 1944, 335-358.

34. Jaky, J. "Pressure in Silos." In Proceedings of the Conference on Soil Mechanics and Foundation Engineering, 1 (June, 1948), 21-30.

35. Janbu, N. "Settlement Calculations Based on the Tangent Modulus Concept." Department of Civil Engineering, The Technical University of Norway, Trondheim, Norway, 1967.

36. Johnson, W. and P. B. Mellor. Engineering Plasticity. Wakingham, Berkshire: Van Nostrand Reinhold Co., 1973.

37. Ladd, C. C. "Stress-Strain Behavior of Saturated Clay and Basic Strength Principles." Research Report R64-17. Soil Mechanics Division, M.I.T., Cambridge, Mass., 1964.

38. Lambe, T. W. "Methods of Estimating Settlement." Design of Foundation for Control of Settlement. New York: American Society of Civil Engineers, 1964, pp. 47-72.

39. Lambe, T. W. "Stress Path Method." Journal of the Soil Mechanics and Foundations Division, ASCE 93, SM 6 (1967), 309-331.

40. Lambe, T. W. and W. A. Marr. "Stress Path Method: Second Edition." Journal of the Geotechnical Engineering Division, 105, GT 6, (1979), 727-738.

41. Lambe, T. W. and R. V. Whitman. Soil Mechanics. New York, N.Y.: John Wiley and Sons, 1969.

42. Lind, N. C. and A. G. Davenport. "Towards Practical Application of Structural Reliability Theory." Probabilistic Design of Reinforced Concrete Buildings, American Concrete Institute, SP-31, 1972, 63-110.

43. Lumb, P. "Variability of Natural Soils." Canadian Geotechnical Journal, 3, No. 2 (May, 1966).

44. Lutenegger, A. J. "The Iowa Continuous K-Test: A Laboratory Test for Measuring Lateral Stresses in Soils Induced by Vertical Applied Loads." M.S. Thesis. Iowa State University, Ames, Iowa, 1977.

45. Mac Gregor, J. G. "Safety and Limit States for Reinforced Concrete." Canadian Journal of Civil Engineers, 3, No. 3 (December, 1976), 484-513.

46. Meyerhof, G. G. "Influence of roughness of base and ground water conditions on the ultimate bearing capacity of foundations." Geotechnique, 5, No. 3 (1955), 227-242.

47. Moore, P. J. and G. K. Spencer. "Settlement of Building on Deep Compressible Soil." ASCE Journal of the Soil Mechanics and Foundations Division, SM 3 (May, 1969), 769-790.

48. Newland, P. L. and G. H. Allely. "Volume Changes in Drained Triaxial Tests on Granular Materials." Geotechnique, No. 7, 1956, 17-34.

49. Peck, R. B. and M. E. Vyanik. "Observed and Computed Settlements of Structures in Chicago." University of Illinois, Urbana, Engineering Experiment Station Bulletin No. 429, 1955.

50. Perloff, W. H. "Pressure Distribution and Settlement." In Foundation Engineering Handbook. Ed. H. F. Winterkorn and H. Fang. New York: Van Nostrand, 1975, 148-196.

51. Polshin, P. F. and R. A. Tokar. "Allowable Settlement of Buildings." In Proceedings of 4th International Conference on Soil Mechanics and Foundation Engineering, I (1957), 402-406.

52. Poulos, H. G. and E. H. Davis. Elastic Solutions for Soil and Rock Mechanics. New York, N.Y.: John Wiley and Sons, 1974.

53. Rohani, V. B. "Mechanical Constitutive Models for Engineering Materials." U.S. Army Engineer Waterways Experiment Station (Vicksburg, Miss.) M.P. 5-77-19, (September, 1977).

54. Sanglerat, G., L. Girousse, and J. Gielly. "Unusual Settlements of a Building at Nantua (France)." Settlement of Structures, London: Penteck Press, 1975, 123-131.

55. SAS User's Guide. Raleigh, N.C.: SAS Institute, Inc., 1979.

56. Schmertmann, J. H. "The Undisturbed Consolidation Behavior of Clay." ASCE Transactions, 120, (1955) 1201-1233.

57. Skempton, A. W. and D. H. Mac Donald. "Allowable Settlement of Buildings." In Proceedings of Institute of Civil Engineers, Part III, 5 (1956), 727-768.

58. Spangler, M. G. and R. L. Handy. Soil Engineering, New York, N.Y.: Intext Educational Publishers, 1973.

59. Terzaghi, K. Theoretical Soil Mechanics. New York, N.Y.: John Wiley and Sons, 1943.

60. Turkstra, C. J. "Choice of Failure Probabilities." Journal of Structural Division, Proceedings American Society of Civil Engineers, ST 6, 93 (December, 1967), 189-200.

61. Turnball, W. C., A. A. Maxwell, and R. G. Ahlvin. "Stresses and Deflections in Homogeneous Soil Masses." In Proceedings of the Fifth International Conference on Soil Mechanics and Foundations Engineering, 1961, 337-345.

62. Vesic, A. S. "Analysis of Ultimate Loads of Shallow Foundations." ASCE Journal of Soil Mechanics and Foundations Division, 99, No. SM 1 (1973), 45-73.

63. Vesic, A. S. "Bearing Capacity of Shallow Foundations." In Foundation Engineering Handbook. Ed. H. F. Winterkorn and H. Fang, New York, N.Y.: Van Nostrand, 1975, pp. 121-147.

64. Winter, G. and A. H. Nilson. Design of Concrete Structures. New York, N.Y.: McGraw-Hill Book Company, 1979.

65. Zienkiewicz, O. C. and C. Humpheson. "Viscoplasticity: a generalized model for description of soil behavior." In Numerical Methods in Geotechnical Engineering. Ed. C. S. Desai and J. T. Christian. New York, N.Y.: McGraw-Hill, 1977.

# APPENDIX A: FLOW RULE DEVELOPMENT

The following development is taken from reference 53 and represents a formalization of Drucker's (17) original work which leads to equation 13.

Drucker's concept of material stability means that work done by stress increments applied to a soil element is positive. Mathematically this can be stated as

$$d\sigma_{ij}\, d\varepsilon_{ij} > 0 \tag{1a}$$

If stress increments are removed, the net work performed during an unload cycle must also be zero or positive. This statement insures that energy is not created and can be expressed as

$$d\sigma_{ij}\, d\varepsilon^{T}_{ij} - d\sigma_{ij}\, d\varepsilon^{E}_{ij} = d\sigma_{ij}\, d\varepsilon^{P}_{ij} \geq 0 \tag{2a}$$

where the superscripts T, E, and P represent total, elastic, and plastic strains. A physical interpretation of Drucker's stable material is one having stress-strain properties displaying no decrease in stress after the ultimate strength is reached (i.e. branch 2 in Figure 2). This restriction is probably invalid for sensitive or strain softening soils.

For an ideal plastic soil, defined as one having stress-strain characteristics following branch 1 in Figure 2, the yield function or surface f is fixed in stress space and plastic flow occurs when f = k.

k is a material constant defining the onset of yield. Thus, during plastic deformation the yield function cannot change which means

$$df = \frac{\partial f}{\partial \sigma_{ij}} d\sigma_{ij} = 0 \tag{3a}$$

The stability condition occurring during plastic yield or along branch 1 of Figure 2 can be written as

$$d\sigma_{ij} \, d\varepsilon^{P}_{ij} = 0 \tag{4a}$$

Since equations 3a and 4a are both identical to zero

$$d\varepsilon^{P}_{ij} = \Lambda \frac{\partial f}{\partial \sigma_{ij}} \tag{5a}$$

$\Lambda$ introduced as a positive scalar factor of proportionality, dependent on the specific form of the yield function. Total strains can then be written as the sum of elastic and plastic components as

$$d\varepsilon^{T}_{ij} = \frac{1+\nu}{E} \sigma_{ij} - \frac{\nu}{E} J_1 \delta_{ij} + \Lambda \frac{\partial f(\sigma_{ij})}{\partial \sigma_{ij}} \tag{6a}$$

Equation 5a is known as the plastic potential while equation 6a represents a constitutive law for a material which deforms elastically until yield; whereupon, increments of plastic deformations are summed to the pre-existing elastic components.

## APPENDIX B: BETA-DISTRIBUTION

The following describes a methodology developed by Harr (28) to define the parameters in the beta-distribution. The general form of the beta-distribution for the random variable, Q, is

$$f(Q) = \frac{1}{(b - a)B(\alpha + 1, \beta + 1)} \left(\frac{Q - a}{b - a}\right)^{\alpha} \left(\frac{b - Q}{b - a}\right)^{\beta} \qquad (1b)$$

cf. Harr (28)

where $\alpha$ and $\beta$ are parameters defining the shape of the distribution, a is the lower limit for the random variable and b is the upper limit. The function $B(\alpha + 1, \beta + 1)$ depends on the gamma function according to

$$B(\alpha + 1, \beta + 1) = \frac{\Gamma(\alpha + 1)\ \Gamma\ (\beta + 1)}{\Gamma(\alpha + \beta + 2)} \qquad \text{cf. Harr (28)} \qquad (2b)$$

Thus,it can be seen that defining the beta-distribution means evaluating the four parameters $\alpha$, $\beta$, a and b.

To establish the bounds for the distribution, Harr suggests using Chebyshev's inequality which states that for a random variable, Q, with an expected value, $\bar{Q}$, and a finite standard deviation, $S_q$, the probability that Q takes on values outside the interval, $\bar{Q} - hS_q/\sqrt{n}$ to $\bar{Q} + hS_q/\sqrt{n}$ can never be greater than $4/9h^2$. Mathematically this statement can be expressed as

$$P[(\bar{Q} - h\, S_q/\sqrt{n}) \leq Q \leq (\bar{Q} + h\, S_q/\sqrt{n})] \geq 1 - \frac{4}{h^2} \qquad (3b)$$

cf. Harr (28)

where h is a parameter and n is the number of samples.

Equation 3b is a powerful tool in that its derivation is independent of the frequency distribution form. Harr's application of equation 3a for determining the bounds a and b involves setting very rigorous standards for the inequality which makes it unlikely that a Q will fall outside the established limits. To find a and b for the example used in this research, a 99 percent chance that a and b contains Q was used. Thus, the following computations can be made:

$$1 - \frac{4}{9h^2} = 0.99$$

$$h = 6.67$$

$$h/\sqrt{n} = 6.67/\sqrt{5} = 3$$

$$a = \bar{Q} - 3(S_q) = 322 - 3(80) = 82$$

$$b = \bar{Q} + 3(S_q) = 322 + 3(80) = 562$$

The parameters defining the shape of the distribution can be determined by matching moments of the experimental data with those of the continuous distribution. This results in the following relations:

$$\alpha = \frac{\left(\frac{\bar{Q} - a}{b - a}\right)^2}{\left(\frac{S_q}{b - a}\right)^2}\left(\frac{b - \bar{Q}}{b - a}\right) - \left(\frac{b - 2a + \bar{Q}}{b - a}\right) \quad \text{cf. Harr (28)} \tag{4b}$$

$$\beta = \left(\frac{b - a}{\bar{Q} - a}\right)(\alpha + 1) - (\alpha + 2) \quad \text{cf. Harr (28)} \tag{5b}$$

Using the mean and standard deviation from the experimental data and the computed values for a and b, in equations 4b and 5b results in:

$$\alpha = \beta = 3.$$

$\alpha = \beta$ means the experimental data indicates a symmetric distribution. Thus, the four parameters needed in equation 1b have been defined and the probability distribution function used in this example is:

$$f(Q) = 2.385 \times 10^{-7} (Q - 82)^3 (562 - Q)^3 \tag{6b}$$